A MATHEMATICAL STUDY OF BOUNDARY LAYER NANOFLUID FLOW USING SPECTRAL QUASILINEARIZATION METHODS

A THESIS SUBMITTED TO THE UNIVERSITY OF KWAZULU-NATAL
FOR THE DEGREE OF DOCTOR OF PHILOSOPHY
IN THE COLLEGE OF AGRICULTURE, ENGINEERING & SCIENCE

By

Mlamuli Dhlamini

School of Mathematics, Statistics & Computer Science

January 2020

Contents

Abstract

Heat and mass transfer enhancement in industrial processes is critical in improving the efficiency of these systems. Several studies have been conducted in the past to investigate different strategies for improving heat and mass transfer enhancement. There are however some aspects that warrant further investigations. These emanate from different constitutive relationships for different non-Newtonian fluids and numerical instability of some numerical schemes. To investigate the convective transport phenomena in nanofluid flows, we formulate models for flows with convective boundary conditions and solve them numerically using the spectral quasilinearisation methods. The numerical methods are shown to be stable, accurate and have fast convergence rates. The convective transport phenomena are studied via parameters such as the Biot number and buoyancy parameter. These are shown to enhance convective transport. Nanoparticles and microorganisms' effects are studied via parameters such as the Brownian motion, thermophoresis, bioconvective Peclet number, bioconvective Schmidt number and bioconvective Rayleigh number. These are also shown to aid convective transport.

Declaration

The work presented in this thesis is my original work conducted under the supervision of Prof. P. Sibanda and Prof. S. S. Motsa in the School of Mathematics, Statistics, & Computer Science, University of KwaZulu-Natal, Pietermaritzburg campus, from September 2016 to January 2020.

No portion of this work has been submitted in any form to any university or institution of learning for any degree or qualification. Where use has been made of the work of others it is duly acknowledged and cited in the reference section.

Signature:..... .....24/06/2020.....

Mlamuli Dhlamini Date

Signature:..... .....

Prof. P. Sibanda Date

Signature:..... .....

Prof. S. S. Motsa Date

To my late father Mr. Jameson Dhlamini, you fought a good fight Mlangeni, Sibalukhulu.

To my mother Mrs. Clara Dhlamini, you stayed strong during tough times to keep the family together. Thank you MaGumede, Mdladla kaSokela.

To Eveline, Nontuthuko, Zandile, and Lincoln, I couldn't have done this without your support, love you so much.

Acknowledgments

I would like to express my heartfelt gratitude to my academic supervisors Prof Precious Sibanda and Prof Sandile S. Motsa. Your support, patience, and guidance throughout my Ph.D. studies were phenomenal.

I would also like to thank the following post-doctoral students and post-graduate students for their assistance and creating a conducive working environment: Dr. Hiranmoy Mondal, Dr. Sicelo Goqo, Mangwiro Magodora, Mohammed Almakki, Samuel F Mutua and Shina D Oloniiju. I would also want to extend my appreciation to the administrative and academic staff in the School of Mathematics, Statistics & Computer Science, University of KwaZulu-Natal, Pietermaritzburg Campus. Not forgetting my colleagues Dr. N J Malunguza and Mr. G G Nyambuya from Nust.

Last but not least, I would like to thank my wife Eveline Dhlamini for the support during my pursuit of this qualification.

List of Publications

M. Dhlamini, H. Mondal, P. Sibanda and, S. Motsa, "Spectral Quasi-Linearization Methods for Powell-Eyring MHD Flow Over a Nonlinear Stretching Surface". *Journal of Nanofluids*, vol. 7, no. 5, pp. 917-927(11), 2018.

For this paper, I transformed the equations to form the boundary value problem using similarity transformations. I wrote the SQLM code for numerical solutions and the draft manuscript.

M. Dhlamini, P. K. Kameswaran, P. Sibanda, S. Motsa and H. Mondal, "Activation energy and binary chemical reaction effects in mixed convective nanofluid flow with convective boundary conditions". *Journal of Computational Design and Engineering*, vol. 6, no. 2, pp 149-158, 2019

In this paper, I transformed the equations to form the boundary value problem using similarity transformations. I wrote the SQLM code for numerical solutions and the draft manuscript.

M. Dhlamini, P. Sibanda, S. Motsa and H. Mondal, "Activation energy and entropy generation in viscous nanofluid with higher-order chemically reacting species". *International Journal of Ambient Energy*, 2020 DOI: 10.1080/01430750.2019.1710564 For this paper I developed the model, analyzed it, wrote the SQLM code for numerical solutions and prepared the draft manuscript.

M. Dhlamini, P. Sibanda, S. Motsa and H. Mondal, "Rotational nanofluids for oxytactic microorganisms with convective boundary conditions using bivariate spectral quasi-linearization method". *Journal of Central South University, Springer*. vol. 27, pp 824-8941, 2020

In this paper, I transformed the equations to form the boundary value problem using similarity transformations. I wrote the BSQLM code for numerical solutions and the draft manuscript.

M. Dhlamini, P. Sibanda, S. Motsa and H. Mondal, "Numerical studies on temperature-dependent viscosity and thermal conductivity on a couple stress fluid". *under review: International Communications On Heat & Mass Transfer*

For this paper, I developed the model, analyzed it, wrote the SQLM code for numerical solutions and prepared the draft manuscript

Signature: ....

Mlamuli Dhlamini Date

Chapter 1

Introduction

1.1 Background

In this thesis, we investigate the impact of convective boundary conditions on the heat and mass transfer in nanofluid flows using the spectral quasilinearisation numerical methods. Fluid dynamics deal with the study of fluids in motion [1]. The study of fluid dynamics seeks to give insights into the structure and behavior of fluid flows [2]. Fluid dynamics has a wide range of industrial and biological applications including, but not limited to, wheezing, blood flow, electricity generation, the design and performance of air and sea crafts, windmills, water sprinklers and missiles [2]. Fluid flow plays a pivotal role in the transport phenomenon, including the transfer of mass, charge, energy and momentum in a wide range of industrial, chemical and biological applications [3]. Of the three modes of heat and mass transport, convection leads to large spatial transportation capabilities over a significantly shorter time scale compared to diffusion [4]. Although several studies on convective transport are found in the literature [5–10], there are aspects that warrant further consideration.

Thermal convection consists of a flowing fluid that is in thermal contact with a solid surface that is in thermal disequilibrium with the fluid [11]. This is the most common setup encountered in many industrial applications resulting in convective boundary conditions. The need to improve heat and mass transfer efficiency in industrial processes is fundamental in fluid dynamics research. There has been advancements in recent years in enhancing heat transfer in industrial applications. One such study is the work of Popov *et al* [12], where they studied the heat transfer enhancement for

power installation. According to Popov *et al* [12], the methods of heat transfer enhancement are focused on reducing the thermal resistance of the near-wall layer during convective heat transfer. This increases the coefficient of heat transfer without increasing the working surface of the apparatus. Convective transport has also been reported to play a crucial role in the transportation of growth factors that were previously thought to be transported by diffusion alone [13]. Convective solute transport is also encountered in interstitial mass transport [14–17]. In climate modeling, convective flow is responsible for the global-wide circulation in the atmosphere [18]. A disruption of the normal convective transport in the atmosphere may lead to temperature inversion [18].

Convective transport lies at the heart of many industrial, chemical, and biological processes. In mathematical modeling, convective transport is accounted for by a nonlinear term. This term normally introduces some numerical instability called convective instability in the solution of the system [19–21]. Developing numerical schemes that are not prone to these numerical instabilities is crucial in the study of heat and mass transfer for industrial applications. Models for flows in different geometries and different fluids with various rheological properties are formulated and solved numerically using a fairly new scheme, the spectral quasilinearisation technique. The accuracy, stability and convergence of the methods are tested and compared with other methods for validation purposes. In the case where no analogous models are found in literature, the residual errors are used to validate the accuracy of the numerical scheme.

Fluids are normally classified as Newtonian or non-Newtonian. Newtonian fluids are fluids that follow Newton's law of viscosity, i.e, the viscous stresses arising from the fluid flow are linearly proportional to the strain rate. Examples of Newtonian fluids include water, kerosene and gasoline. Fluids that do not obey this relationship, i.e shear stress is not linearly dependent on strain rate, are classified as non-Newtonian. These fluids include, among many others, coal slurries, colloidal suspension, blood and asphalt [1, 2]. Other rheological properties may be used in the classification of a fluid as Newtonian or non-Newtonian. When modeling the fluid flow, it is important to correctly capture the rheology of the fluid and represent this adequately in the mathematical model. Due to the variability and complexity of non-Newtonian fluids, there is no single constitutive relationship that correctly models all non-Newtonian fluids [22, 23]. As such, different models have been de-

veloped for different non-Newtonian fluids. Some of the models developed for this purpose are Casson, couple stress fluids, Jeffery, Maxwell, micropolar, Oldroyd-B and Powell-Eyring. These models capture some peculiar aspects of a particular fluid that may need emphasis, for example, the Powell-Eyring model accounts for fluids that behave like Newtonian fluids under low and high strain rate [23] and the couple stress seeks to account for the forces in the fluid due to additives [24].

1.2 Heat and mass transfer

Heat and mass transfer are two kinetic processes that can be studied separately or jointly. Lately, it has been found to be more judicious to study the two jointly, especially in engineering settings as they often influence one another. This is normally encountered or explained as the Soret and Dufour effects [25–27]. The Soret effect is mass flux due to a temperature gradient and the Dufour effect is the energy flux due to a concentration gradient. We investigated heat and mass transfer in nanofluid flow. They were interested in establishing how heat that is either fed to the system or produced during an industrial process affects the fluid and flow properties. Similarly, we were also interested in establishing how the concentration gradients in a fluid affect the fluid and flow properties too.

Heat transfer is thermal energy in transit due to a spatial temperature gradient [28]. If heat and heat transfer are not properly managed thermal runaways may occur leading to accidents, entropy generation and poor performance by a thermal system [29–31]. Entropy generation is considered in Chapter 4 where the study sought to understand the processes that lead to entropy generation and how this can be minimized.

When a temperature gradient occurs in a stationary medium, heat transfer proceeds by conduction. If the medium is a moving fluid, then heat transfer is by convection. The third mode of heat transfer is thermal radiation. This is thermal energy that is emitted as electromagnetic waves, by a body at a higher temperature, to a body with low temperature. This mode of transport does not need a

medium for transport.

In conduction, heat transfer occurs at the molecular or atomic level. Molecules with a higher thermal energy vibrate and collide with molecules with a lower thermal energy and in the process they transfer some of their thermal energy. Conduction depends mainly on four factors, namely the temperature gradient, the cross-sectional area of the material involved, length of the path and the properties of the materials involved. To quantify the amount of heat transfer by conduction the Fourier's law is used. This is given as,

$$q''_x = -k\frac{dT}{dx}, \tag{1.1}$$

where q''_x is the heat flux (W/m^2), k is the heat transport property of the fluid (W/m.K) and dT/dx is the temperature gradient. The negative sign indicates that heat transfer is in the direction of decreasing temperature.

In convection, there are two mechanisms for heat transfer. The first one is the diffusion process, due to the random movement of molecules and the second one is advection or bulk transport in the flow. If temperature gradients exist in moving fluid then heat transfer occurs by convection. In this thesis, the problems that were studied consisted of a solid surface moving through a fluid at a different temperature. Such problems are said to have convective boundary conditions and this phenomenon in the thermal boundary conditions at the surface.

When close to a surface, diffusion is the dominant mechanism for heat transfer due to the no-slip condition. When far from the surface, advection dominates. Convection can be classified as forced convection if an external device is used to drive the flow, or natural convection if the flow is driven by buoyancy forces resulting from temperature differences in the fluid. The rate equation for convective heat transfer is,

$$q'' = h\left(T_s - T_\infty\right), \tag{1.2}$$

where q'' is the convective heat flux $(W/m^2.K)$, T_s and T_∞ are the surface and ambient fluid temperatures and h is the convection heat transfer coefficient $(W/m^2.K)$.

The third mode of heat transfer is thermal radiation. In this thesis, we investigated the influence of thermal radiation in Chapters 2 and 5. Thermal radiation is the energy emitted by a body that is at a nonzero temperature [28]. The emitted energy is transported by electromagnetic waves or photons. No medium is required for this form of heat transfer, in fact, radiation transfer is most effective in a vacuum [28]. The rate at which the radiation energy is released by a body is termed the surface emissive power E. The Stefan-Boltzman law is used to approximate the energy emitted by a body (W/m^2) as,

$$E_b = \sigma T_s^4, \tag{1.3}$$

where T_s is the absolute temperature of surface and σ is the Stefan-Boltzman constant $(\sigma = 5.67 \times 10^{-10} W/m^2)$. Equation (1.3) represents the heat flux emitted by a black-body. The heat flux emitted by real surfaces is normally modeled by including a radiative property term for the surface called the emissivity $0 \leq \varepsilon \leq 1$, so that,

$$E = \varepsilon \sigma T_s^4. \tag{1.4}$$

The concept of mass transfer is analogous to that of heat transfer. Mass transfer is solute in transit as a result of spatial solute differences [3, 28]. The basic types of mass transfer include diffusion in a quiescent medium and mass exchange between phases [32]. The models investigated in this thesis considered mainly mass transfer in laminar flow. Mass transfer by diffusion is driven by a concentration gradient in a medium. Fick's law is used to describe this type of mass movement and is given by

$$\dot{Q} = -\kappa_{diff} A \frac{dC}{dx}, \tag{1.5}$$

where $\dot{Q}$ is the mass flow rate, κ_{diff} is the diffusion coefficient, A is the area normal to the flow direction and dC/dx is the concentration gradient.

The diffusion coefficient and subsequent diffusion are dependent on the temperature [1]. Higher temperatures increase the velocity of the molecules and thus increase diffusion. Diffusive mass transport is further influenced by the molecular spacing or mean free path. Diffusion is high if the molecular spacing is high because particles/molecules have a longer distance to travel before colliding with another particle/molecule. As such, diffusion is highest in gases followed by liquids and lastly in solids. Although there are many diffusion mechanisms, they were not discussed in detail at this point due to their limited consideration in this thesis.

Mass convection or convective mass transport is the mass transfer between a surface and a moving fluid through both diffusion and bulk fluid motion [1]. If the mass is constantly supplied from a surface in a moving fluid, a solute boundary layer will develop just like in the case of convective heat transport. If the fluid stops or is stationary, then mass transport reduces to diffusion only. When close to the surface, diffusion transport is dominant due to the no-slip boundary condition. When further from the surface, the fluid has significant momentum and the bulk transport will begin to dominate.

1.3 Nanofluids

Nanofluids are a class of emerging industrial fluids. They are more desirable over convectional fluids due to their unique thermal properties. The term nanofluid was introduced by Choi and Eastman in 1995 [33] to describe fluids in which nano-sized particles are added to a base fluid to enhance certain properties. Nanofluids have a wide range of applications that include antibacterial activity, cooling systems, solar water heating, diesel combustion, application in transformers,

targeted drug delivery, nuclear reactors and many others [34–37]. A typical nanoparticle is a stable metal (Al, Cu, Ag, Au, Fe), an oxide (Al_2O_3, CuO, TiO_2, SiO_2), carbide (SiC), nitrate (AlN, SiN) or a non-metal (graphite). The common base fluids are water, ethylene glycol, oil, polymer or bio-fluid [38]. Some previous studies have suggested that metallic nanoparticles enhance the thermal and electrical conductivity of the base fluids [39]. The idea of improving the conductivity of a fluid by the use of solid particles had been reported before by Maxwell [40]. The results of these studies were not commercialised because these fluids tended to damage mechanical pumps and clog flow passages due to the particles settling [39, 41] and this presented a major challenge towards commercialisation.

The use of a nanofluid improves conductive and convective heat transfer [42]. The enhancement of thermal conductivity is attributed to nanoparticle aggregation. Particle aggregation is believed to lead to percolation paths which enhance the thermal conductivity parameter beyond what is predicted by the mean-path theory for well-distributed nanoparticles [42–45]. Some researchers, however, do not subscribe to the theory of nanoparticle aggregation as the primary cause of the thermal conductivity parameter enhancement. Although similar hypotheses have been put forward for the convective heat transfer coefficient, no conclusive mechanism has been attributed to the convective heat transfer coefficient enhancement [42].

It has been suggested that nanoparticles also play a vital role in altering other fluid properties, among them, the specific heat capacity and the viscosity [42, 46–50]. For these properties, nanoparticles are believed to have a deleterious effect. The specific heat of the nanofluid mixture is generally below that of a pure liquid since the specific heat capacity of the solids is less than that of fluids [42]. Viscosity tends to increase with an increase in the nanoparticle volume fraction. This is attributed to nanoparticle aggregation and/or nanoparticle size [42]. The addition of more than a certain optimum amount of particles is thus detrimental to the heat transfer of a system [42].

Buongiorno [51] suggested that the convective heat transfer in nanofluids is mainly driven by Brownian diffusion and thermophoresis. This is the main reason for the inclusion of the two terms when modeling the flow of a nanofluid. As the nanoparticles move in the fluid, convective heat transfer is enhanced by the nanoparticle dragging the fluid surrounding it. The results for this phe-

nomenon were reported in chapters 2 to 6.

In chapter 6, we study the effect of rotation and bioconvection on the fluid and flow properties of a nanofluid. Bioconvection is the convective motion that is initiated and maintained by microorganisms in a fluid medium [52–57]. Microorganisms respond to some external stimuli such as oxygen consumption (oxytactic), gravitational torque (gyrotactic), chemical concentration (chemotactic), thermal changes (thermotaxis) or light (phototactic) [38, 58–60]. The common microorganisms include algae, bacteria, dinoflagellates and diatomic [53, 61]. The swimming microorganisms are denser than the base fluid. The aggregation of these microorganisms at the upper surface of the fluid initiates an overturning instability synonymous with Rayleigh-Benard convection [62]. The falling plumes are believed to deliver oxygen to the bottom of the tank in the case of oxytactic microorganisms faster than diffusion [52, 63, 64]. Although the drive towards the use of 'green technologies' in the industry is a major driving force towards the utilisation of bioconvection mechanisms [53], most of the theories surrounding bioconvection are still not fully understood or proven [52]. Most experimental evidence to support mass enhancement have been inconclusive. It is for this reason that we sought to study the influence of bioconvection from a theoretical perspective to gain some insight into the subject area. In as much as there are many theoretical studies on bioconvection [38, 58, 59, 65–69], most, if not all, did not investigate the rotational effects of the fluid with a floating insulated plate. These two aspects form the focus of the study and were presented in Chapter 6.

1.4 Non-dimensionalisation and numerical techniques

In modeling fluid flow, the transport equations are generally highly nonlinear partial differential equations that do not have analytic solutions. To gain some insights into the flow dynamics, we use numerical simulations to approximate the solutions. Although there are several techniques for solving differential equations, most methods work only for a limited class of problems [70]. Similarity transformations have in the past yielded solutions to nonlinear partial differential equations which would be intractable to a standard solution technique. A similarity solution of partial differ-

ential equations occurs if the number of independent variables can be reduced by at least one from the original number.

In this thesis, we solve systems of equations describing fluid flows using the similarity transformations to first transform the set of equations to a system of ordinary differential equations. The methods of determining the similarity transformations can be classified into two categories, the direct methods and group methods.

1.4.1 Direct Methods

Direct methods do not invoke any group invariance. These methods include dimensional analysis, free parameter and separation of variables method. Although these methods are straight forward in determining similarity transformations, they are often limited to a few contrived cases.

Dimensional analysis reduces the number and complexity of the variables required to describe a given phenomenon by making use of information implied by the units of the physical quantities involved. This is a technique for restructuring the original variables using dimensions of the problem into a set of dimensionless problems using the constraints imposed upon them by their dimensions. Such non-dimensional variables are fewer and have a more appropriate interpretation than the original variables [71]. The Buckingham π-theorem provides a way of computing these dimensionless parameters even if the form of the equation is unknown [72].

The free parameter method depends on the unknown transformation function of independent variables occurring in a particular function suggested by possible similarity. One of the functions of this product is a function of all independent variables except one, and the other depends on a single parameter, say η. η is a variable involving all independent variables [71]. If we let u be the dependent variable for a certain partial differential equation with independent variable given by $x_1, x_2, \cdots, x_n, y$, u can be expressed in the form,

$$u = \Phi(x_1, x_2, \cdots, x_n) F(\eta), \tag{1.6}$$

where

$$\eta = \eta(x_1, x_2, \cdots, x_n, y).$$

The separation of the variable method was introduced by Winternitz and Fris [73] and works similar to the free parameter method. The difference is that in the separation of variables method η is assumed to be separable and initially specified while the free parameter method makes no such specification on η [71].

The direct method by Clarkson and Kruskal [74] was used to find a similarity transformation for the first, second and fourth Painvele equations that could not be established using the Lie group method [74]. The direct method however often leads to tedious algebraic manipulations especially for huge and highly nonlinear systems of partial differential equations. This presents a major setback for the method.

1.4.2 Group methods

The underlying idea with this method is to find a set of transformations such that the system is invariant when applied [70, 75]. The group theoretic approach is further divided into two distinct categories, which are: Those methods that search for finite group transformations such as the Birkhoff (1948) and Mogan's method (1952), Moran and Gaggioli method (1968) as well as the Hellums-Churchill method (1964) and those methods that search for infinitesimal groups of transformations such as the classical method by Lie (1922), nonclassical method by Bluman and Cole (1974) and characteristic function method by Na and Hansen (1969) [71].

1.4.3 Numerical methods

Due to the high nonlinearity and complexity of the systems for modeling fluid flow, analytical solutions are often difficult to find, hence the reason numerical methods are employed. Although there are known methods for evaluating analytic solutions for solving nonlinear partial differential

equations such as Adomian decomposition, homotopy and the *tanh*-function method, they have major drawbacks. Some of these drawbacks include slow convergence rates and that they may be cumbersome to use [76].

The standard homotopy analysis method by Liao [77] often works well, it is reported to have a low convergence rate and limited region where the solutions are valid [76]. The finite difference scheme, on the other hand, is a well-established and simple numerical scheme to implement [78]. The method uses a point-wise approximation of the equations. Its accuracy improves with an increasing number of grid points. This presents a problem because using more grid points requires more resources and thereby takes long to compute. Although some differential equations may be solved using finite differences, it becomes difficult to use the method if complex geometries are encountered or unusual specifications to boundary conditions are made [79, 80].

The finite element method has gained popularity as a numerical method of choice in engineering from structural analysis, heat transfer, fluid flow, mass transport and electromagnetic potential. The finite element method works by dividing the domain into small sub-domains called elements. This process, called discretisation of the domain, has the net effect of reducing the continuum problem with an infinite number of unknowns to one with a finite number of unknowns at specified points called nodes [78]. Besides, it has several advantages that include: an accurate representation of complex geometries; the inclusion of material with non-homogeneous properties; easy representation of the total solution that captures the local effects and produces sparse matrices that can be solved at a fraction of the cost compared to their full matrices counterparts [81]. Each sub-domain is represented by a set of element equations. These element equations approximate the original equation locally. The method works by constructing an integral of the inner product of residuals and the weight functions and then sets the integral to zero. In simpler terms, it minimizes the error of approximation by fitting trial functions into the differential equation [78]. The finite control volume, on the other hand, is obtained using constant weights. A global system of equations is generated by combining the element equations. Despite all the positives that the finite element method has over the finite difference method, the method has its disadvantages. Some of these in-

clude; a general closed-form solution, which allows one to examine system response to changes in various parameters, is not attained; the method only produces approximate solutions; the method has some inherent errors and mistakes by users can be fatal [81].

Spectral methods are a class of numerical methods used to solve differential equations arising in applied mathematics, science and engineering. The name spectral method is derived from the fact that the solution is expressed as a series of orthogonal eigenfunctions of some linear operator. In this form, the numerical solution is related to its spectrum, hence the name [81, 82]. The basic idea behind the spectral methods is to write the solution of a differential equation as a sum of basis functions of the complex exponentials, Chebyshev or Legendre polynomials [83] and choose the coefficients in a manner that the differential equation is satisfied. Spectral methods and finite element methods are built on similar principles. There are however some fundamental differences between the two methods. The first difference is that the finite element sub-divides the domain into sub-intervals and chooses local polynomial functions of fixed degree which are non-zero and only over a couple of sub-intervals. Spectral methods, on the other hand, use global basis functions which are polynomials of a high order and are non-zero, except at isolated points over the entire domain [81]. The second difference is that the finite element method produces sparse matrices that are easier to compute while spectral methods produce full matrices that are more computationally demanding. Another difference is that the basis functions in spectral methods can be differentiated analytically and each coefficient a_n can be determined by all grid points. That being said, it means the spectral methods are N-point formula, unlike their finite element method counterparts that are 3-point and finite difference methods that are normally low order methods [81]. This is the property that makes spectral methods a better numerical scheme as compared to finite element and finite difference methods. Spectral methods are however more difficult to program, irregular domains lead to severe losses in accuracy although there have been some improvements over the years for these setbacks [81].

Upon applying the similarity transformations the partial differential equation is reduced to an ordinary boundary value problem with normally one or two independent variables. The resulting boundary value problem is solved using a numerical scheme. Although there are numerous com-

mon numerical schemes such as the Runge-Kutta methods, finite element method, finite difference method, Adomian decomposition method, Keller-box and the homotopy method that have been developed and used over the years, these have presented some limitations. Some of these limitations include; small regions for convergence, the requirement for more grid points for approximation leading to a high demand in memory and time thus becoming computationally expensive, inefficiency in cases involving singularities, discontinuities and problems with multiple solutions [84]. In the current study, we used spectral based methods to solve the resulting boundary value problem. Spectral methods are the best choice for solving differential equations (ordinary and partial differential equations) at a high accuracy on a simple domain if the data defining the problem is smooth [85]. The quasilinearisation method (QLM) is a generalization of the Newton-Raphson's method [86]. A direct implementation of a numerical scheme is not an easy task with most nonlinear systems due to either the high order of both dimensions and differential operator or nonlinearity [87]. quasilinearisation is a systematic way of obtaining linear boundary functions to an otherwise nonlinear system [88]. The method provides a sequence of functions which in general converges rapidly to the original equations. The unique feature of the quasilinearisation technique is the quadratic convergence and monotonicity, which render the method superior [89]. The derivation of the QLM is based on the linearization of the nonlinear components of the governing equations using the Taylor series assuming that the difference between successive iterations, that is at $r+1$, and r is negligibly small. In this thesis we depended on two methods, the spectral quasilinearisation method (SQLM) that was proposed by Mosta *et al* [90] and the bivariate spectral quasilinearisation method (BSQLM) that was introduced by Mosta *et al* [76]. Although the SQLM has a very high convergence it is limited to cases where there is only one independent variable. The BSQLM, on the other hand, works when there are two independent variables and requires fewer grid points [81, 91]. The BSQLM is used to solve the problem in Chapter 5 where the similarity variables has two variable η and ξ; and for the rest of the problems, the SQLM suffices since the similarity variables have one variable η.

1.5 Problem statement

Due to different constitutive relationships, non-Newtonian fluids have different and complex mathematical models to describe them. Often times, these models do not have analytical solutions and thus require numerical methods to solve them. Although numerical techniques offer a solution to this challenge, there are stillsome draw-backs associated with using numerical schemes. The major ones are; numerical instability when solving reaction-diffusion equations, slow convergence and stability of the numerical scheme.

1.6 Objectives

1.6.1 Main Objective

The main objective of this thesis is to test the accuracy, stability and convergence rate of a fairly new numerical scheme; the spectral quasilinearisation method in solving the nonlinear advection-diffusion type of equations with convective boundary conditions.

Specific Objectives The specific objective are:

- formulate models for different non-Newtonian fluids,
- solve these models numerically using the spectral quasilinearization method,
- test for accuracy of the model by plotting the residual errors and the convergence rate by the number of iteration needed for the scheme to converge,
- investigate the impact of physical parameters of interest on the flow properties of these fluids.

1.7 Significance of the study

The findings of this study will prove insightful knowledge in computational fluid dynamics and forging a way forward in the implementation of spectral methods in commercial softwares.

1.8 Structure of the thesis

The remainder of the thesis is structured as follows:

In Chapter 2, we study momentum, heat and mass transfer in a Powell-Eyring MHD flow over a nonlinear stretching surface. In this chapter, a model with non-convective boundary conditions is considered. The remainder of the chapters focus on models with convective boundary conditions considering some aspects that have an impact on it, either positive or negative. In Chapter 3, we formulate and analyse a model for an unsteady flow for Arrhenius activation energy and binary chemical reaction of nanofluid with convective boundary conditions. In Chapter 4, a study of the effect of the order of a chemical reaction, entropy generation and activation energy with convective boundary conditions is conducted. In this chapter, we investigate whether the order of a chemical reaction plays a role in heat and/or mass transfer. In Chapter 5 we study the impact of oxytactic microorganisms in a rotational nanofluid with convective boundary conditions. There is also a consideration of a metal plate that is either dragged by the fluid, drags the fluid, floats on the fluid or is moving in the opposite direction affects the flow dynamics. In this section, we are interested in assessing the extent of heat and/or mass transfer enhancement by the use of microorganisms. In Chapter 6, we study the effect of temperature-dependent viscosity and thermal conductivity on couple stress nanofluid with convective boundary conditions. A new formulation and analysis for variable thermal conductivity is presented. In this section, we investigate the convective heat and mass transfer using the fact that viscosity and thermal conductivity are non-constant in the boundary layer. The assumption of constant viscosity and thermal conductivity is not true for certain temperature ranges. Lastly, in Chapter 7, we present a general discussion and conclusion.

Chapter 2

Spectral Quasilinearisation Methods for Powell-Eyring MHD Flow Over a Nonlinear Stretching Surface

In this chapter, we study the flow of a Powell-Eyring magnetohydrodynamic over a nonlinearly stretching sheet. The Powel-Eyring model is suitable for a non-Newtonian shear-thinning fluid [92] that behaves like a Newtonian fluid under low and high shear stress [93, 94]. This behavior is attributed to two types of molecular bonds that must be broken before the fluid flows. The type I strong bonds permit the flow of the fluid according to the non-Newtonian law and the type II bonds allow the flow of the fluid according to the Newtonian law [95]. This model has been adopted in modeling pseudo-plastics [96] and greases [95]. The current model seeks to analyse the convective flow of a Powell-Eyring nanofluid over a nonlinear stretching surface. Thermal radiation and viscous dissipation effects are the other factors that have not been considered for Powell-Eyring nanofluid flow over a stretching surface in the past.

AMERICAN SCIENTIFIC PUBLISHERS

Journal of Nanofluids
Vol. 7, pp. 917–927, 2018
(www.aspbs.com/jon)

ARTICLE

Spectral Quasi-Linearization Methods for Powell-Eyring MHD Flow Over a Nonlinear Stretching Surface

Mlamuli Dhlamini, Hiranmoy Mondal*, Precious Sibanda, and Sandile Motsa

School of Mathematics, Statistics and Computer Science, University of KwaZulu-Natal, Private Bag X01, Scottsvile, Pietermaritzburg-3209, South Africa

In most industrial processes heat generation is an important aspect for production. Heat affects the quality of the end product and if it is not properly regulated this may lead to thermal runaways. In this paper we address the problem of the flow of a Powell-Eyring nanofluid over a nonlinear stretching surface with processes that either generate heat or result in heat loss, such as viscous dissipation, thermal radiation, nanoparticle Brownian motion and thermophoresis. An electrically conducting fluid is considered and a magnetic field is applied transverse to the stretching sheet. The nonlinear ordinary differential equations are solved numerically using the spectral quasi-linearization method. We showed that increasing the thinning parameter leads to an overshoot in the temperature and an increase in the thermal boundary layer thickness accompanied by an increase in flow velocity. The Brownian motion parameter was shown to reduce the fluid velocity due to generation of long velocity fields by Brownian particles in the surrounding fluid. Although there is an overshoot in temperature for certain parameter values, the steady-state is eventually attained in the long run. This is because of heat advection due to the ascending buoyant fluid and chemical species in the fluid.

KEYWORDS: Powell-Eyring Fluid, Spectral Quasi-Linearization Method, Stretching Sheet, Nanoparticles, Viscous Dissipation, Thermophoresis, Thermal Radiation, Thermal Runaway.

1. INTRODUCTION

The study of the flow of non-Newtonian fluids is a popular area of research because these fluids are important in industrial applications. These fluids are found in several industrial technological processes such as the continuous stretching of plastic films, coal-oil slurries, metal spinning, metal extrusion, continuous casting, glass blowing, extrusion of polymer sheet from die etc. Heat transfer in stretching surfaces is a crucial area of research for industrial and manufacturing processes. In these processes the quality of the final product depends significantly on heat transfer rate. It is therefore important that proper cooling rates are attained for the best quality product. Most industrial fluids deviate from the Newtonian model, and thus the usual Navier-Stokes equations fail to adequately describe the flow of these fluids. The Powell-Eyring fluid model has some advantages over the Newtonian fluid model in that, it is derived from the kinetic theory of fluids rather than from empirical relations and secondly it reduces to a Newtonian fluid under very low and high shear stress. Heat is generated as adjacent fluid layers slide over each other in a process known as viscous dissipation. This occurs when a flowing viscous fluid converts some of its kinetic energy into internal energy resulting in an increase in temperature. Bearing in mind that the quality of product from a stretching, blowing or extrusion processes depends on the cooling rate, it becomes important to investigate any process that may lead to changes in the temperature of the fluid.

On the other hand nanofluids present a new kind of fluid for energy transport. Nanofluids consist of nanopartices, normally aluminum, gold, iron oxide, platinum, silica, silver etc. of sizes ranging from 1 to 100 nanometers suspended in a base fluid to increase/improve their thermal performance. Nanofluids have a wide range of applications such as in cooling systems, solar water heating and improving diesel generator efficiency. Thermophoresis is a phenomenon where different particles exhibit different responses to the force of a temperature gradient. It is a well known fact that energy fluxes arise due to temperature and

*Author to whom correspondence should be addressed.
Email: hiranmoymondal@yahoo.co.in
Received: 3 November 2017
Accepted: 15 January 2018

concentration gradients and also that mass transfer may occur as a result of temperature gradients.

The effect of thermal diffusion and diffusion thermo on heat and mass transfer in a mixed convective boundary layer for a Powell-Eyring fluid over a nonlinear stretching surfaced was investigated by Panigrahi et al.[1] They concluded that both the Soret and Dafour effects enhance the concentration and the temperature in the boundary layer. Panigrahi et al.[2] studied the magnetohydrodynamic (MHD) effect on mixed convection boundary-layer flow of a Powell-Eyring fluid past a nonlinear stretching surface. They observed that the momentum boundary thickness increased and the thermal boundary layer decreased with an increase in thinning parameter. The momentum boundary layer decreased while the thermal boundary layer increased for increase in the shearing rate parameter for both aiding and opposing mixed convection flows. The boundary layer flow of the Powell-Eyring fluid over a linearly stretching sheet was analyzed by Javed[3] and Jalil.[4] Malik[5] studied the analytic solution for the steady flow of a Powell-Erying fluid due to a stretching cylinder with temperature dependent variable viscosity. Khan et al.[6] analyzed the numerical and analytical solution of MHD Powell Eyring fluid flow with effects of joule heating, thermophoresis and chemical reaction. Hayat[7] studied the steady two-dimensional flow of a Powell-Eyring fluid over a stretching surface with homogeneous-heterogeneous reactions. The study showed that the boundary layer thickness increases by increasing the thinning parameter whereas it decreases by increasing the shearing rate parameter. The concentration is also an increasing function of Schmidt number and decreasing function of strength of homogeneous reaction. Lastly mass transfer rate increases for larger rate of heterogeneous reaction. The study of the stagnation point flow of a MHD Powell-Eyring fluid over a non-linearly stretching sheet in the presence of heat source/sink was presented by Vittal et al.[8] The findings in that study were that for the free stream velocity dominating the stretching velocity, the velocity field increases and the momentum boundary layer thickness decreases; however the boundary layer thickness and flow field velocity increases for shrinking. Also the thermal boundary layer thickness decreased for heat sink and increased for heat source. Mushtaq et al.[9] investigated the effect of exponentially stretching Sheet in a Powell-Eyring fluid. The study revealed that the momentum boundary layer thickness increase with an increase in the rheological fluid parameter and this increase was accompanied by larger wall shear stress.

A study of a steady, laminar, two-dimensional boundary layer flow and heat transfer of an incompressible, viscous non-Newtonian fluid over a non-isothermal stretching sheet in the presence of viscous dissipation and internal heat generation/absorption was given by Prasad et al.[10] The study concluded that increasing values of material parameters increased the velocity and hence the boundary layer thickness. An increase in the shear thinning parameter was noted to cause a decrease in the skin friction coefficient. The temperature distribution was observed to be unity at the wall in the prescribed surface temperature case and less than unity at the wall in the prescribed heat flux case. They further noticed that increasing the material parameter and injection parameter increased the thermal boundary layer thickness. Pal and Mondal[11] studied the influence of thermophoresis and Soret–Dufour on magnetohydrodynamic heat and mass transfer over a non-isothermal wedge with thermal radiation and Ohmic dissipation. Mondal et al.[12] analyzed the MHD three-dimensional nanofluid flow on a vertical stretching surface with heat generation/absorption and thermal Radiation.

The aim of the present paper is to study the effects of mixed convection Powell-Eyring nanofluid over a nonlinear stretching with nonlinear thermal radiation, viscous dissipation and thermophoresis parameter. The nonlinear differential equations are solved numerically. It is hoped that the results obtained will serve as a complement to the previous studies. The present study has many applications in cooling of metallic plate, movement of biological fluids, melt spinning, heat exchangers technology, and oceanography. The conversations equations are solved using the spectral quasi-linearization method (SQLM). The behavior of velocity, temperature and nanoparticles volume fraction are studied and visualize graphically.

2. MATHEMATICAL FORMULATION OF THE PROBLEM

A steady two-dimensional laminar boundary layer flow of an incompressible viscous fluid over a semi-infinite permeable nonlinear stretching surface is considered. The surface is stretched along the positive x-direction at a velocity $U_w(x) = cx^m$ and also stretched non-linearly along the y-direction at a velocity $V_w(x) = dx^n$ such that the origin remains fixed. Heat and chemical species are supplied from the plate at constant rates into the fluid thereby inducing a buoyancy force.

The Cartesian coordinate system is chosen in such a way that the x-axis is along the plate and y-axis is normal to it. The plate is maintained at a constant temperature and concentration of T_w and C_w respectively. The ambient temperature and concentration in the free stream, far away from the plate/wall are T_∞ and C_∞ respectively.

The physical set-up of the problem is shown in Figure 1.

The governing equations for the Powell-Eyring fluid are given by:

$$\frac{\partial u}{\partial x} + \frac{\partial u}{\partial y} = 0 \tag{1}$$

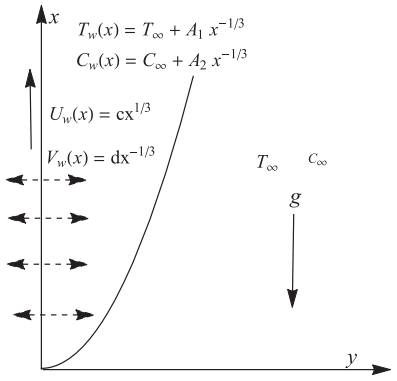

Fig. 1. Physical set-up.

$$u\frac{\partial u}{\partial x}+v\frac{\partial u}{\partial y}=\frac{1}{\rho}\frac{\partial \tau_{xy}}{\partial y}-\frac{\sigma B(x)^2 u}{\rho}+g\beta_T(T-T_\infty)+g\beta_C(C-C_\infty) \quad (2)$$

$$u\frac{\partial T}{\partial x}+v\frac{\partial T}{\partial y}=\frac{\kappa}{\rho C_p}\frac{\partial^2 T}{\partial y^2}+\tau\left[D_B\frac{\partial C}{\partial y}\frac{\partial T}{\partial y}+\frac{D_T}{T_\infty}\left(\frac{\partial T}{\partial y}\right)^2\right]-\frac{1}{\rho C_p}\frac{\partial q_r}{\partial y}+\frac{\mu}{\rho C_p}\left(\frac{\partial u}{\partial y}\right)^2 \quad (3)$$

$$u\frac{\partial C}{\partial x}+v\frac{\partial C}{\partial y}=D_B\frac{\partial^2 C}{\partial y^2}+\frac{D_T}{T_\infty}\frac{\partial^2 T}{\partial y^2} \quad (4)$$

The shear stress component τ_{xy} for the Powell-Eyring fluid having dynamic viscosity μ, the fluid material parameters β and γ with dimensions S^{-1} and Pa^{-1} respectively is given by

$$\tau_{xy}=\mu\frac{\partial u}{\partial y}+\frac{1}{\beta}\sinh^{-1}\left(\frac{1}{\gamma}\frac{\partial u}{\partial y}\right) \quad (5)$$

The inverse sine hyperbolic function accounts for the shear thinning of the fluid. (u, v) are the fluid velocity components in the x and y directions. $B(x)$, T and C are the magnetic field, temperature of the fluid and concentration of nano-particles. σ is the conductivity of the fluid, g the gravitational acceleration, β_T and β_C are the volumetric coefficients of thermal and mass expansion, κ is the thermal conductivity, ρ is the density, C_p is the specific heat at constant pressure for the fluid, τ is the ratio between effective heat capacity of the nanoparticles and the base fluid, D_B and D_T are the coefficients of mass and thermophoretic diffusion, q_r is the radiative heat, T_∞ and C_∞ are the free stream temperature and concentration (outside the boundary layer), k^* is mean absorption coefficients and σ^* is the Stephan-Boltzman constant. We use non-linear radiative heat flux given by Rosseland approximation which allows one to obtain results for both small and large differences between T_w and T_∞. The thermal radiation q_r and the wall temperature excess ratio are given by

$$q_r=-\frac{4\sigma^*}{3k^*}\frac{\partial T^4}{\partial y},\qquad \theta_w=\frac{T_w}{T_\infty} \quad (6)$$

where $T^4=T_\infty^4[1+(\theta_w-1)\theta]^4$.[13] The following similarity variable and stream function are used to transform the partial differential equations (PDE).

$$\eta=y\sqrt{\frac{2cx^{-2/3}}{3\nu}},\quad \psi=f(\eta)\sqrt{\frac{3c\nu x^{4/3}}{2}},\quad \theta(\eta)=\frac{T-T_\infty}{T_w-T_\infty},\quad \phi(\eta)=\frac{C-C_\infty}{C_w-C_\infty},\quad u=\frac{\partial\psi}{\partial y},\quad v=-\frac{\partial\psi}{\partial x} \quad (7)$$

we obtain

$$u=cx^{1/3}f',\quad v=\frac{1}{3}[\eta f'-2f]\sqrt{\frac{3c\nu x^{-2/3}}{2}} \quad (8)$$

The stretching velocity U_w, the succussion velocity V_w, and wall temperature T_w, the wall concentration C_w are considered as

$$U_w=cx^{1/3},\quad V_w=dx^{-1/3},\quad T_w=T_\infty+A_1x^{-1/3},\quad C_w=C_\infty+A_2x^{-1/3} \quad (9)$$

Here c, d, A_1 and A_2 are taken to be constants. The boundary conditions for the problem are are given as

$$u=U_w=cx^{1/3},\quad v=V_w=dx^{-1/3},\quad T=T_w=T_\infty+A_1x^{-1/3},\quad C=C_w=C_\infty+A_2x^{-1/3}\ \text{at}\ y=0$$
$$u\to 0,\quad T\to T_\infty,\quad \text{and}\quad C\to C_\infty\quad \text{as}\ y\to\infty \quad (10)$$

The transformation leads to the following set of ordinary differential equations (ODE)

$$f'''+\frac{f'''}{\rho\beta\gamma\nu\sqrt{1+(2c^3(f'')^2/3\nu\gamma^2)}}+ff''-\frac{1}{2}(f')^2-\frac{3}{2}Mf'+\frac{3}{2}\lambda_1\theta+\frac{3}{2}\lambda_2\phi=0 \quad (11)$$

Table I. Residual errors for different iterations.

i	$f(\eta)$	$\theta(\eta)$	$\phi(\eta)$
1	2.046325×10^{-2}	4.310583×10^{0}	1.727172×10^{-2}
2	1.231527×10^{-3}	3.160801×10^{-2}	8.817625×10^{-4}
3	9.984863×10^{-6}	2.405911×10^{-5}	8.539702×10^{-6}
4	1.258113×10^{-6}	1.372335×10^{-9}	8.086167×10^{-10}
5	3.325615×10^{-7}	5.168923×10^{-10}	1.416281×10^{-10}
6	4.026294×10^{-7}	3.977156×10^{-10}	7.236286×10^{-10}
7	4.947002×10^{-6}	1.718940×10^{-9}	1.562538×10^{-10}
8	3.690998×10^{-6}	1.325910×10^{-9}	5.479845×10^{-10}
9	4.199970×10^{-7}	8.244765×10^{-10}	4.920113×10^{-10}
10	2.499023×10^{-6}	3.059624×10^{-10}	1.444410×10^{-10}

ARTICLE

$$\frac{1}{Pr}\theta'' + Nb\theta'\phi' + Nt(\theta')^2 + \frac{1}{2}f'\theta + f\theta' + Ec(f'')^2 + \frac{N_r}{Pr}\{3[1+(\theta_w-1)\theta]^2(\theta_w-1)(\theta')^2 + [1+(\theta_w-1)\theta]^3\theta''\} = 0 \quad (12)$$

$$\frac{1}{Le}\phi'' + \frac{1}{Le}\frac{Nt}{Nb}\theta'' + \frac{1}{2}f'\phi + f\phi' = 0 \quad (13)$$

where M is the magnetic parameter, λ_1 is the mixed convection parameter, λ_2 is the solutal buoyancy parameter, Pr is the Prandtl number, N_r is the thermal radiation coefficient, N_t is the thermophoresis parameter, N_b is the Brownian motion parameter, Le is the Lewis number and Ec is the Eckert number.

$$M = \frac{\sigma B_0^2}{c^2}, \quad \lambda_1 = \frac{g\beta_T A_1}{c^2}, \quad \lambda_2 = \frac{g\beta_C A_2}{c^2},$$

$$Pr = \frac{\rho C_p \nu}{\kappa}, \quad N_r = \frac{16\sigma^* T_\infty^3}{3\kappa k^*}, \quad N_t = \frac{\tau D_T (T_w - T_\infty)}{\nu T_\infty},$$

$$N_b = \frac{\tau D_B (C_w - C_\infty)}{\nu}, \quad Le = \frac{\nu}{D_B}, \quad Ec = \frac{(cx^{1/3})^2}{C_p(T_w - T_\infty)} \quad (14)$$

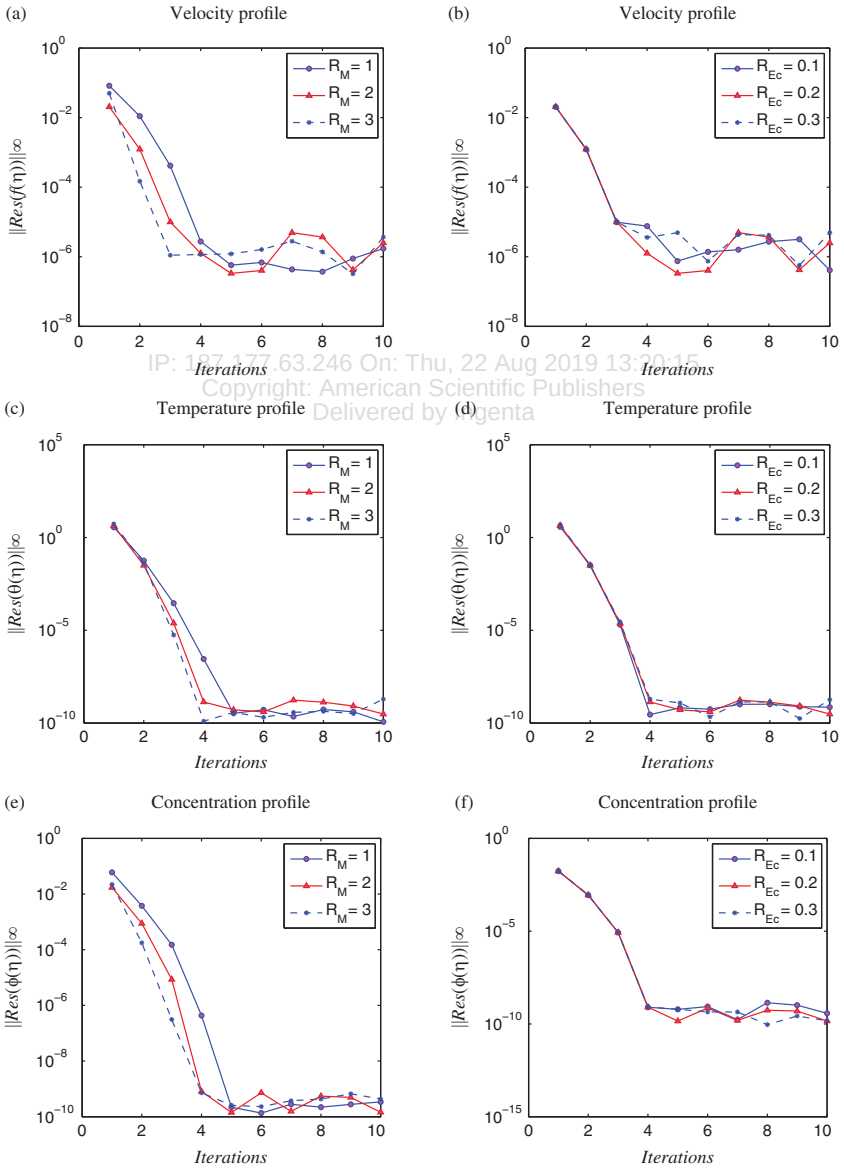

Fig. 2. The residual errors on $f(\eta)$, $\theta(\eta)$ and $\phi(\eta)$ for different iterations.

Using the binomial expansion to evaluate on the second term of Eq. (11) we obtain

$$\frac{1}{\sqrt{1+(2c^3(f'')^2/3\nu\gamma^2)}} \approx 1-\frac{c^3(f'')^2}{3\nu\gamma^2} \tag{15}$$

By neglecting all higher order terms for $|f''^2/\gamma^2| \ll 1$. The equation reduces to

$$(1+\epsilon)f''' - \frac{\epsilon\delta}{3}f'''(f'')^2 + ff'' - \frac{1}{2}(f')^2 - \frac{3}{2}Mf' + \frac{3}{2}\lambda_1\theta + \frac{3}{2}\lambda_2\phi = 0 \tag{16}$$

where $\epsilon = 1/(\rho\beta\nu\gamma)$ and $\delta = c^3/(\nu\gamma^2)$ are the Powell-Eyring fluid parameters, the thinning and shearing rate parameters respectively. If the fluid parameters are zero the equation reduces to that of a viscous fluid. The boundary conditions are

$$f(0) = f_w, \quad f'(0) = 1, \quad \theta(0) = 1, \quad \phi(0) = 1, \quad f'(\infty) = 0, \quad \theta(\infty) = 0, \quad \phi(\infty) = 0 \tag{17}$$

where

$$f_w = -d\sqrt{\frac{3}{2c\nu}} \tag{18}$$

is the blowing or suction parameter.

Using the Taylor's series expansion of order 3 to approximate $\sinh^{-1}(1/\gamma(\partial u/\partial y))$ we obtain,

$$\frac{1}{\beta}\sinh^{-1}\left(\frac{1}{\gamma}\frac{\partial u}{\partial y}\right) = \frac{1}{\beta\gamma}\frac{\partial u}{\partial y} - \frac{1}{6\beta\gamma^3}\left(\frac{\partial u}{\partial y}\right)^3 \tag{19}$$

The wall shear stress $\tau_w = \tau(y=0)$ is given as

$$\tau_w = \left(\mu + \frac{1}{\beta\gamma}\right)\left(\frac{\partial u}{\partial y}\right)_{|y=0} - \frac{1}{6\beta\gamma^3}\left(\frac{\partial u}{\partial y}\right)^3_{|y=0} \tag{20}$$

The skin friction coefficient C_f, the local Nusselt number Nu_x and the local Sherwood Sh_x are given by

$$C_f = \frac{\tau_w}{(1/2)\rho U_w^2(x)}, \quad Nu_x = \frac{xq_w}{\kappa(T_w - T_\infty)}, \quad Sh_x = \frac{xq_m}{D(C_w - C_\infty)}, \quad q_w = -\kappa\left(\frac{\partial T}{\partial y}\right)_{|y=0}, \quad q_m = -D\left(\frac{\partial C}{\partial y}\right)_{|y=0} \tag{21}$$

κ and D are the thermal conductivity and molecular diffusivity, so that these equations yield

$$C_f Re_x^{1/2} = 2\sqrt{\frac{2}{3}}\left[(1+\epsilon)f''(0) - \frac{\epsilon\delta}{9}(f''(0))^3\right], \quad Nu_x Re_x^{-1/2} = -\sqrt{\frac{2}{3}}\theta'(0), \quad Sh_x Re_x^{-1/2} = -\sqrt{\frac{2}{3}}\phi'(0) \tag{22}$$

where $Re_x = (xU_w(x))/\nu$ is the local Reynolds number.

3. NUMERICAL SOLUTION USING SPECTRAL QUASI-LINEARIZATION METHOD

If one wishes to solve an ordinary differential equation (ODE) or a partial differential equation (PDE) to a high level of accuracy on a simple domain, then spectral methods are usually the best tool to use. The connection between the smoothness of a function and the rate of decay of its Fourier transform determines the size of aliasing errors introduced by discretisation. Motsa et al.[14] studied the quasi-linearization method for systems of nonlinear boundary value problems. These connections explain how the smoothness depends on function being approximated.[15] There are a number of other iterative numerical methods in literature that are used to solve coupled non-linear equations. Some of theses methods include the

Table II. Variation in $f''(0)$, $-\theta'(0)$ and $-\phi'(0)$ for $\lambda_1 = 0.5$, $\lambda_2 = 0.4$, $N_r = 0.5$, $\theta_w = 2$, $P_r = 6.8$, $f_w = 0$ and varying other parameters.

ϵ	δ	N_b	N_t	Le	Ec	M	$f''(0)$	$-\theta'(0)$	$-\phi'(0)$
0.1	0.2	0.5	0.5	0.22	0.2	2	−1.19136195	0.41251485	−0.21667967
0.2							−1.14629696	0.41949441	−0.22260059
0.3							−1.10614681	0.42577077	−0.22783812
0.4							−1.07011047	0.43145288	−0.23250056
0.5							−1.03755150	0.43662750	−0.23667403
0.2	0.4	0.5	0.5	0.22	0.2	2	−1.15040631	0.41915360	−0.22228759
	0.6						−1.15462518	0.41880747	−0.22196951
0.2	0.2	0.4	0.5	0.22	0.2	2	−1.12717724	0.43987207	−0.32591778
		0.3					−1.09362760	0.46569524	−0.50432873
0.2	0.2	0.5	1.0	0.22	0.2	2	−1.07186677	0.39888090	−0.49299203
			1.5				−1.00824126	0.37093923	−0.69180135
0.2	0.2	0.5	0.5	2.4	0.2	2	−1.24660167	0.16762400	0.49624915
				5			−1.29034370	0.12433024	0.86412238
0.2	0.2	0.5	0.5	0.22	0.3	2	−1.14543184	0.37309477	−0.17686001
					0.5		−1.14372801	0.28057920	−0.08564542
0.2	0.2	0.5	0.5	0.22	0.2	2.5	−1.36635599	0.37608605	−0.19469218
						3	−1.56402718	0.33536311	−0.16646609

ARTICLE

continuation method,[16] homotopy analysis method (HAM). Prashanth[17] established a semilocal convergence of the continuation method combing the Chebyshev method and the convex acceleration of the Newton's method that produced superior results compared to the convectional methods. The coupled nonlinear ordinary differential Eqs. (12), (13) and (16) are solved numerically using a spectral quasi-linearization method (SQLM). The nonlinear components of the system of ordinary differential equations give the following iterative sequences of linear differential equations

$$\begin{aligned} &a_{0,r}f'''_{r+1}+a_{1,r}f''_{r+1}+a_{2,r}f'_{r+1}+a_{3,r}f_{r+1}\\ &\quad+a_{4,r}\theta_{r+1}+a_{5,r}\phi_{r+1}=R_f,\\ &b_{0,r}\theta''_{r+1}+b_{1,r}\theta'_{r+1}+b_{2,r}\theta_{r+1}+b_{3,r}f''_{r+1}+b_{4,r}f'_{r+1}\\ &\quad+b_{5,r}\phi'_{r+1}+b_{6,r}f_{r+1}=R_\theta,\\ &c_{0,r}\phi''_{r+1}+c_{1,r}\phi'_{r+1}+c_{2,r}\phi+c_{3,r}f'_{r+1}+c_{4,r}f_{r+1}\\ &\quad+c_{5,r}\theta''_{r+1}=R_\phi \end{aligned} \tag{23}$$

where $a_{0,r}=(1+\epsilon)-(\epsilon\delta/3)f''^{2}_{r}$, $a_{1,r}=f_r-(2\epsilon\delta/3)f'''_rf''_r$, $a_{2,r}=-f'_r-(3/2)M$, $a_{3,r}=f''_r$, $a_{4,r}=(3/2)\lambda_1$, $a_{5,r}=(3/2)\lambda_2$, $b_{0,r}=1+Nr(1+(\theta_w-1)\theta_r)^3$, $b_{1,r}=6N_r(\theta_w-1)(1+(\theta_w-1)\theta_r)^2\theta'_r+Prf_r+PrNb\phi'_r+2PrNt\theta'_r$, $b_{2,r}=3Nr\theta''_r(1+(\theta_w-1)\theta_r)^2(\theta_w-1)+6Nr(\theta_w-1)^2(\theta'_r)^2$ $(1+(\theta_w-1)\theta_r)$, $b_{3,r}=2PrEcf''_r$, $b_{4,r}=PrNb\theta'_r$, $b_{5,r}=Pr\theta'_r$, $c_{0,r}=1$, $c_{1,r}=Lef_r$, $c_{2,r}=1/2Lef'_r$, $c_{3,r}=1/2Le\phi_r$, $c_{4,r}=Le\phi'_r$, $c_{5,r}=Nt/Nb$, subject to the boundary conditions

$$\begin{gathered} f_{r+1}(0)=f_w,\quad f'_{r+1}(0)=1,\quad f'_{r+1}(\infty)=0,\quad \theta_{r+1}(0)=1,\\ \theta_{r+1}(\infty)=0,\quad \phi_{r+1}(0)=1,\quad \phi_{r+1}(\infty)=0 \end{gathered} \tag{24}$$

The initial guesses are selected such that they satisfy the boundary conditions, and these were chosen as $f_0(\eta)=f_w-(e^{-\eta}-1)$, $\theta_0(\eta)=e^{-\eta}$ and $\phi_0(\eta)=e^{-\eta}$. Upon applying the spectral quasi-linearization technique we obtain the system

$$\begin{aligned} A_{1,1}f+A_{1,2}\theta+A_{1,3}\phi&=R_f,\\ A_{2,1}f+A_{2,2}\theta+A_{2,3}\phi&=R_\theta,\\ A_{3,1}f+A_{3,2}\theta+A_{3,3}\phi&=R_\phi \end{aligned} \tag{25}$$

Here $A_{i,j}$ $(i,j=1,2,3)$ and R_m $(m=f,\theta,\phi)$ are given as:

$$\begin{aligned} \mathbf{A}_{1,1}&=\mathrm{diag}(a_{0,r})D3+\mathrm{diag}(a_{1,r})D2+\mathrm{diag}(a_{2,r})D1\\ &\quad+\mathrm{diag}(a_{3,r})I,\\ \mathbf{A}_{1,2}&=\mathrm{diag}(a_{4,r})I,\quad \mathbf{A}_{1,3}=\mathrm{diag}(a_{5,r})I,\\ \mathbf{A}_{2,1}&=\mathrm{diag}(b_{3,r})D2+\mathrm{diag}(b_{4,r})D1+\mathrm{diag}(b_{6,r})I,\\ \mathbf{A}_{2,2}&=\mathrm{diag}(b_{0,r})D2+\mathrm{diag}(b_{1,r})D1+\mathrm{diag}(b_{2,r})I, \end{aligned}$$

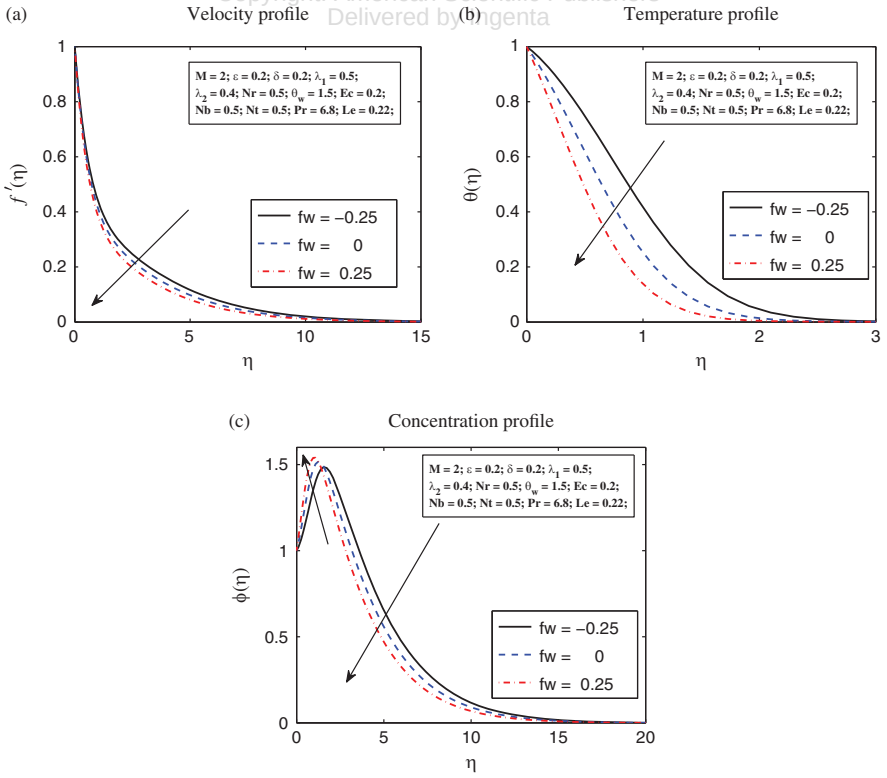

Fig. 3. The effect of suction/injection f_w on (a) velocity, (b) temperature and (c) concentration.

$$\mathbf{A}_{2,3} = \text{diag}(b_{5,r})D1, \quad \mathbf{A}_{3,1} = \text{diag}(c_{3,r})D1 + \text{diag}(c_{4,r})I,$$
$$\mathbf{A}_{3,2} = \text{diag}(c_{5,r})D2,$$
$$\mathbf{A}_{3,3} = \text{diag}(c_{0,r})D2 + \text{diag}(c_{1,r})D1 + \text{diag}(c_{2,r})I,$$
$$\mathbf{R}_f = f_r f_r'' - \frac{1}{2}f_r'^2 - \frac{2\epsilon\delta}{3}f'''f''^2,$$
$$\mathbf{R}_\theta = PrNt\theta'^2 + PrEcf''^2 + 3Nr(1+(\theta_w-1)\theta)^2(\theta_w-1)\theta'^2$$
$$+\{3Nr\theta_r''(1+(\theta_w-1)\theta_r)^2(\theta_w-1)$$
$$+6Nr(\theta_w-1)^2\theta_r'^2(1+(\theta_w-1)\theta_r)\}\theta,$$
$$\mathbf{R}_\phi = Lef\phi' + \frac{1}{2}Lef'\phi \tag{26}$$

In matrix for this can be written as

$$\begin{bmatrix} A_{1,1} & A_{1,2} & A_{1,3} \\ A_{2,1} & A_{2,2} & A_{2,3} \\ A_{3,1} & A_{3,2} & A_{3,3} \end{bmatrix} \begin{bmatrix} f_{r+1} \\ \theta_{r+1} \\ \phi_{r+1} \end{bmatrix} = \begin{bmatrix} R_f \\ R_\theta \\ R_\phi \end{bmatrix}$$

To validate the accuracy of the numerical scheme and it convergence we use the residual errors given in Table I and the plots for these residuals for graphical representation are given in Figure 2. The residual errors for different number of iterations are plotted for the functions $f(\eta)$, $\theta(\eta)$ and $\phi(\eta)$ with $M = 2$ and $Ec = 0.2$. An average of five iterations was found to be sufficient to guarantee residual errors of orders of $||10^{-7}||$, $||10^{-10}||$ and $||10^{-10}||$ for the functions $f(\eta)$, $\theta(\eta)$ and $\phi(\eta)$ respectively. We can

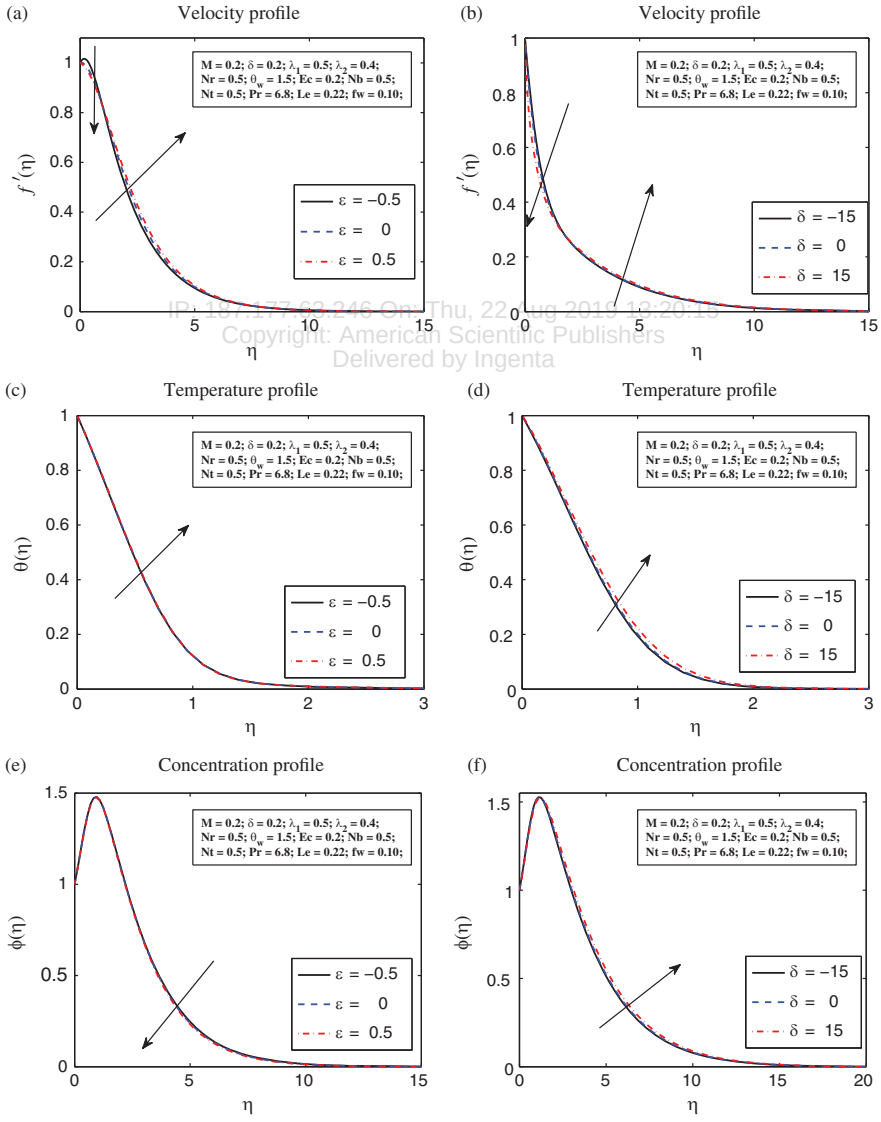

Fig. 4. The effect of fluid parameters ϵ and δ on velocity, temperature and concentration.

therefore conclude that the SQLM has a fast convergence rate making it a suitable numerical tool to use in these types of nonlinear boundary value problems.

We investigate the effect of varying some parameter on the non-dimensional local skin friction coefficient, the non-dimensional local Nusselt number and the non-dimensional local Sherwood number for our Powell-Eyring fluid. These are given by values that are proportional to $f''(0)$, $-\theta'(0)$ and $-\phi'(0)$ respectively. The results are shown in Table II.

4. DISCUSSION OF RESULTS

In order to assess the impact of certain parameters on the flow velocity, temperature and concentration, we plot the graphs of velocity $(f'(\eta))$, temperature $(\theta(\eta))$ and concentration $(\phi(\eta))$ by varying one parameter of interest and keeping the rest fixed. We begin by investigating the effect of suction or injection, that is the effect of f_w. We have a suction if f_w is positive otherwise it is an injection and this is depicted in Figure 3. Suction reduces the the velocity and temperature in the boundary layer. In heat transfer laminar flow is associated with with Nusselt number that is close to one. A Nusselt number of one means that convection and conduction heat transfer are of the same magnitudes thereby enhancing heat transfer between the solid surface and the fluid. Close to the solid surface suction increases the concentration. This due to the bulk movement of the chemical species with the fluid towards the surface and this movement dominates other processes like diffusion that may otherwise result in the chemical

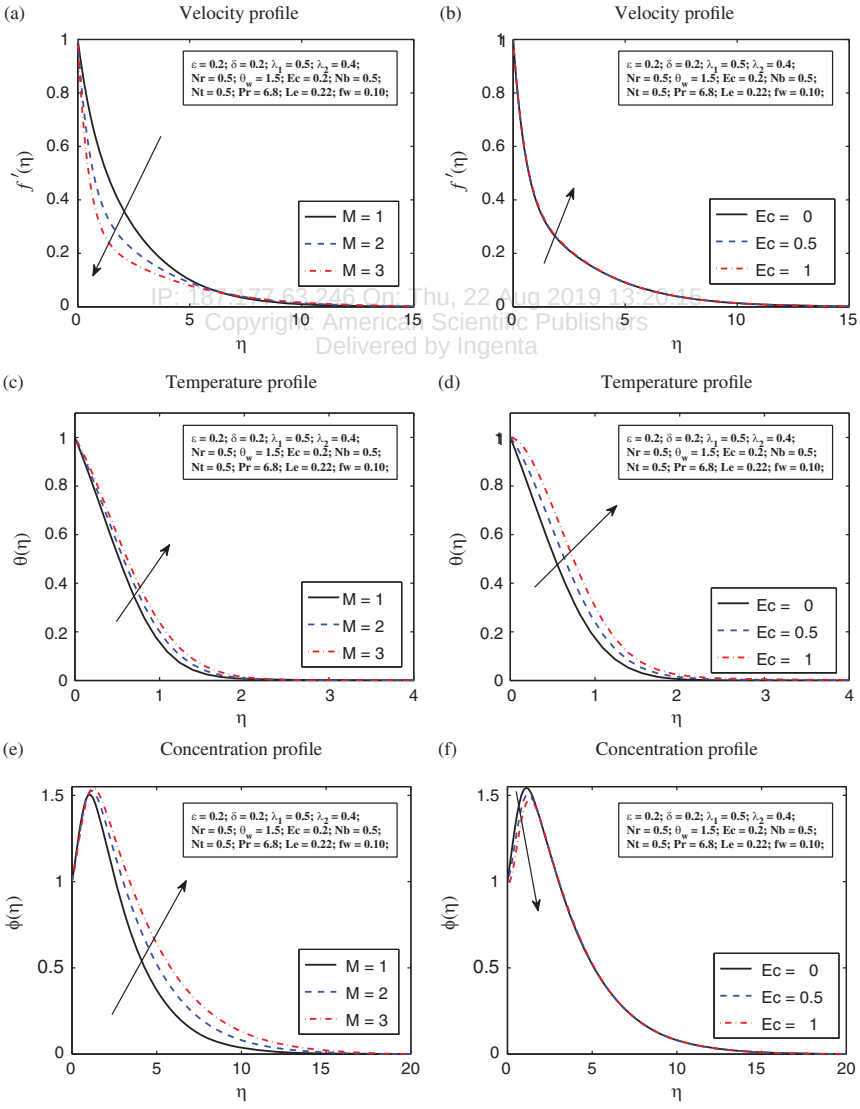

Fig. 5. The magnetic effect M and viscous dissipation Ec on velocity, temperature and concentration.

species moving away from the solid surface. Far away from the solid surface suction reduces the concentration of the chemical species.

In order to analyze the influence of the thinning parameter ϵ and shear rate parameter δ we plot the velocity, temperature and concentration graphs by varying these parameters illustrated in Figure 4. The thinning parameter increases the velocity of the fluid. This is attributed to a decrease in the fluid viscosity resulting in the observed phenomenon. An increase on the thinning parameter however causes the temperature to decrease and an overshoot in the concentration within the boundary layer. There are no noticeable changes due to the different values of shear rate parameter except for an overshoot in the concentration within the boundary layer.

The influence of the magnetic effect and viscous dissipation are illustrated in Figure 5 on the velocity, temperature and concentration profiles. The magnetic effect reduces the velocity for increasing values of M. This is because the magnetic effect introduces a retarding force which acts transverse to the direction of applied magnetic field. However for increasing values of M increases the temperature and concentration increase within the boundary layer. Viscous dissipation increases the velocity and temperature. An increase in the the fluid velocity may be attributed to a reduction in fluid viscosity as a result of frictional heating making the fluid more 'easy' to flow. The increase in the velocity is however insignificant as the heat generation takes place in a smaller region compared to the rest of the fluid and this explains the decrease in temperature as we

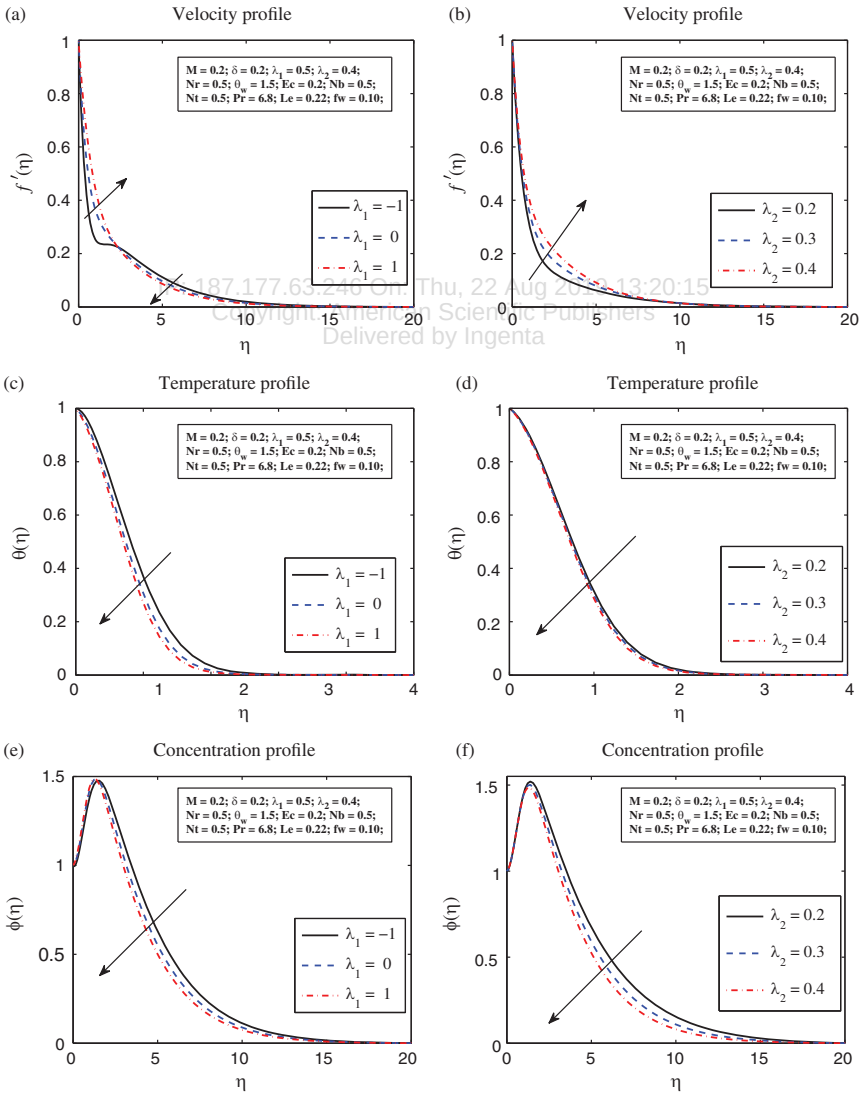

Fig. 6. The effect of λ_1 and λ_2 on velocity, temperature and concentration.

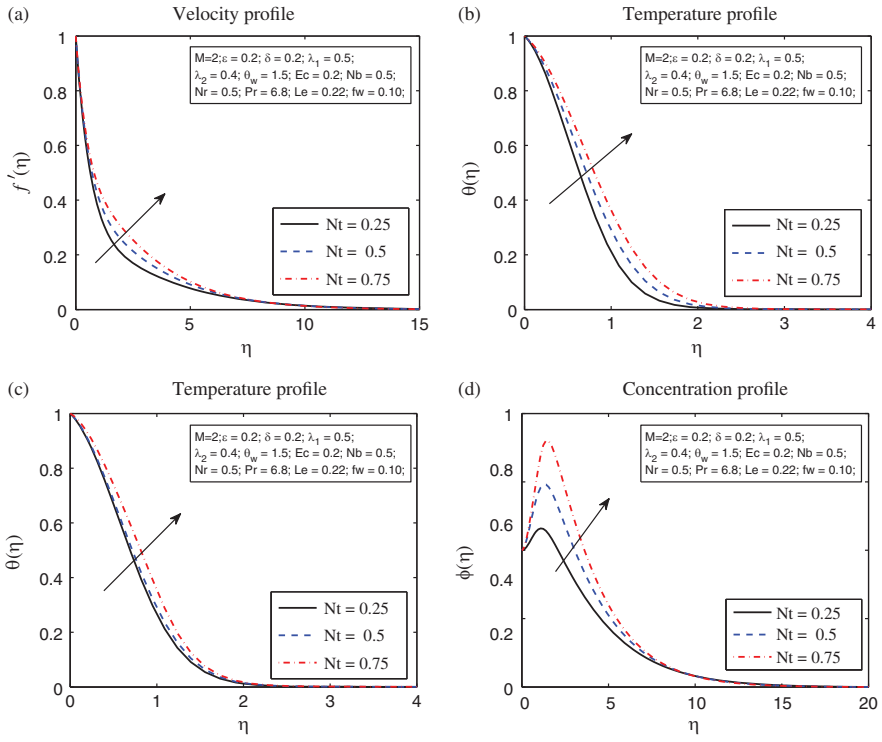

Fig. 7. The effect of thermal radiation N_r and thermophoresis N_t on velocity, temperature and concentration.

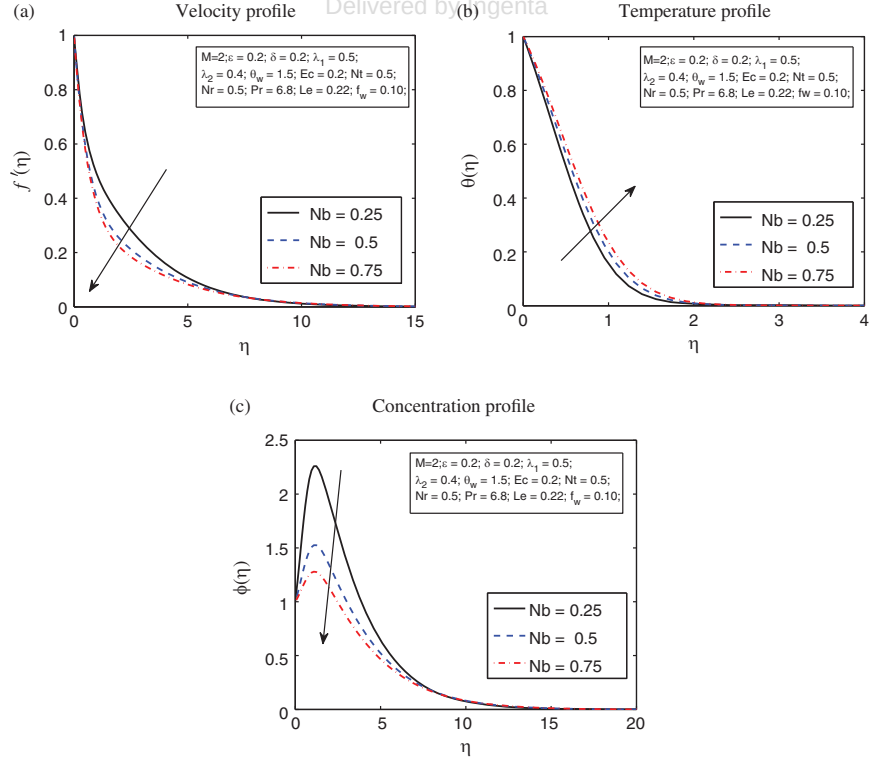

Fig. 8. The effect of Brownian motion parameter N_b on velocity, temperature and concentration.

move further into the free stream away from the surface. Viscous dissipation also causes an increase of the concentration and the concentration boundary layer, however this effect decreases for increasing values of the Eckert number.

In Figure 6 we analyze the influence of thermal and concentration buoyancy on the velocity, temperature and concentration in the boundary layer. The two parameters have the same effect on the velocity, temperature and concentration. Both parameters λ_1 and λ_2 increase the velocity for increasing values. Heat is lost in both cases for thermal and solutal buoyancy parameter through advection by ascending fluid and chemical particles. This leads to a decrease in the temperature for increasing values of both the thermal and solutal buoyancy parameters.

The impact of thermal radiation parameter N_r and thermophoresis parameter N_t are analyzed in Figure 7. Both the thermal radiation parameter and thermophoresis parameter increase the temperature of the in the boundary layer. There is no significant effect of thermal radiation on velocity and concentration and as such we omit the graphs. An increase in the thermophoretic parameter is associated with an increase in the velocity and concentration of the chemical species.

The influence of Brownian motion is studied in Figure 8. The velocity is observed to decrease as the Brownian motion parameter increase. This is attributed to generation of a long velocity field by each Brownian particle in the surrounding fluid. The temperature increases with increasing values of Brownian motion parameter. An increase in the Brownian motion will increase the movement of the nanoparticles close to the surfaces and this increases the thermal conductivity of the fluid resulting in the observed phenomenon, although some researcher believe that this contribution is very small if not insignificant. Increasing the Brownian motion decreases the concentration of solute in the boundary layer. Increasing the Brownian motion parameter will result in more species ‘leaving’ the boundary layer than those ‘coming’ into the boundary layer because the boundary layer is relatively thin compared to the free stream and hence the observed phenomenon.

5. CONCLUSIONS

The MHD flow of Powell-Eyring nanofluid with thermal radiation, viscous dissipation and thermophoresis was analyzed. Numerical solutions were obtained using the spectral quasi-linearisation method. Parameters of interest were investigated to ascertain their influence on fluid flow characteristics, and these are, the flow velocity, temperature and concentration. The following important observations were made;

- the Brownian motion of nanoparticles reduce the fluid velocity by generating long velocity fields,
- although viscous dissipation, thermal radiation, thermophoresis and magnetic effect led to an increase in the temperature within the boundary layer, there were no thermal runaways suggesting that the cooling was effective and there is no overheating during the process,
- the Powell-Eyring fluid respond more to the fluid thinning parameter ϵ than shear rate parameter δ, thus adjustment to thinning parameter may lead to more variability in the quality of final product than that of shear rate parameter,
- both thermal and solutal buoyancy parameters have the same effect to the fluid flow.

Other observations are consistent with previously published work such as[1,2] on the impact of magnetic field and buoyancy parameters. They showed that the magnetic field reduces the velocity of the fluid in the boundary layer. The buoyancy parameters increased the velocity while decreasing the temperature in the boundary layer.

Acknowledgments: The authors would like to thanks Claude Leon Foundation Postdoctoral Fellowship, University of KwaZulu-Natal, South Africa, financially supported the research work.

References and Notes

1. S. Panigrahi, M. Reza, and K. Mishra, *Procedia Engineering* 127, 645 (**2015**).
2. S. Panigrahi, M. Reza, and A. K. Mishra, *Appl. Math. Mec.-Engl.* 35, 1525 (**2014**).
3. T. Javed, N. Ali, Z. Abbas, and M. Sajid, *Chemical Engineering Communications* 200, 327 (**2013**).
4. M. Jalil, S. Asghar, and S. M. Imran, *International Journal of Heat and Mass Transfer* 65, 73 (**2013**).
5. M. Y. Malik, A. Hussain, and S. Nadeem, *Scientia Iranica B* 20, 313 (**2013**).
6. N. A. Khan, F. Sultan, and N. A. Khan, *International Journal of Chemical Reactor Engineering* 13, 37 (**2015**).
7. T. Hayat, M. Imtiaz, and A. Alsaedi, *J. Cent. South Univ.* 22, 3211 (**2015**).
8. C. H. Vittal, M. C. K. Reddy, and M. Monica, *Journal of Progressive Research in Mathematics* 8, 1290 (**2016**).
9. A. Mushtaq, M. Mustafa, T. Hayat, M. Rahi, and A. Alsaedi, *Numerical and Series Solutions Natureforsch* 68a, 791 (**2013**).
10. K. V. Prasad, P. S. Datti, and B. T. Raju, *Int. Journal of Math. Arc.* 4, 230 (**2013**).
11. D. Pal and H. Mondal, *Journal of Magnetism and Magnetic Materials* 331, 250 (**2013**).
12. H. Mondal, P. De, S. Chatterjee, P. Sibanda1, and P. K. Roy, *Journal of Nanofluids* 6, 1 (**2017**).
13. D. Pal and H. Mondal, *Nucl. Eng. Des.* 256, 350 (**2013**).
14. S. Motsa, P. Sibanda, and S. Shateyi, *Mathematical Methods in the Applied Sciences* 34, 1406 (**2011**).
15. C. Canuto, A. Quarteroni, M. Y. Hussaini, and T. A. Zang Jr., Spectral Methods in Fluid Dynamics, Springer (**1986**).
16. M. Prashanth and D. K. A. Gupta, *International Journal of Computaional Methods* 10, 1 (**2013**).
17. M. Prashanth and D. K. A. Gupta, *J. App. Math. Comput.* 39, 253 (**2012**).

Summary

In this chapter, a Powell-Eyring MHD nanofluid flow over a nonlinear stretching surface was studied. The resulting system of equations was solved numerically using the spectral quasilinearisation method. Important physical and flow properties were studied via the analysis of specific parameters of interests. Brownian motion and thermophoresis parameters are key in the velocity, thermal and solute boundary layer profiles. The shearing parameter thickens the thermal and solute boundary layers. There are no noticeable effects for the thinning parameter.

Chapter 3

Activation energy and binary chemical reaction effects in mixed convective nanofluid flow with convective boundary conditions

In this chapter, we study the effect of activation energy in a binary chemical reaction flow. A binary chemical reaction is one that occurs in two stages. The concept of fluid flow with binary chemical reaction and activation energy was introduced by Bestman [97]. Activation energy is important to consider when dealing with chemical reactions. It is defined as the minimum energy required to initiate a chemical reaction. A study was done on the combined effects of activation energy and binary chemical reactions in convective nanofluid flow with convective boundary, being the aspects that have not been studied before this study. The system of equations was solved using the spectral quasilinearisation method.

Journal of Computational Design and Engineering 6 (2019) 149–158

Contents lists available at ScienceDirect

Journal of Computational Design and Engineering

journal homepage: www.elsevier.com/locate/jcde

Activation energy and binary chemical reaction effects in mixed convective nanofluid flow with convective boundary conditions

Mlamuli Dhlamini [a], Peri K. Kameswaran [b], Precious Sibanda [a], Sandile Motsa [a,c], Hiranmoy Mondal [a,*]

[a] School of Mathematics, Statistics and Computer Science, University of KwaZulu-Natal, Private Bag X01, Scottsvile, Pietermaritzburg 3209, South Africa
[b] Department of Mathematics, School of Advanced Sciences, VIT University, Vellore 632014, India
[c] Department of Mathematics, University of Swaziland, Private Bag 4, Kwaluseni, Swaziland

ARTICLE INFO

Article history:
Received 13 March 2018
Received in revised form 25 June 2018
Accepted 4 July 2018
Available online 29 July 2018

Keywords:
Arrhenius activation energy
Binary chemical reaction
Viscous dissipation
Brownian motion
Thermophoresis

ABSTRACT

In this paper, we present a theoretical study of the combined effects of activation energy and binary chemical reaction in an unsteady mixed convective flow over a boundary of infinite length. The current study incorporates the influence of the Brownian motion, thermophoresis and viscous dissipation on the velocity of the fluid, temperature of the fluid and concentration of chemical species. The equations are solved numerically to a high degree of accuracy using the spectral quasilinearization method. Brownian motion was noted as the main process by which the mass is transported out of the boundary layer. The effect of thermophoretic parameter seems to be contrary to the expected norm. We expect the thermophoretic force to 'push' the mass away from the surface thereby reducing the concentration in the boundary layer, however, concentration of chemical species is seen to increase in the boundary layer with an increase in the thermophoretic parameter. The use of a heated plate of infinite length increased the concentration of chemical species in the boundary layer. The Biot number which increases and exceeds a value of one for large heated solids immersed in fluids increases the concentration of chemical species for its increasing values.

1. Introduction

The study of boundary layer flow of a mixture of fluids with heat and mass transfer past a continuous surface has a lot of applications in aerodynamics, extrusion of plastic and rubber sheets, crystal growing and so on (Makinde & Olanrewaju, 2011; Shafique, Mustafa, & Mushtaq, 2016). The Arrhenius activation term was introduced in 1889 by Svante Arrhenius. It models the minimum energy which must be available to a chemical system with potential reactants to produce a chemical reaction. Lazaridis, Savara, and Argyrakis (2014) suggested that in a successful reaction, it is reasonable to assume that a reaction occurs with a certain nonzero probability. In the study, the researchers investigated the effect of varying this probability on the rate of reaction. A binary chemical reaction is a reaction that occurs in two steps. These types of reaction are common in deposition processes, both chemical vapour deposition (CVD) and chemical liquid deposition (CLD). Chemical deposition has industrial applications such as coating of metallic objects and glasses, manufacture of electronic devices eg diodes and transistors, gas-permeation barriers and many other applications (Pedersen & Elliott, 2014). In a binary chemical reaction, the activation energy has been shown to be a significant factor (Shafique et al., 2016). During a chemical deposition process, the reaction must occur on the surface of the substrate (Pedersen & Elliott, 2014). Since the reactor chamber is heated from outside, some reactions may occur away from the substrate surface leading to a processes known as the gas phase nucleation and this presents a major problem (Rana, Chandrashekhar, & Sudarshan, 2012). In order to ensure that atomic layer deposition (ALD) surface reactions take place and not the CVD-like reactions, one can execute a purge step after each half-cycle to remove the residual precursor or reactants (Profijt, Potts, Van de Sanden, & Kessels, 2011). Despite not being understood fully, the liquid phase deposition (LPD) or chemical liquid deposition is superior to other deposition techniques because of low processing temperature, the simplicity of the equipment, high growth rate ($12nm/h$) and low operational cost (Sun & Sun, 2004). In order to improve/enhance thermal properties of fluid for industrial applications, ordinary fluids are normally replaced with nanofluids. The term nanofluid was coined by Choi in 1995 (Choi & Eastman, 1995) to describe fluids where nano-sized particles are added. The material used range

Peer review under responsibility of Society for Computational Design and Engineering.

* Corresponding author.
E-mail address: hiranmoymondal@yahoo.co.in (H. Mondal).

https://doi.org/10.1016/j.jcde.2018.07.002
2288-4300/

from stable metals, oxides, carbides, nitrates and non-metals (Das, Sharma, & Sarkar, 2016; Muhammad & Nadeem, 2017; Muhammad, Nadeem, & Mustafa, 2018; Nadeem, Ahmad, & Muhammad, 2018). In this study, we focus on the flow of a binary chemically reacting fluid with Arrhenius activation energy and convective boundary conditions. This study seeks to address the impact that activation energy and frictional heating among other factors have on the flow of such fluids. An understanding of the influence of frictional heating on a binary chemical reaction may help in the elimination of premature reactions occurring away from the surface of the substrate and thus improve the deposition. Heat transport in stretching or moving sheets and ambient fluid has become very critical in most engineering applications (Muhammad, Nadeem, & Haq, 2017). In this study we consider the concentration of one of the end products of the chemical reaction rather than tracking the concentration of the reactants. The study of the combined effects of activation energy and binary chemical reactions have been considered by several researcher (Abbas, Sheikh, & Motsa, 2016; Daniel, Aziz, Ismail, & Salah, 2017; Makinde, Olanrewaju, & Charles, 2011; Maleque, 2013a, 2013b; Nadeem, Ahmad, Muhammad, & Mustafa, 2017).

Makinde and Olanrewaju's (Makinde & Olanrewaju, 2011) study focused on the buoyancy parameter, i.e. thermal and solutal Grashof number. They showed that the momentum boundary layer thickness generally decreased with increasing buoyancy parameter values. Reverse flow within the boundary layer was shown to occur with increasing buoyancy values. Wall suction causes the momentum boundary layer to decrease while injection causes the momentum boundary layer to increase. An increase in the Damkohler parameter was shown to increase the temperature of the fluid. An increase in the Damkohler parameter reduced the concentration of chemical species in the boundary layer. The Schmidt number was however shown to have a reverse effect on the boundary layer. An increase in the Schmidt number causes the species concentration to increase within the boundary layer. Results from (Makinde et al., 2011) show that a reverse flow within the boundary layer is enhanced with an increase in the intensity of buoyancy forces, injection, destructive chemical reaction, radiation absorption, and thermo-diffusion effect and a decrease in the diffusion-thermal effect and also that fluid temperature increases. The species concentration decreases with an increase in Soret number and a decrease in Dufour number. Abbas et al. (2016) conclude that increasing values of non-dimensional activation energy enhances the concentration profile within the boundary layer. Maleque (2013a) found that a small decrease in temperature profile is found for increasing values of the preexposure parameter for exothermic reaction, but opposite effects are found for endothermic reaction. The chemical reaction rate decreases with increasing activation energy. He further concluded that the velocity and temperature profiles increase with increasing chemical reaction rate constant for exothermic reaction, but opposite effects are found for endothermic reaction. Buoyancy and heat generation/absorption were shown to have marked effects on the boundary layer and velocity profile in Maleque (2013b). The effect of heat generation coefficient is to expand the boundary layer thickness, and the opposite effect is found for heat absorption. Thus, the heat generation/absorption coefficient has the same effects on skin-friction coefficients. The effect of rotation was studied by Awad, Motsa, and Khumalo (2014). He showed that for small values of the rotation rate parameter a monotonic exponential decay in the velocity profiles was observed and an oscillatory decay for large values.

The objective of this study is to investigate the unsteady flow with activation energy and binary chemical reaction over a boundary of infinite length. The temperature condition at the boundary depends on the Biot number. The model equations are solved numerically using a recently developed spectral quasi-linearization method. The second objective is to explore the accuracy and convergence of the method through the evaluation of the residual errors norms and to investigate the impact of flow parameters on the transport processes. The results may give insights as to the choice of parameter values that may be used in engineering applications. The influence of pertinent parameters on the physical quantities has been examined graphically.

2. Mathematical analysis

Consider the flow of an unsteady one-dimensional viscous nanofluid over an infinitely long flat plate moving with velocity U_0 in a binary chemical mixture. Since the plate is infinite and the motion is unsteady all the flow variables depend only on y and time t. The temperature and concentration far from the wall are T_∞ and C_∞.

The geometry of the problem is chosen in the Cartesian coordinate system (x, y) such that the velocity component u is parallel to the plate and is taken to be the x-axis while v is perpendicular to the plate and is taken to be in the y-axis. The flow is assumed to be parallel to the plate, that is, along the x-axis. The geometry of the problem is given in Fig. 1.

The system of equations for the flow of a nanofluid with thermophoresis and a binary chemical reaction with Arrhenius activation energy can be written as follows.

$$\frac{\partial v}{\partial y}=0, \tag{1}$$

$$\frac{\partial u}{\partial t}+v\frac{\partial u}{\partial y}=\frac{\mu}{\rho f_\infty}\frac{\partial^2 u}{\partial y^2}+(1-C_\infty)g\beta\rho f_\infty(T-T_\infty) - \left(\rho_p-\rho f_\infty\right)g(C-C_\infty), \tag{2}$$

$$\frac{\partial T}{\partial t}+v\frac{\partial T}{\partial y}=\alpha\frac{\partial^2 T}{\partial y^2}+\frac{\mu}{(\rho c_p)_f}\left(\frac{\partial u}{\partial y}\right)^2+\tau\left\{D_B\frac{\partial T}{\partial y}\frac{\partial C}{\partial y}+\frac{D_T}{T_\infty}\left(\frac{\partial T}{\partial y}\right)^2\right\}, \tag{3}$$

$$\frac{\partial C}{\partial t}+v\frac{\partial C}{\partial y}=D_B\frac{\partial^2 C}{\partial y^2}-k_r^2\left(\frac{T}{T_\infty}\right)^n \mathrm{Exp}\left(-\frac{E_a}{kT}\right)(C-C_\infty)+\frac{D_T}{T_\infty}\frac{\partial^2 T}{\partial y^2}. \tag{4}$$

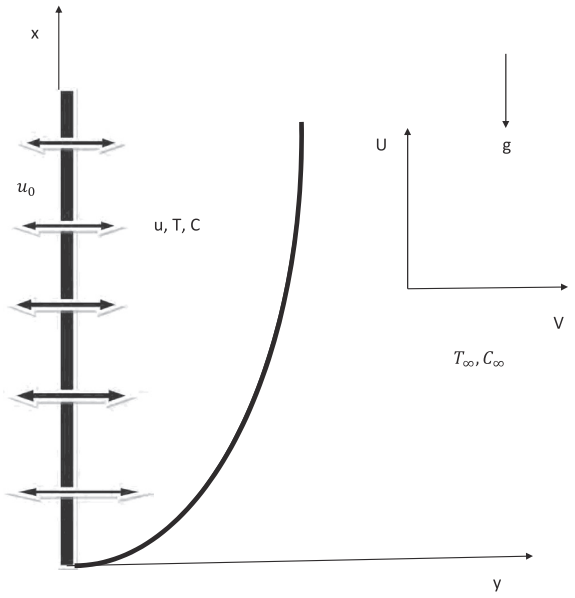

Fig. 1. Flow configuration and coordinate system.

$$\alpha = \frac{k_m}{(\rho c)_f} \quad \text{and} \quad \tau = \frac{(\rho c)_p}{(\rho c)_f}$$

The boundary conditions for Eqs. (1)–(4) are given in the form:

$$u = U_0, \quad -k_f \frac{\partial T}{\partial y} = h_f (T_f - T), \quad D_B \frac{\partial C}{\partial y} + \frac{D_T}{T_\infty} \frac{\partial T}{\partial y} = 0, \quad \text{at} \quad y = 0, \quad t > 0$$
$$u \to 0, \quad T \to T_\infty, \quad C \to C_\infty \quad \text{as} \quad y \to \infty, \quad t > 0 \tag{5}$$

where (u, v) are the velocity components along (x, y) directions, respectively, μ is the viscosity, ρf_∞ is the density of the base fluid, g is the acceleration due to gravity, β is the volumetric thermal expansion coefficient of the nanofluid, ρ_p is the density of nanoparticle, T is the temperature, C is the concentration of the fluid, α is the thermal diffusivity of the base fluid, c_p is the specific heat at constant pressure, τ is the ratio of the effective heat capacity of the nanoparticle material and heat capacity of the fluid, D_B is the Brownian diffusion coefficient, D_T is the thermophoretic diffusion coefficient, k_m is the thermal conductivity, $(\rho c)_f$ is the heat capacity of the base fluid and $(\rho c)_p$ is the effective heat capacity of the nanoparticle material, k_r^2 is the chemical reaction rate constant, $(T/T_\infty)^n \mathrm{Exp}(-E_a/kT)(C - C_\infty)$ is Arrhenius function, n is a constant exponent and E_a is the Activation energy.

3. Transformation of equations

The velocity components are given by (Maleque, 2013a, 2013b)

$$u = U_0 f(\eta) \quad \text{and} \quad v = -\frac{v_0 v}{\delta(t)}, \tag{6}$$

where η is the similarity variable $\left(\eta = \frac{y}{\delta(t)}\right)$, $\delta(t)$ is a scaling parameter, f represents the scaled velocity and v_0 is the suction/injection velocity.

The temperature and concentrations are represented as

$$T = T_\infty + (T_f - T_\infty)\theta(\eta) \quad \text{and} \quad C = C_\infty + (C_w - C_\infty)\phi(\eta) \tag{7}$$

$\theta(\eta)$ is the dimensionless temperature and $\phi(\eta)$ is the dimensionless concentration. On using Eqs. (6) and (7), Eqs. (2)–(4) transform into the following boundary value problem

$$f''' + (A\eta + v_0) f'' + \frac{Gr}{Re}(\theta - Nr\phi) = 0, \tag{8}$$
$$\theta'' + Pr(A\eta + v_0)\theta' + PrEcf''^2 + PrNb\theta'\phi' + PrNt\theta'^2 = 0, \tag{9}$$
$$\phi'' + Sc(A\eta + v_0)\phi' - Sc\lambda^2(1 + n\gamma\theta)\,\mathrm{Exp}\left(-\frac{E}{1 + \gamma\theta}\right)\phi + \frac{Nt}{Nb}\theta'' = 0, \tag{10}$$
$$f(0) = 1, \quad f(\infty) \to 0, \tag{11}$$
$$\theta'(0) = -Bi(1 - \theta(0)), \quad \theta(\infty) \to 0, \tag{12}$$
$$Nb\phi' + Nt\theta'(0) = 0, \quad \phi(\infty) \to 0. \tag{13}$$

The prime denotes differentiation with respect to η. The parameters in Eqs. (8)–(13) are the unsteadiness parameter A, scaling parameter δ, Grashof number Gr which is the ratio of the buoyancy to viscous force acting on a fluid, Reynolds number Re which is the ratio of inertial forces to viscous forces, Buoyancy ratio parameter Nr which is an upward force exerted on an object that is immersed in a fluid, Prandtl Pr, a ratio of momentum diffusivity to thermal diffusivity, Eckert number Ec which is ratio of advective transport to heat dissipation potential, Brownian motion parameter Nb the random movement of particles in a fluid, thermophoresis parameter Nt which is the movement of microscopic particles due to a force of a temperature gradient, Schmidt number Sc, a ratio of momentum diffusivity and mass diffusivity, the dimensionless chemical reaction rate constant λ^2, the temperature relative parameter γ, the dimensionless activation energy E and Biot number Bi which is the ratio of the heat transfer resistances inside of and at the surface of a body. These parameters are defined as;

$$A = \frac{\delta\delta'}{v}, \quad \delta(t) = \sqrt{2Avt + L^2},$$
$$Gr = \frac{(1 - C_\infty) g\beta\rho f_\infty \triangle T\delta^3}{v^2}, \quad Re = \frac{U_0\delta}{v},$$
$$Nr = \frac{\left(\rho_p - \rho f_\infty\right)\triangle C}{(1 - C_\infty)\rho f_\infty \beta \Delta T}, \quad Pr = \frac{v}{\alpha}, \quad Ec = \frac{U_0^2}{c_p(T_f - T_\infty)},$$
$$Nb = \frac{\tau D_B \triangle C}{v},$$
$$Nt = \frac{\tau D_T \triangle T}{v T_\infty}, \quad Sc = \frac{v}{D_B}, \quad \lambda^2 = \frac{k_r^2 \delta^2}{v}, \quad \gamma = \frac{T_f - T_\infty}{T_\infty},$$
$$E = \frac{E_a}{kT_\infty}, \quad Bi = \frac{h_f}{k_f}\delta(t).$$

4. Heat and mass transfer coefficients

The heat transfer rate from the surface of the plate is given by

$$q_w = -k\left[\frac{\partial T}{\partial y}\right]_{y=0}, \tag{14}$$

The local Nusselt number is defined as

$$Nu = \frac{\delta q_w}{k(T_f - T_\infty)}. \tag{15}$$

$$Nu = -\theta'(0). \tag{16}$$

The mass flux at the surface of the wall is given by

$$q_m = -D_m\left[\frac{\partial C}{\partial y}\right]_{y=0} \tag{17}$$

The local Sherwood is defined as

$$Sh = \frac{\delta q_m}{D_m(C_w - C_\infty)}. \tag{18}$$

Using Eq. (17) in Eq. (18) the dimensionless Sherwood number obtained as

$$Sh = -\phi'(0). \tag{19}$$

5. Numerical solution using spectral quasi-linearization method

The set of ordinary differential Eqs. (8)–(10) together with the boundary conditions (11)–(13) are solved using the spectral quasi-linearization method to get a high accuracy. The fundamental principle of spectral collocation methods is that, given discrete data on a grid, interpolate the data globally and, then evaluate the derivatives of the interpolant on the grid (Canuto, Hussaini, Quarteroni, & Zang, 1988; Trefethen, 2000). The quasi-linearization method (QLM) is a generalization of the Newton-Raphson method (Bellman & Kalaba, 1965). The derivation of the QLM is based on the linearization of the nonlinear components of the governing equations using the Taylor series assuming that the difference between successive iterations, that is at $r + 1$, and r is negligibly small. We solve the nonlinear system of ordinary differential equations with boundary conditions (11)–(13) using the spectral quasi-linearization method (SQLM). The nonlinear components of the system of ordinary differential equations give

the following iterative sequences of linear differential equations. First define functions F, Θ and Φ for Eqs. (8)–(10) respectively as;

$$F = f'' + (A\eta + v_0)f' + \frac{Gr}{Re}(\theta - Nr\phi), \tag{20}$$

$$\Theta = \theta'' + Pr(A\eta + v_0)\theta' + PrEcf''^2 + PrNb\theta'\phi' + PrNt\theta'^2, \tag{21}$$

$$\Phi = \phi'' + Sc(A\eta + v_0)\phi' - Sc\lambda^2(1 + n\gamma\theta)\mathrm{Exp}\left(-\frac{E}{1+\gamma\theta}\right)\phi + \frac{Nt}{Nb}\theta''. \tag{22}$$

We construct the errors from the iterative process for Eqs. (8)–(10) as given by (23)–(25) respectively

$$a_{0r}f''_{r+1} + a_{1r}f'_{r+1} + a_{2r}\theta_{r+1} + a_{3r}\phi_{r+1} - F = R_f, \tag{23}$$

$$b_{0r}\theta''_{r+1} + a_{1r}\theta'_{r+1} + b_{2r}f'_{r+1} + b_{3r}\phi'_{r+1} - \Theta = R_\theta, \tag{24}$$

$$c_{0r}\phi''_{r+1} + c_{1r}\phi'_{r+1} + c_{2r}\phi_{r+1} + c_{3r}\theta''_{r+1} + c_{4r}\theta_{r+1} - \Phi = R_\phi. \tag{25}$$

subject to the boundary conditions

$$f_{r+1}(0) = 1, \quad f_{r+1}(\infty) \to 0 \tag{26}$$

$$\theta'_{r+1}(0) = -Bi(1 - \theta(0)), \quad \theta_{r+1}(\infty) \to 0 \tag{27}$$

$$Nb\phi'_{r+1}(0) + Nt\theta'_{r+1}(0) = 0, \quad \phi_{r+1}(\infty) \to 0 \tag{28}$$

where the coefficients in (23)–(25) are given as;

$$\begin{aligned}
&a_{0,r} = 1, \quad a_{1,r} = (A\eta + v_0), \quad a_{2,r} = \tfrac{Gr}{Re}, \quad a_{3,r} = -\tfrac{GrNr}{Re}, \quad b_{0,r} = 1,\\
&b_{1,r} = Pr(A\eta + v_0) + PrNb\phi'_r + 2PrNt\theta'_r, b_{2,r} = 2PrEcf'_r,\\
&b_{3,r} = PrNb\theta'_r,\\
&c_{0,r} = 1, \quad c_{1,r} = Sc(A\eta + v_0),\\
&c_{2,r} = -Sc\lambda^2(1 + n\gamma\theta_r)e^{-E/(1+\gamma\theta_r)}, \quad c_{3,r} = \tfrac{Nt}{Nb}\\
&c_{4,r} = -\tfrac{Sc\lambda^2 e^{-E/(1+\gamma\theta_r)}(E+n+n(2+E)\gamma\theta_r+n\gamma^2\theta_r^2)}{(1+\gamma\theta_r)^2}
\end{aligned} \tag{29}$$

The initial guesses are selected as functions that satisfy the boundary conditions, and these were chosen as

$$f_0(\eta) = e^{-\eta}, \quad \theta_0(\eta) = \tfrac{Bi}{1+Bi}e^{-\eta}, \quad \phi_0(\eta) = -\tfrac{Nt}{Nb}\tfrac{Bi}{(1+Bi)}e^{-\eta}. \tag{30}$$

In order to apply the SQLM to solve the system of nonlinear ordinary differential (23)–(25) we transform the domain from $0 \leqslant \eta \leqslant L_x$ to $-1 \leqslant x \leqslant 1$ using the transformation $\eta = L_x(x+1)/2$ (Kameswaran, Sibanda, & Motsa, 2013). We use the Gauss-Lobatto collocation points defined by

$$x_i = \cos\left(\frac{\pi i}{N}\right), \quad i = 0, 1, 2, \cdots, N \tag{31}$$

The spectral collocation method uses a differentiation matrix (D) to approximate the derivative of unknown variables at the collocation points as a matrix vector product. The D-matrix is constructed for the domain $[-1, 1]$ so we scale this matrix for the domain $[0, L_x]$ by taking $D1 = 2D/L_x$, so that

$$\frac{dF_r^{(1)}}{d\eta}(\eta_j) = \sum_{k=0}^{n} D1f(\eta_k) = D1F_m, \quad j = 0, 1, 2, \cdots, N \tag{32}$$

where $F = [f(\eta_0), f(\eta_1), f(\eta_2), \cdots, f(\eta_N)]^T$ represent the vector function at the collocation points. Higher order derivatives are given as powers of the scaled differentiation matrix

$$F^{(p)} = D1^p F_r. \tag{33}$$

Using the scaled differentiation matrix on (23)–(25) we obtain;

$$\begin{aligned}
A_{11}f_{r+1} + A_{12}\theta_{r+1} + A_{13}\phi_{r+1} &= R_f\\
A_{21}f_{r+1} + A_{22}\theta_{r+1} + A_{23}\phi_{r+1} &= R_\theta\\
A_{31}f_{r+1} + A_{32}\theta_{r+1} + A_{33}\phi_{r+1} &= R_\phi
\end{aligned} \tag{34}$$

In matrix for this can be written as

$$\begin{bmatrix} A_{11} & A_{12} & A_{13} \\ A_{21} & A_{22} & A_{23} \\ A_{31} & A_{32} & A_{33} \end{bmatrix} \begin{bmatrix} f_{r+1} \\ \theta_{r+1} \\ \phi_{r+1} \end{bmatrix} = \begin{bmatrix} R_f \\ R_\theta \\ R_\phi \end{bmatrix}$$

where

$$\begin{aligned}
&A11 = diag(a_{0,r})D2 + diag(a_{1,r})D1,\\
&A12 = diag(a_{2,r})I, \ A13 = diag(a_{3,r})I\\
&A21 = diag(b_{2,r})D1,\\
&A22 = diag(b_{0,r})D2 + diag(b_{1,r})D1, \ A23 = diag(b_{3,r})D1\\
&A31 = Zeros(N+1, N+1), \ A32 = diag(c_{3,r})D2 + diag(c_{4,r})I,\\
&A33 = diag(c_{0,r})D2 + diag(c_{1,r})D1 + diag(c_{2,r})I
\end{aligned}$$

Residual error analysis

We validate the accuracy and convergence of the SQLM by performing a residual error analysis. We tabulate the residual errors in Table 1 and Fig. 2.

From Table 1 we note that the smallest values for residual errors were attained after 2 iterations for $f(\eta)$ and 4 iterations for $\theta(\eta)$ and $\phi(\eta)$. This shows that the SQLM is an accurate method with a good convergence rate. In order to have a clearer picture on the convergence rates, we plot the residual errors against the number of iterations in Fig. 2.

6. Discussion of results

In this paper, we investigate the impact that the activation energy has on a binary chemical reacting nanofluid with convective boundary conditions. We investigate the influence that the thermal and chemical parameters have on the velocity, temperature and concentration of the fluid in the boundary layer. We begin by investigating how the drag, heat transfer and mass transfer on the solid boundary are affected by certain parameters. We do so by varying a parameter of interest while keeping the rest constant and note the changes to the local skin friction coefficient (C_f), local Nusselt (Nu) number and local Sherwood number (Sh). The results are given in Table 2.

In Table 3 we give a summary of the parameter values in the model and the sources from which they were obtained.

The unsteady parameter A is investigated in Fig. 3 by plotting the velocity, temperature and concentration profiles for different values of the parameter. Increasing the unsteady parameter from the steady value of 0, led to a decrease in the velocity, temperature and concentration in the boundary layer. As the fluid transition from laminar flow to turbulent flow the velocity, heat transfer and mass transfer all decrease. Results from the current study are consistent with results from (Maleque, 2013a). The overshoot in the concentration profile can be attributed other factors, not the unsteady parameter. The effect of the unsteady parameter is

Table 1
Residual error for different iterations.

i	$f(\eta)$	$\theta(\eta)$	$\phi(\eta)$
1	7.867129×10^{-11}	3.191528×10^{-1}	2.535005×10^{-1}
2	3.159872×10^{-11}	7.612455×10^{-4}	1.025387×10^{-3}
3	8.640200×10^{-11}	4.233677×10^{-9}	4.432544×10^{-7}
4	8.753887×10^{-11}	9.773146×10^{-11}	2.045453×10^{-11}
5	9.731593×10^{-11}	2.188154×10^{-10}	6.840795×10^{-11}
6	1.182343×10^{-10}	7.860722×10^{-10}	2.582401×10^{-11}
7	7.753442×10^{-11}	3.279255×10^{-10}	5.194600×10^{-11}
8	5.161382×10^{-11}	3.652539×10^{-10}	4.351142×10^{-11}
9	3.808154×10^{-11}	3.276447×10^{-10}	5.004180×10^{-11}
10	8.185452×10^{-11}	5.311367×10^{-10}	2.323225×10^{-11}

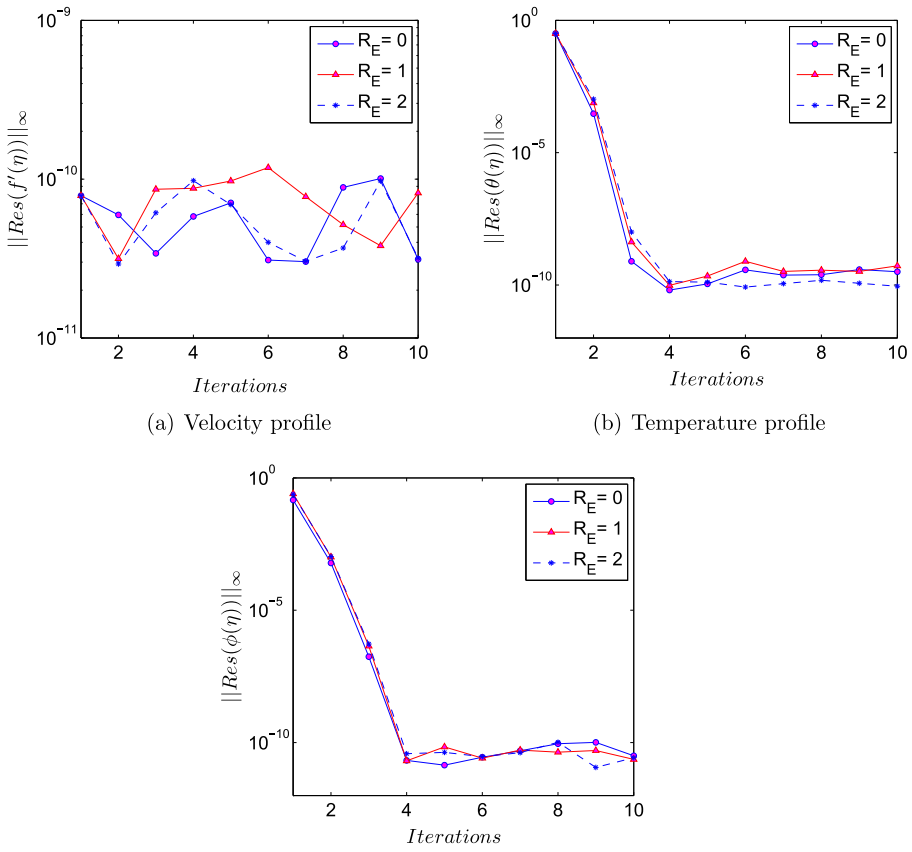

(a) Velocity profile

(b) Temperature profile

(c) Concentration profile

Fig. 2. Residual errors for velocity, temperature and concentration profiles.

Table 2
Effect of varying parameters on skin friction coefficient (C_f), local Nusselt number (Nu) and local Sherwood number (Sh) and $v_0 = 2, Gr = 1.5, Re = 1, Bi = 100, Ec = 0.2, \gamma = 1, n = 1, Pr = 6.8$.

A	Sc	Nr	Nb	Nt	E	λ	$-f'(0)$	$-\theta'(0)$	$-\phi'(0)$
0.0	0.6	0.5	0.3	0.1	1.0	5.0	1.912449	9.865404	−2.739898
0.5	0.6	0.5	0.3	0.1	1.0	5.0	2.126137	9.941617	−2.759319
1.0	0.6	0.5	0.3	0.1	1.0	5.0	2.293911	10.037429	−2.785280
1.0	0.3	0.5	0.3	0.1	1.0	5.0	2.322190	10.238323	−2.987516
1.0	0.0	0.5	0.3	0.1	1.0	5.0	2.789233	10.291383	−3.400554
1.0	0.6	0.25	0.3	0.1	1.0	5.0	2.269238	10.052712	−2.790421
1.0	0.6	0.0	0.3	0.1	1.0	5.0	2.244563	10.067812	−2.795502
1.0	0.6	0.5	0.2	0.1	1.0	5.0	2.318582	10.021971	−4.170131
1.0	0.6	0.5	0.1	0.1	1.0	5.0	2.392579	9.974499	−8.292432
1.0	0.6	0.5	0.3	0.2	1.0	5.0	2.332045	9.108249	−4.947295
1.0	0.6	0.5	0.3	0.3	1.0	5.0	2.367588	8.191294	−6.501718
1.0	0.6	0.5	0.3	0.1	0.5	5.0	2.283544	9.900079	−2.607755
1.0	0.6	0.5	0.3	0.1	0.0	5.0	2.274071	9.751707	−2.413290
1.0	0.6	0.5	0.3	0.1	1.0	2.5	2.322548	10.342466	−3.182157
1.0	0.6	0.5	0.3	0.1	1.0	0.0	2.346528	10.524261	−3.413481

analyzed by comparing the curves for different values of the unsteady parameter.

We note that the velocity and temperature are not affected by most parameters and as such we turn our focus to parameters that are associated with the activation energy and chemical reaction. The graphs for the effect of different parameters on the concentration profiles are given in Fig. 4. An increase in the activation energy parameter E and the thermophoretic parameter Nt leads to an increase in the chemical species concentration at the boundary layer. The observation on the thermophoretic parameter is not consistent with the expected outcomes. Thermophoresis leads to a net movement of particles from a hotter region to a colder region. This has applications in removing small particles from gas streams and determining exhaust gas projectiles. Results from Malvandi

Table 3
Parameters in the model and their values.

Parameter	Symbol	Value	Source
Grashof number	Gr	(0.1,5)	Makinde and Olanrewaju (2011)
Reynolds number	Re	1	assumed
Buoyancy parameter	Nr	(0.3,1.2)	Pal and Mondal (2011)
Prandtl number	Pr	(6.8,7.2)	Abbas et al. (2016)
Eckert number	Ec	(0.1,0.4)	Makanda et al. (2013)
Brownian motion parameter	Nb	0.5	Sithole et al. (2018)
Thermophoresis parameter	Nt	0.5	Sithole et al. (2018)
Schmidt number	Sc	0.6	Makinde and Olanrewaju (2011) and Maleque (2013a)
Chemical reaction constant	λ^2	5	Makinde and Olanrewaju (2011) and Maleque (2013a, 2013b)
temperature relative parameter	γ	(0,5)	Awad et al. (2014)
Activation energy	E	1	Makinde and Olanrewaju (2011), Maleque (2013a), and Awad et al. (2014)
Biot number	Bi	(0.1,100)	Uddin et al. (2012), RamReddy et al. (2013), and Kameswaran et al. (2013)
suction/injection parameter	v_0	(−3,3)	Makinde and Olanrewaju (2011) and Maleque (2013a)
Steadiness parameter	A	(0,1)	Maleque (2013a)
Constant exponent	n	(−1,1)	Maleque (2013a) and Awad et al. (2014)

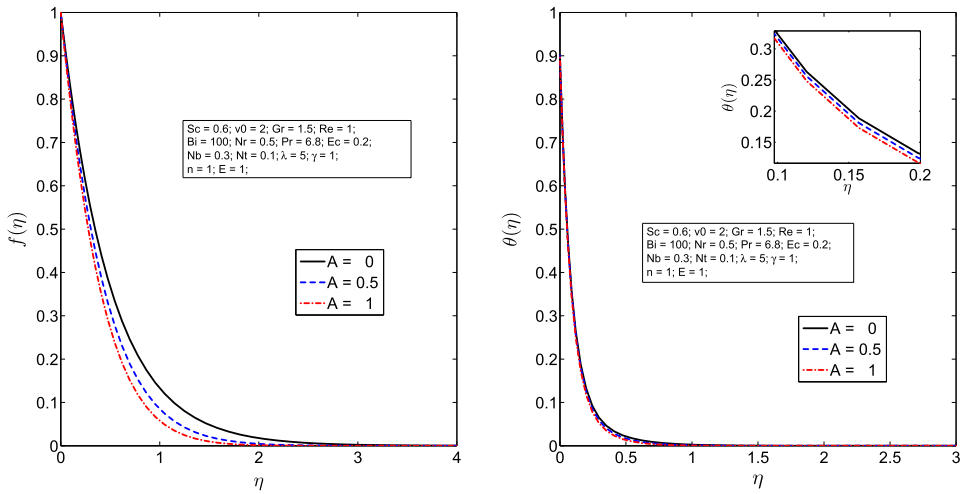

(a) Velocity profile (b) Temperature profile

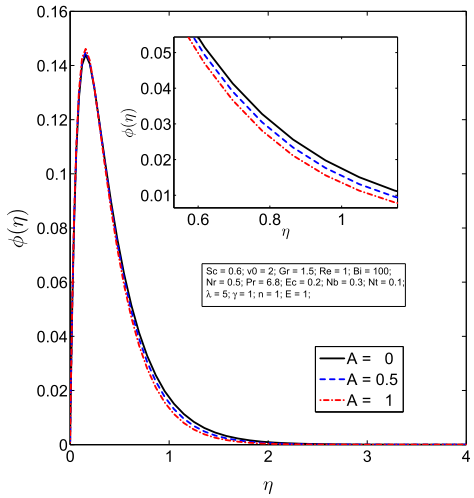

(c) Concentration profile

Fig. 3. Effect of unsteady parameter A.

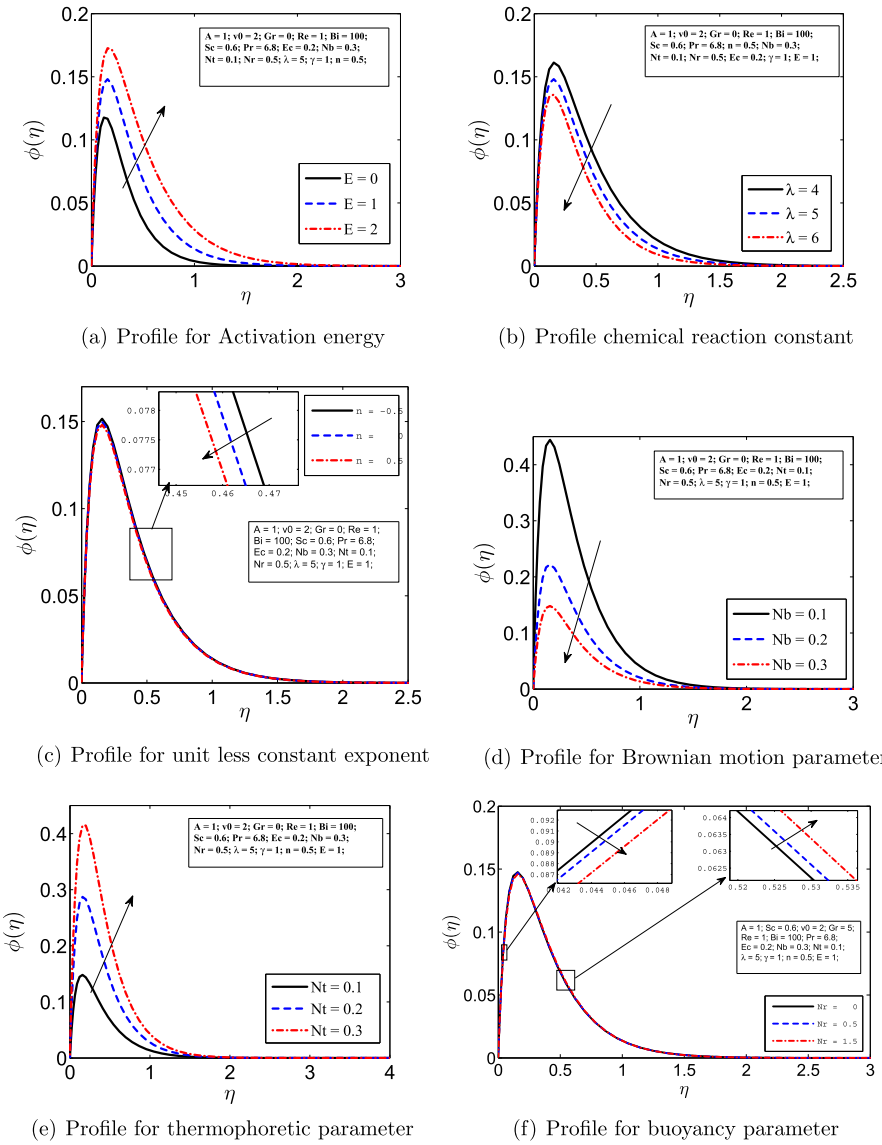

(a) Profile for Activation energy

(b) Profile chemical reaction constant

(c) Profile for unit less constant exponent

(d) Profile for Brownian motion parameter

(e) Profile for thermophoretic parameter

(f) Profile for buoyancy parameter

Fig. 4. Concentration profiles for different parameters.

and Ganji (2014) showed that the concentration of the nanoparticles was higher on the cold wall (nanoparticle accumulation) and lower near the adiabatic wall(nanoparticle depletion). Similar results were obtained by Malvandi and Ganji (2014) who showed that the concentration of nanoparticles in the core of the microchannel was higher than near the heated wall. In this study the results are contrary to the expected results, that is, the concentration is seen to increase with increasing values of thermophoretic parameter in the boundary layer. This observation can be attributed to the confounding effect of the thermophoretic parameter and activation energy. An increase in the thermophoretic parameter is associated with an increase in temperature Fig. 5, which is also associated with an increase in activation energy thereby increasing the rate of chemical reaction leading to a high concentration in the boundary layer. Similar results can be found in Mabood, Khan, and Ismail (2015). However increasing the constant exponent n, Brownian motion parameter Nb and the chemical reaction constant λ causes a decrease in the chemical species within the boundary layer. These results are consistent with the expected results. The Brownian motion parameter increases the 'indecisive' random movement of molecules. Increasing the Brownian motion increases the movement of molecules in and out of the boundary layer and the free stream. Since the free stream is relatively large compared to the boundary layer some of the molecules that enter the free stream may not 'come back' into the boundary layer resulting in a net decrease in concentration of molecules in the boundary layer. Similar results for Brownian were drawn by Mustafa, Khan, Hayat, and Alsaedi (2017) and Mabood et al. (2015).

The viscous dissipation is analyzed by making observations of changes in the temperature profile for varying values of the Eckert number Ec in Fig. 5. Increasing the Eckert number increases the temperature of the fluid leading to thickening of the thermal boundary layer which is consistent with heat generation due to the frictional effects of the fluid. These observations are consistent

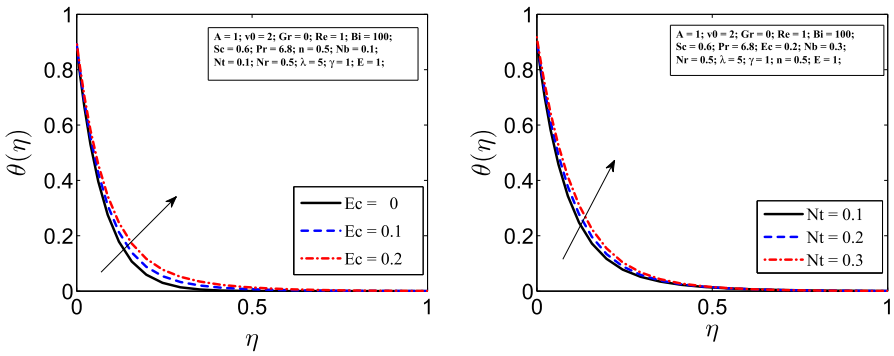

(a) Profile for Eckert number (b) Profile for thermophoresis

Fig. 5. Temperature profile for the Eckert number and thermophoresis.

with those found in literature such as (Mahdy & Chamkha, 2010; Yazdi, Abdullah, Hashim, & Sopian, 2011). We also observe the positive correlation between the temperature and the thermophoretic force. Increasing the temperature of the fluid will result in an increase in the thermophoretic parameter.

We analyze the effect of Biot number on the temperature and concentration in Fig. 6. It is shown that increasing the Biot number will result in an increase in both the temperature and concentration in the boundary layer. Since we considered a plate of infinite length, this means the length scale is long enough so that the Biot number exceeds one. This implies that heat resistance offered at the surface is less than heat resistance offered within the solid plate. Temperature gradients within the solid are no longer negligible, we can no longer assume constant temperature within the solid. This is so since the plate is heated to maintain a constant temperature yet it is constantly being cooled at the surface by the fluid it comes in contact with. The transfer of thermal energy from the solid to the fluid results in an increase in the thermal energy of the fluid leading to an increase in the fluid temperature and concentration of the chemical species as a result of an increase in the chemical reaction. The result on the effect of Biot number on concentration in this study concurs with the result by Makinde and Aziz (2011). They showed that concentration increased for increasing values of the Biot number.

Fig. 7 seeks to give an analysis of the chemical reaction constant λ by taking values from 0 to 1 in the step of 0.1. It is shown that the chemical reaction constant causes the concentration to decrease in a nonlinear pattern in the boundary layer. Pal and Mondal (2012) also drew a similar conclusion for this parameter. The analysis is done for different values of Brownian motion *Nb* and thermophore-

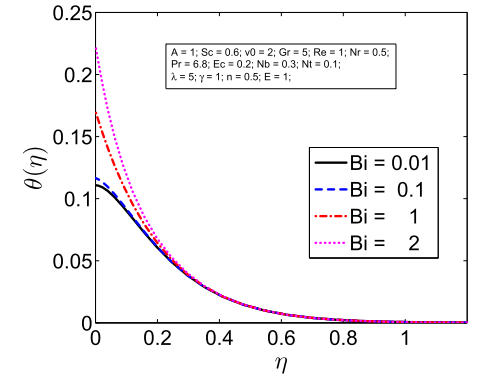

(a) Temperature profile

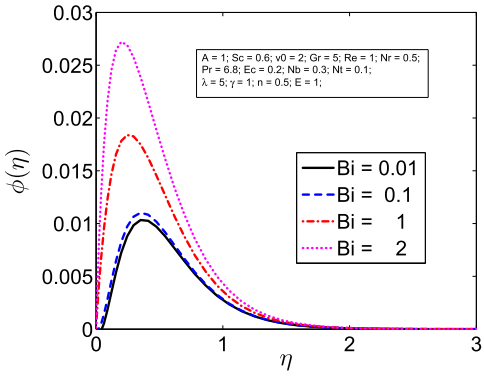

(b) Concentration profile

Fig. 6. An analysis of the influence of Biot number on temperature and concentration profiles.

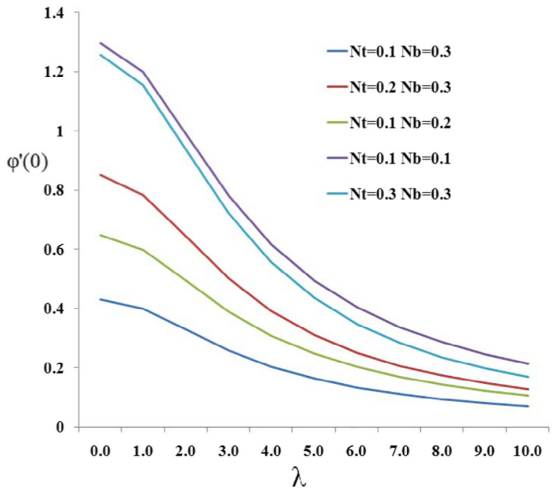

(a) Concentration profile for chemical reaction rate constant λ

Fig. 7. Analysis of the effect of chemical reaction parameter (λ) on the concentration for different values of Nb and Nt.

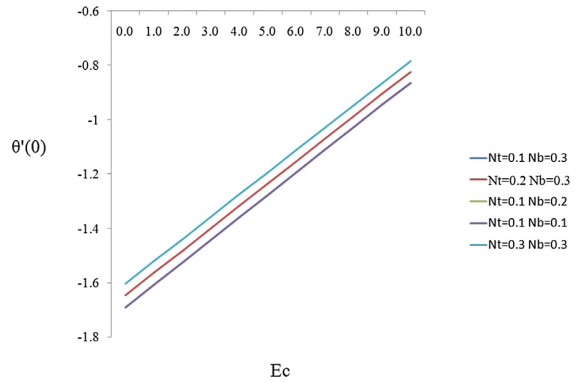

Fig. 8. Temperature profile for the Eckert number with varying Nt and Nb.

sis *Nt* by fixing values for one parameter and varying the other parameter in three steps (0.1, 0.2 and 0.3). The least concentration occurs when both *Nb* and *Nt* have values of 0.3 and is highest when both parameters have values of 0.1. For fixed values of *Nb* (0.3) and varying *Nt* the concentration increases with increasing values of *Nt* and this is consistent with the observation made earlier on the influence of thermophoresis on concentration. The concentration showed a decreasing trend for increasing values of *Nb* and fixed values of *Nt* (0.1). This too is consistent with the earlier observation made for the effect of Brownian motion on concentration.

Fig. 8 seek to give an analysis of the effect of varying the Eckert number on the temperature for different values of the Brownian motion parameter and thermophoresis parameter. Increasing the thermophoresis parameter increases the temperature while the Brownian motion has no effect on the temperature. This observation is consistent with the previous observation that we made, the thermophoretic force is in the direction of a lower temperature and this will result in temperature increase in that region and Brownian motion is by a random process that has no bearing on the temperature difference of any two regions and thus it does not affect the temperature.

7. Conclusion

In this paper, we considered the effect of activation energy, Brownian motion and thermophoresis on a binary chemical unsteady nanofluid with convective boundary conditions. The governing nonlinear partial differential equations are reduced to second order nonlinear ordinary differential equations using an appropriate similarity transformation and solved using the spectral quasi-linearization method. The following observations were made.

- The unsteady parameter reduces the velocity and temperature of the fluid while on the other hand increases the concentration of the chemical species in the boundary layer.
- The activation energy and thermophoresis parameters increase the concentration of the chemical species in the boundary layer while the Brownian motion and the chemical reaction constant reduces the concentration of the chemical species in the same region.
- The Eckert and the thermophoresis parameters are found to increase the temperature of the fluid.

Conflict of interest

The authors declare that there is no conflict of interests regarding the publication of this paper.

Acknowledgment

This work was supported by the Claude Leon Foundation Postdoctoral Fellowship, and the University of KwaZulu-Natal, South Africa.

References

Abbas, Z., Sheikh, M., & Motsa, S. S. (2016). Numerical solution of binary chemical reaction on stagnation point flow of Casson fluid over a stretching/shrinking sheet with thermal radiation. *Energy, 95*, 12–20.

Awad, F. G., Motsa, S., & Khumalo, M. (2014). Heat and mass transfer in unsteady rotating fluid flow with binary chemical reaction and activation energy. *PloS One, 9*(9), e107622.

Bellman, R. E., & Kalaba, R. E. (1965). *Quasilinearization and Nonlinear Boundary-Value Problems. Modern Analytic and Computional Methods in Science and Mathematics* (vol. 3) New York, NY, USA: American Elsevier.

Canuto, C., Hussaini, M. Y., Quarteroni, A., & Zang, T. A. (1988). *Spectral Methods in Fluid Dynamics*. Berlin: Springer-Verlag.

Choi, S. U. S., & Eastman, J. A. (1995). *Enhancing thermal conductivity of fluids with nanoparticles. Technical report*. IL (United States): Argonne National Lab.

Daniel, Y. S., Aziz, Z. A., Ismail, Z., & Salah, F. (2017). Thermal stratification effects on mhd radiative flow of nanofluid over nonlinear stretching sheet with variable thickness. *Journal of Computational Design and Engineering, 5*(2), 232–242.

Das, K., Sharma, R. P., & Sarkar, A. (2016). Heat and mass transfer of a second grade magnetohydrodynamic fluid over a convectively heated stretching sheet. *Journal of Computational Design and Engineering, 3*(4), 330–336.

Kameswaran, P. K., Sibanda, P., & Motsa, S. S. (2013). A spectral relaxation method for thermal dispersion and radiation effects in a nanofluid flow. *Boundary Value Problems, 2013*(1), 242.

Kameswaran, P. K., Sibanda, P., & Murti, A. S. N. (2013). Nanofluid flow over a permeable surface with convective boundary conditions and radiative heat transfer. *Mathematical Problems in Engineering*, 11. Article ID 201219.

Lazaridis, F., Savara, A., & Argyrakis, P. (2014). Reaction efficiency effects on binary chemical reactions. *The Journal of Chemical Physics, 141*(10), 104103.

Mabood, F., Khan, W. A., & Ismail, A. I. M. d. (2015). Mhd boundary layer flow and heat transfer of nanofluids over a nonlinear stretching sheet: A numerical study. *Journal of Magnetism and Magnetic Materials, 374*, 569–576.

Mahdy, A., & Chamkha, A. J. (2010). Chemical reaction and viscous dissipation effects on Darcy-Forchheimer mixed convection in a fluid saturated porous media. *International Journal of Numerical Methods for Heat & Fluid Flow, 20*(8), 924–940.

Makanda, G., Makinde, O. D., & Sibanda, P. (2013). Natural convection of viscoelastic fluid from a cone embedded in a porous medium with viscous dissipation. *Mathematical Problems in Engineering*, 11. Article ID 934712.

Makinde, O. D., & Aziz, A. (2011). Boundary layer flow of a nanofluid past a stretching sheet with a convective boundary condition. *International Journal of Thermal Sciences, 50*(7), 1326–1332.

Makinde, O. D., & Olanrewaju, P. O. (2011). Unsteady mixed convection with soret and dufour effects past a porous plate moving through a binary mixture of chemically reacting fluid. *Chemical Engineering Communications, 198*(7), 920–938.

Makinde, O. D., Olanrewaju, P., & Charles, W. M. (2011). Unsteady convection with chemical reaction and radiative heat transfer past a flat porous plate moving through a binary mixture. *Afrika Matematika, 22*(1), 65–78.

Maleque, Kh. A. (2013a). Effects of exothermic/endothermic chemical reactions with arrhenius activation energy on mhd free convection and mass transfer flow in presence of thermal radiation. *Journal of Thermodynamics*, 11. Article ID 692516.

Maleque, Kh. A. (2013b). Effects of binary chemical reaction and activation energy on mhd boundary layer heat and mass transfer flow with viscous dissipation and heat generation/absorption. *ISRN Thermodynamics*, 9. Article ID 284637.

Malvandi, A., & Ganji, D. D. (2014). Effects of nanoparticle migration on force convection of alumina/water nanofluid in a cooled parallel-plate channel. *Advanced Powder Technology, 25*(4), 1369–1375.

Malvandi, A., & Ganji, D. D. (2014). Brownian motion and thermophoresis effects on slip flow of alumina/water nanofluid inside a circular microchannel in the presence of a magnetic field. *International Journal of Thermal Sciences, 84*, 196–206.

Muhammad, N., & Nadeem, S. (2017). Ferrite nanoparticles Ni-ZnFe2O4, Mn-ZnFe2O4 and Fe2O4 in the flow of ferromagnetic nanofluid. *The European Physical Journal Plus, 132*(9), 377.

Muhammad, N., Nadeem, S., & Haq, R. Ul. (2017). Heat transport phenomenon in the ferromagnetic fluid over a stretching sheet with thermal stratification. *Results in Physics, 7*, 854–861.

Muhammad, N., Nadeem, S., & Mustafa, M. T. (2018). Analysis of ferrite nanoparticles in the flow of ferromagnetic nanofluid. *PloS One, 13*(1), e0188460.

Mustafa, M., Khan, J. A., Hayat, T., & Alsaedi, A. (2017). Buoyancy effects on the mhd nanofluid flow past a vertical surface with chemical reaction and activation energy. *International Journal of Heat and Mass Transfer, 108*, 1340–1346.

Nadeem, S., Ahmad, S., & Muhammad, N. (2018). Computational study of Falkner-Skan problem for a static and moving wedge. *Sensors and Actuators B: Chemical, 263*, 69–76.

Nadeem, S., Ahmad, S., Muhammad, N., & Mustafa, M. T. (2017). Chemically reactive species in the flow of a maxwell fluid. *Results in Physics, 7*, 2607–2613.
Pal, D., & Mondal, H. (2011). The influence of thermal radiation on hydromagnetic Darcy-Forchheimer mixed convection flow past a stretching sheet embedded in a porous medium. *Meccanica, 46*(4), 739–753.
Pal, D., & Mondal, H. (2012). Influence of chemical reaction and thermal radiation on mixed convection heat and mass transfer over a stretching sheet in Darcian porous medium with Soret and Dufour effects. *Energy Conversion and Management, 62*, 102–108.
Pedersen, H., & Elliott, S. D. (2014). Studying chemical vapor deposition processes with theoretical chemistry. *Theoretical Chemistry Accounts, 133*(5), 1476.
Profijt, H. B., Potts, S. E., Van de Sanden, M. C. M., & Kessels, W. M. M. (2011). Plasma-assisted atomic layer deposition basics, opportunities, and challenges. *Journal of Vacuum Science & Technology A, Vacuum, Surfaces, and Films, 29*(5), 050801.
RamReddy, C. h., Murthy, P. V. S. N., Chamkha, A. J., & Rashad, A. M. (2013). Soret effect on mixed convection flow in a nanofluid under convective boundary condition. *International Journal of Heat and Mass Transfer, 64*, 384–392.
Rana, T., Chandrashekhar, M. V. S., & Sudarshan, T. S. (2012). Elimination of silicon gas phase nucleation using tetrafluorosilane (sif4) precursor for high quality thick silicon carbide (sic) homoepitaxy. *Physica Status Solidi (a), 209*(12), 2455–2462.
Shafique, Z., Mustafa, M., & Mushtaq, A. (2016). Boundary layer flow of maxwell fluid in rotating frame with binary chemical reaction and activation energy. *Results in Physics, 6*, 627–633.
Sithole, H., Mondal, H., & Sibanda, P. (2018). Entropy generation in a second grade magnetohydrodynamic nanofluid flow over a convectively heated stretching sheet with nonlinear thermal radiation and viscous dissipation. *Results in Physics, 9*, 1077–1085.
Sun, J., & Sun, Y. C. (2004). Chemical liquid phase deposition of thin aluminum oxide films. *Chinese Journal of Chemistry, 22*(7), 661–667.
Trefethen, L. N. (2000). *Spectral methods in MATLAB* (Vol. 10). Siam.
Uddin, M. d., Khan, W. A., & Ismail, A. I. (2012). Scaling group transformation for mhd boundary layer slip flow of a nanofluid over a convectively heated stretching sheet with heat generation. *Mathematical Problems in Engineering*, 20. Article ID 934964.
Yazdi, M. H., Abdullah, S., Hashim, I., & Sopian, K. (2011). Effects of viscous dissipation on the slip mhd flow and heat transfer past a permeable surface with convective boundary conditions. *Energies, 4*(12), 2273–2294.

Summary

This study focused on the unsteady convective flow of a binary chemically reacting nanofluid with Arrhenius activation energy and convective boundary conditions. The flow of chemically reacting fluids is critical in many industrial processes hence the need to fully understand the underlying dynamics. In this study, activation energy was shown to increase the solute boundary layer. The thermal and solute boundary layer decrease for increasing values of the Biot number. This is due to an increase in both velocity and temperature in the boundary layer.

Chapter 4

Activation energy and entropy generation in viscous nanofluid with higher order chemically reacting species

In Chapter 3, we studied the impact of activation energy and binary chemical reaction effects in mixed convective nanofluid flow with convective boundary conditions. The study is extended to consider the effect of the order of a chemical reaction and entropy generation. The order of a chemical reaction for a reactant is the power the concentration is raised to in the rate equation [98]. It gives the relationship between the concentration of a reactant and the rate of the reaction. In this study, we sought to gain some insights into heat and mass transfer phenomena as well as the flow properties of nanofluid flow with a higher-order chemically reacting species.

Another important aspect that was considered was the entropy generation. Entropy is a thermodynamic quantity that represents a system's thermal energy unavailability for conversion to mechanical energy [99, 100]. Entropy generation is due to irreversible processes in momentum, heat and mass transfer. It is for this reason that entropy generation was studied to understand the processes that lead to entropy generation and how these can be minimised. The concept of entropy generation minimisation is important in the design of efficient mechanical systems. Entropy minimization has been studied by researchers such as Adrian Bejan [101]. [1]

[1] In press, International Journal of Ambient Energy: 13 December 2019

International Journal of Ambient Energy

Taylor & Francis
Taylor & Francis Group

42

ISSN: 0143-0750 (Print) 2162-8246 (Online) Journal homepage: https://www.tandfonline.com/loi/taen20

Activation energy and entropy generation in viscous nanofluid with higher order chemically reacting species

Mlamuli Dhlamini, Hiranmoy Mondal, Precious Sibanda & Sandile Motsa

To cite this article: Mlamuli Dhlamini, Hiranmoy Mondal, Precious Sibanda & Sandile Motsa (2020): Activation energy and entropy generation in viscous nanofluid with higher order chemically reacting species, International Journal of Ambient Energy, DOI: 10.1080/01430750.2019.1710564

To link to this article: https://doi.org/10.1080/01430750.2019.1710564

Accepted author version posted online: 03 Jan 2020.

Publisher: Taylor & Francis
Journal: International Journal of Ambient Energy
DOI: 10.1080/01430750.2019.1710564

Activation energy and entropy generation in viscous nanofluid with higher order chemically reacting species

Mlamuli Dhlamini[a], Hiranmoy Mondal[a], Precious Sibanda[a], Sandile Motsa[a,b]

[a]*School of Mathematics, Statistics and Computer Science,University of KwaZulu-Natal, Private Bag X01, Scottsvile, Pietermaritzburg-3209, South Africa*

[b]*Department of Mathematics, University of Swaziland, Private Bag 4, Kwaluseni, Swaziland*

Received 29 Aug 2019, Revised 26 Nov 2019, Accepted 13 Dec 2019

Abstract

In this paper, we investigate the boundary layer flow of a steady viscous nanofluid with activation energy and a high order chemical reaction. The flow equations are solved to a high degree of accuracy using the spectral quasi-linearization method with residual errors less than 10^{-08}. The changes in the local skin friction coefficient, local Nusselt number and local Sherwood number with flow parameters are analyzed. Both the activation energy and order of the chemical reaction are shown to enhance the momentum and solute boundary layers while decreasing the thermal boundary layer. Increasing the activation energy and the order of the chemical reaction reduces the Bejan number, indicating that viscous dissipation and mass transfer-induced entropy dominate irreversibility of the heat transfer. The impact of particle Brownian motion and thermophoresis are also discussed in detail. Heat generation is shown to increase heat transfer irreversibility as evidenced by an increase in the Bejan number when the parameter is increased.

Keywords: Order, Chemical reaction, Activation energy, Nanofluids, Entropy generation, Bejan number, Brownian motion, Thermophoresis

1. Introduction

Most manufacturing processes involve the flow of reactive fluids or fluids with dissolved reactants. The study of heat and mass transfer in the boundary layer flow of viscous incompressible nanofluids driven by stretching sheet is at the center of of the studies in heat and mass transfer. Such flows are encountered in industrial processes such as, metal and plastic extrusion, glass blowing and polymer extrusion [39, 60, 26].

The quality of most industrial end products depend on cooling rates [66] and chemical reactions [65], this could be be either the rate of reaction or the type of chemical reaction itself. Heat is generated or absorbed during a

*Corresponding author
Email address: hiranmoymondal@yahoo.co.in (Hiranmoy Mondal)

chemical reaction [39, 46], thus managing heat or heat transfer is critical. Some of the strategies that have been used for controlling the heat transfer rate include the use of a transverse magnetic field [39, 12] and the use of nanofluids [3, 42]. Nanofluids consist of nanoparticles, normally aluminum, gold, iron oxide, platinum, silica, silver etc of sizes ranging from 1 to 100 nanometers suspended in a base fluid to increase/improve the thermal performance of base liquids. Nanofluids have a wide range of applications such as in cooling systems, solar water heating and improving diesel generator efficiency [37, 28, 29].

Other important factors in the fluid flow with a chemical reaction are the activation energy and order of chemical reaction. Activation energy is the minimum energy which must be available for potential reactants to produce a chemical reaction [56, 46]. We include the activation energy in this model, which most researchers have not incorporated in previous studies [48, 18, 20]. Order of a chemical reaction is given as the sum of powers of reactants in a rates equation. It shows how the reaction is affected by the concentration of a particular chemical. Some examples of high order chemical reactions (second order) are dimerization, decomposition of NO_2 and HI. We are interested in knowing if order of a chemical reaction and activation energy have a significant impact on flow and fluid properties of a fluid in a moving surface, an aspect that is normally ignored by many researchers [39, 36, 54, 31]. The Cattaneo-Christov heat flux model and Casson fluid with homogeneous-heterogeneous reactions studied by Hayat et al. [23, 24, 34, 32].

Makinde and Sibanda [39, 59], investigated the effects of a chemical reaction on boundary layer flow past a vertical stretching surface with internal heat generation. They found that for positive buoyancy, the local skin friction and mass transfer coefficients increase with Eckert and Schmidt numbers while on the other hand the heat transfer coefficient decreases with both the Eckert and Schmidt numbers. However, the study did not consider the activation energy, nanoparticle effect and order of the chemical reaction. These are new aspects that we incorporated in the current model. Olanrewaju *et al.* [46] studied the effects of internal heat generation on a thermal boundary layer with a convective surface boundary condition. They observed that for weak plate heating, the surface temperature increased rapidly as the local internal heat generation increased. The issue of heat generation is shown to be of great concern hence the need to fully understand the phenomena surrounding its generation. Their model however did not include the concentration equation thus no mass transfer was considered. Reddy *et al.* [55] studied free convection, heat and mass transfer flow in a chemically reactive and radiation absorption fluid in an aligned magnetic field. The concentration was shown to decrease with increasing chemical reaction rates which also reduced the solute boundary layer thickness. It was further noted that increasing the radiation parameter caused a decrease in the fluid velocity. The velocity attained a peak in the absence of the radiation parameter. Palani *et al.* [48] studied the MHD flow of an upper-convected Maxwell fluid with a higher order chemical reaction. The main conclusion drawn from this study was that the thickness of the species distribution increased with increasing order of a chemical reaction. However the study did not incorporate the energy transport and activation energy. Olanrewaju *et al*, [46] and Palani *et al.* [48] studied similar problems without the energy equation, we feel that it is critical to incorporate and study momentum, mass and heat transfer simultaneous so that we get a clearer picture since these factors are correlated. It is in this spirit that we develop and analyze a model that captures all three factors.

The current work seeks to investigate momentum, heat and mass transport in a nanofluid with a high order chemical reaction. Important factors such as activation energy, heat generation, buoyancy effect, viscous dissipation, magnetic effect and thermophoresis are considered to ascertain their impact on the momentum, heat or/and mass transfer characteristics. We consider convective boundary condition in this work for the simple fact that the surface is kept at a different constant temperature to the ambient temperature of the fluid.

2. Mathematical Analysis

We consider a two-dimensional steady boundary layer flow of a viscous incompressible nanofluid due to a sheet moving at a constant velocity. The flow configuration and equations for the flow are given as:

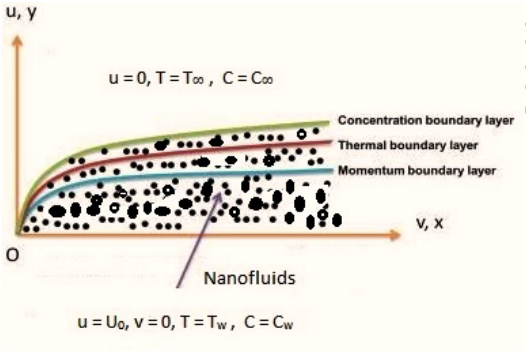

Figure 1: Flow configuration and coordinate system

$$\frac{\partial u}{\partial x}+\frac{\partial v}{\partial y}=0, \tag{1}$$

$$u\frac{\partial u}{\partial x}+v\frac{\partial u}{\partial y}=\nu\frac{\partial^2 u}{\partial y^2}-\frac{\sigma B^2(x)}{\rho}u+g\beta_T(T-T_\infty)+g\beta_C(C-C_\infty), \tag{2}$$

$$u\frac{\partial T}{\partial x}+v\frac{\partial T}{\partial y}=\alpha\frac{\partial^2 T}{\partial y^2}+\frac{\nu}{c_p}\left(\frac{\partial u}{\partial y}\right)^2+\tau\left[D_B\frac{\partial T}{\partial y}\frac{\partial C}{\partial y}+\frac{D_T}{T_\infty}\left(\frac{\partial T}{\partial y}\right)^2\right]+\frac{Q_0}{\rho c_p}(T-T_\infty), \tag{3}$$

$$u\frac{\partial C}{\partial x}+v\frac{\partial C}{\partial y}=D_B\frac{\partial^2 C}{\partial y^2}-k_1\left(\frac{T}{T_\infty}\right)^m\exp\left(-\frac{E_a}{\kappa_B T}\right)(C-C_\infty)^n+\frac{D_T}{T_\infty}\frac{\partial^2 T}{\partial y^2}. \tag{4}$$

The boundary conditions for equations (1)-(4) are given in the form:

$$\begin{aligned} &u=U_0,\quad v=0,\quad -k_w\frac{\partial T}{\partial y}=h_w(T_w-T),\quad D_B\frac{\partial C}{\partial y}+\frac{D_T}{T_\infty}\frac{\partial T}{\partial y}=0,\quad \text{at}\quad y=0,\quad t>0\\ &u\to 0,\quad T\to T_\infty,\quad C\to C_\infty\quad \text{as}\quad y\to\infty,\quad t>0 \end{aligned} \tag{5}$$

where (u, v) are the velocity components in the (x, y) directions, $B(x)$, T and C are the magnetic field, temperature and concentration respectively, ν is the kinematic viscosity, ρ is the fluid density, g is the gravitational acceleration, σ is the fluid conductivity, β_T and β_C are the volumetric coefficients of thermal and mass expansion, α is the thermal diffusivity, C_p is the specific heat capacity at constant pressure, τ is the ratio of effective heat capacity of

nanoparticles and the base fluid, D_B and D_T are the mass and thermophoretic diffusion, k_1 is the chemical reaction parameter, $(T/T_\infty)^m Exp(-E_a/\kappa T)$ is the Arrhenius activation energy, E_a is the activation energy, κ is the heat diffusivity constant, n represents the order of the chemical reaction, κ_w and h_w are the thermal conductivity of the solid and the convective heat transfer coefficient.

Transformation of equations

The system of partial differential equations model the flow is a complex system. Solving such a system is very difficult if not impossible. We resort to a method of converting the partial differential equation to an ode via Lie symmetry transformations. We use the similarity variable $\eta(x, y)$ and stream function $\psi(x, y)$ given as,

$$\eta(x, y) = y\sqrt{\frac{U_0}{\nu x}}, \quad \psi(x, y) = \sqrt{U_0 \nu x} f(\eta). \tag{6}$$

We calculate the velocity components $u = \partial\psi/\partial y$ and $v = -\partial\psi/\partial x$ and these are given as;

$$u = U_0 f'(\eta) \qquad v = \frac{1}{2}\sqrt{\frac{U_0\nu}{x}}(\eta f' - f), \tag{7}$$

and also introduce the transformations for temperature and concentrations and these are represented as

$$T = T_\infty + (T_w - T_\infty)\theta(\eta) \quad \text{and} \quad C = C_\infty + (C_w - C_\infty)\phi(\eta), \tag{8}$$

where $\theta(\eta)$ is the dimensionless temperature and $\phi(\eta)$ is the dimensionless concentration. On using Eqs. (6)- (8), Eqs. (2)-(4) and the boundary conditions (5) are transformed to the following boundary value problem

$$f''' + \frac{1}{2}f''f - Mf' + \lambda_1\theta + \lambda_2\phi = 0, \tag{9}$$

$$\theta'' + Pr\left[\frac{1}{2}f\theta' + Ecf''^2 + Nb\theta'\phi' + Nt\theta'^2 + \delta\theta\right] = 0, \tag{10}$$

$$\phi'' + Sc\left[\frac{1}{2}f\phi' - \gamma[1 + \epsilon\theta]^m \exp\left(-\frac{E}{1 + \epsilon\theta}\right)\phi^n\right] + \frac{Nt}{Nb}\theta'' = 0, \tag{11}$$

$$f'(0) = 1, \quad f(0) = 0, \quad f'(\infty) \to 0, \tag{12}$$

$$\theta'(0) = -Bi(1 - \theta(0)), \quad \theta(\infty) \to 0, \tag{13}$$

$$Nb\phi'(0) + Nt\theta'(0) = 0, \quad \phi(\infty) \to 0. \tag{14}$$

The prime denotes differentiation with respect to η. The parameters in equations (9)-(14) are the magnetic parameter M which measures the applied magnetic force, the thermal Grashof number Gr_T which is the ratio of the buoyancy to viscous force acting on a fluid due to a temperature difference in the fluid, the concentration/solute Grashof number Gr_C, the Reynolds number Re which is the ratio of inertial forces to viscous forces, the Prandtl number Pr which is the ratio of momentum diffusivity to thermal diffusivity, the Eckert number Ec which is the ratio of advective transport to heat dissipation potential, the Brownian motion parameter Nb which accounts for random movement of particles in a fluid, the thermophoresis parameter Nt which is the movement of microscopic particles due to a force of a temperature gradient, the heat generation parameter δ that measure the internal

generation of heat, Schmidt number Sc which is the ratio of momentum diffusivity and mass diffusivity, the dimensionless chemical reaction rate constant γ, the temperature relative parameter ϵ, the dimensionless activation energy E which is the minimum energy required for a chemical reaction to occur and Biot number Bi the ratio of the heat transfer resistances inside of and at the surface of a body. These parameters are defined as;

$$M = \frac{\sigma B^2 x}{\rho U_0}, \quad Gr_T = \frac{g\beta_T (T_w - T_\infty)x^3}{\nu^2}, \quad Gr_C = \frac{g\beta_C (C_W - C_\infty)x^3}{\nu^2}, \quad Re = \frac{U_0 x}{\nu},$$
$$Pr = \frac{\nu}{\alpha}, \quad Ec = \frac{U_0^2}{c_p\left(T_f - T_\infty\right)}, \quad Nb = \frac{\tau D_B (C_W - C_\infty)}{\nu}, \quad Nt = \frac{\tau D_T (T_W - T_\infty)}{\nu T_\infty},$$
$$\delta = \frac{Q_0 x}{\rho c_p U_0}(T_w - T_\infty), \quad Sc = \frac{\nu}{D_B}, \quad \gamma = \frac{k_1 (C_w - C_\infty)^{n-1} x}{U_0}, \quad \epsilon = \frac{T_w - T_\infty}{T_\infty},$$
$$E = \frac{E_a}{kT_\infty}, \quad Bi = \frac{h_w}{k_w}\frac{x}{\sqrt{Re}}, \quad \lambda_1 = \frac{Gr_T}{Re^2}, \quad \lambda_2 = \frac{Gr_C}{Re^2}.$$

3. Momentum, heat and mass transfer coefficients

The shear stress at the surface of the plate is given by

$$\tau_w = -\mu\left[\frac{\partial u}{\partial y}\right]_{y=0}, \tag{15}$$

where the local skin friction coefficient is defined as

$$C_f = \frac{\tau_w}{\frac{1}{2}\rho U_0^2}, \tag{16}$$

so that

$$C_f Re^{\frac{1}{2}} = -2f''(0). \tag{17}$$

The heat transfer rate from the surface of the plate is given by

$$q_w = -k\left[\frac{\partial T}{\partial y}\right]_{y=0}, \tag{18}$$

with the local Nusselt number defined as

$$Nu = \frac{xq_w}{k\left(T_f - T_\infty\right)}. \tag{19}$$

Hence

$$NuRe^{-\frac{1}{2}} = -\theta'(0). \tag{20}$$

The mass flux at the surface of the wall is given by

$$q_m = -D_m\left[\frac{\partial C}{\partial y}\right]_{y=0} \tag{21}$$

The local Sherwood is defined as

$$Sh = \frac{xq_m}{D_m(C_w - C_\infty)}. \tag{22}$$

The dimensionless Sherwood number obtained as

$$ShRe^{-\frac{1}{2}} = -\phi'(0). \tag{23}$$

4. Entropy generation analysis

Convective heat transfer is the study of heat transport processes in a moving fluid by fluid flow. In the design of industrial appliances such as heat exchangers, the main goal is to improve the thermal contact and reduce power during pumping in order to improve thermodynamic efficiency of the system [2, 5]. An efficient thermodynamic system/appliance is one that basically reduces the generation of entropy or one that minimizes the destruction of exergy, the energy that is available for use by the system [35, 47]. Entropy generation analysis clarifies energy losses in a system evidently in many energy-related applications such as the heat exchangers as previously mentioned, cooling of electronic devices and geothermal energy systems [25, 27, 52]. Entropy generation consists of three factors; conduction, or Heat Transfer Irreversibility (HTI), Fluid Friction Irreversibility (FFI) and Diffusive Irreversibility (DI) [51, 19, 53]. The volumetric entropy generation is defined as;

$$S'''_{gen} = \frac{\kappa}{T_\infty^2}\left[\left(\frac{\partial T}{\partial x}\right)^2 + \left(\frac{\partial T}{\partial y}\right)^2\right] + \frac{\mu}{T_\infty}\left[\left(\frac{\partial u}{\partial x}\right)^2 + \left(\frac{\partial u}{\partial y}\right)^2\right] + \frac{\sigma B_0^2}{T_\infty^2}u^2 + \frac{RD_B}{C_\infty}\left[\left(\frac{\partial C}{\partial x}\right)^2 + \left(\frac{\partial C}{\partial y}\right)^2\right] + \frac{RD_B}{T_\infty}\left[\left(\frac{\partial C}{\partial x}\frac{\partial T}{\partial x}\right) + \left(\frac{\partial C}{\partial y}\frac{\partial T}{\partial y}\right)^2\right], \tag{24}$$

and the characteristic rate of entropy generation S'''_0 as

$$S'''_0 = \frac{\kappa(T_w - T_\infty)^2}{x^2 T_\infty^2}. \tag{25}$$

Equation (24) gives the constituent components that give rise to entropy. The first component is is entropy generation due heat transfer irreversibility, the second component is the entropy due to viscous dissipation, the third component is the entropy generation due to the applied magnetic field, the fourth and fifth components describe entropy generation due mass transfer irreversibility.

We evaluate the entropy generation number (N_G) as,

$$N_G = \frac{S'''_{gen}}{S'''_0} = \left(\frac{\eta^2}{4} + Re\right)\theta'^2(\eta) + \left(\frac{\eta^2}{4} + Re\right)\frac{Br}{\epsilon}f''^2(\eta) + \frac{ReBrM}{\epsilon}f'^2(\eta) + \left(\frac{\eta^2}{4} + Re\right)\zeta\left(\frac{\chi}{\epsilon}\right)^2\phi'^2(\eta) + \left(\frac{\eta^2}{4} + Re\right)\zeta\left(\frac{\chi}{\epsilon}\right)\theta'(\eta)\phi'(\eta), \tag{26}$$

where Br, χ, and ζ are the Brinkman number, a dimensionless parameter that is related to heat conduction from a wall to a flowing fluid, concentration relative parameter and a constant parameter. These are defined as;

$$Br = \frac{\mu U_0^2}{\kappa(T_w - T_\infty)}, \quad \chi = \frac{C_w - C_\infty}{C_\infty}, \quad \zeta = \frac{RD_B C_\infty}{\kappa}. \tag{27}$$

An important parameter in the study of entropy generation is the Bejan number, Be. It is the ratio of entropy generation due to heat transfer irreversibility to the total entropy generation:

$$Be = \frac{Entropy\ generation\ due\ to\ heat\ transfer}{Total\ entropy\ generation} = \frac{N1}{N_G}, \tag{28}$$

where

$$N1 = \left(\frac{\eta^2}{4} + Re\right)\theta'^2(\eta).$$

For $Be << 0.5$ represents a situation where entropy generation due to viscous dissipation irreversibility dominates entropy generation due to heat transfer irreversibility. For $Be >> 0.5$ represents a situation where entropy generation due to heat transfer irreversibility dominates entropy generation due to viscous dissipation irreversibility. When Be = 0.5, the heat transfer irreversibility and the fluid friction irreversibility are equal [11, 13, 4].

5. Numerical Solution using Spectral Quasi-linearization Method

The set of ordinary differential equations resulting from the use of similarity transformations (9)-(11) together with the boundary conditions (12)-(14) are solved numerically to a high level of accuracy using the spectral quasi-linearization method (SQLM). The fundamental principle of the spectral method is to discretize the domain, then interpolate the data globally and evaluate the derivatives of the interpolants on the grid [62, 14]. The quasi-linearization method (QLM) is a generalization of the Newton-Raphson's method [**?**]. The derivation of the QLM is based on the linearization of the nonlinear components of the governing equations using the Taylor series assuming that the difference between successive iterations, that is at $r + 1$, and r is negligibly small. We solve the nonlinear system of ordinary differential equations with boundary conditions (9)-(14) using the spectral quasi-linearisation method (SQLM). The nonlinear components of the system of ordinary differential equations give the following iterative sequences of linear differential equations. First define the functions F, Θ and Φ for the equations (9)-(11) respectively as;

$$F = f''' + \frac{1}{2}f''f - Mf' + \lambda_1\theta + \lambda_2\phi, \tag{29}$$

$$\Theta = \theta'' + Pr\left[\frac{1}{2}f\theta' + Ecf''^2 + Nb\theta'\phi' + Nt\theta'^2 + \delta\theta\right], \tag{30}$$

$$\Phi = \phi'' + Sc\left[\frac{1}{2}f\phi' - \gamma\left[1 + \epsilon\theta\right]^m Exp\left(-\frac{E}{(1+\epsilon\theta)}\right)\phi^n\right] + \frac{Nt}{Nb}\theta''. \tag{31}$$

We construct the errors from the iterative process for the the equations (9)-(11) as give below by (32)-(34) respectively

$$a_{0r}f'''_{r+1} + a_{1r}f''_{r+1} + a_{2r}f'_{r+1} + a_{3r}f_{r+1} + a_{4r}\theta_{r+1} + a_{5r}\phi_{r+1} - F = R_f, \tag{32}$$

$$b_{0r}\theta''_{r+1} + b_{1r}\theta'_{r+1} + b_{2r}\theta_{r+1} + b_{3r}f''_{r+1} + b_{4r}f_{r+1} + b_{5r}\phi'_{r+1} - \Theta = R_\theta, \tag{33}$$

$$c_{0r}\phi''_{r+1} + c_{1r}\phi'_{r+1} + c_{2r}\phi_{r+1} + c_{3r}f_{r+1} + c_{4r}\theta''_{r+1} + c_{5r}\theta_{r+1} - \Phi = R_\phi, \tag{34}$$

subject to the boundary conditions

$$f_{r+1}(0) = 0, \quad f'_{r+1}(0) = 1, \quad f'_{r+1}(\infty) \to 0, \tag{35}$$

$$\theta'_{r+1}(0) = -Bi(1 - \theta_r(0)), \quad \theta_{r+1}(\infty) \to 0, \tag{36}$$

$$Nb\phi'_{r+1}(0) + Nt\theta'_{r+1}(0) = 0, \quad \phi_{r+1}(\infty) \to 0. \tag{37}$$

The coefficients in equation (32)-(34) are given as

$$\begin{aligned}
&a_{0,r} = 1, \quad a_{1,r} = \frac{1}{2}f_r, \quad a_{2,r} = -M, \quad a_{3,r} = \frac{1}{2}f''_r, \quad a_{4,r} = \lambda_1, \quad a_{5,r} = \lambda_2,\\
&b_{0,r} = 1, \quad b_{1,r} = Pr\left[\tfrac{1}{2}f_r + Nb\phi'_r + 2Nt\theta'_r\right], \quad b_{2,r} = Pr\delta, \quad b_{3,r} = 2PrEcf''_r, \quad b_{4,r} = \tfrac{1}{2}Pr\theta'_r,\\
&b_{5,r} = PrNb\theta'_r, \quad c_{0,r} = 1, \quad c_{1,r} = \tfrac{1}{2}Scf_r, \quad c_{2,r} = -nSc\gamma\left[1 + \epsilon\theta_r\right]^m Exp\left(-\tfrac{E}{1+\epsilon\theta_r}\right)\phi^{n-1},\\
&c_{3,r} = \tfrac{1}{2}Sc\phi'_r, \quad c_{4,r} = \tfrac{Nt}{Nb}, \quad c_{5,r} = -Sc\gamma\left[1 + \epsilon\theta_r\right]^{m-2}\left[m(1 + \epsilon\theta_r) + E\right] Exp\left(-\tfrac{E}{1+\epsilon\theta_r}\right)\phi^n.
\end{aligned} \tag{38}$$

The initial guesses are selected as functions that satisfy the boundary conditions, and these were chosen as

$$f_0(\eta) = 1 - e^{-\eta}, \quad \theta_0(\eta) = \frac{Bi}{1 + Bi}e^{-\eta}, \quad \phi_0(\eta) = -\frac{Nt}{Nb}\frac{Bi}{(1 + Bi)}e^{-\eta}. \tag{39}$$

In order to apply the SQLM to the system of nonlinear ordinary differential (23)-(25) we transform the domain from $0 \le \eta \le L_x$ to $-1 \le x \le 1$ using the transformation $\eta = Lx(x + 1)/2$ [30] where,

$$x_i = \cos\left(\frac{\pi i}{N}\right), \quad i = 0,\ 1,\ 2,\ \cdots,\ N \tag{40}$$

are the Gauss-Lobatto collocation points. The spectral collocation method will construct a differentiation matrix (D) to approximate the derivative of unknown variables at the collocation points as a matrix vector product. The D-matrix is constructed for the domain [-1, 1] so we scale this matrix for the domain $[0, L_x]$ by taking $D1 = 2D/L_x$, so that

$$\frac{dF_r^{(1)}}{d\eta_j}(\eta) = \sum_{k=0}^{n} D1f(\eta_k) = D1F_m, \quad j = 0,\ 1,\ 2,\ \cdots,\ N, \tag{41}$$

where $F = [f(\eta_0), f(\eta_1), f(\eta_2), \cdots, f(\eta_N)]^T$ represent the vector function at the collocation points. Higher order derivatives are given as powers of the scaled differentiation matrix

$$F^p = D1^p F_r. \tag{42}$$

Using the scaled differentiation matrix on (32)-(34) we obtain;

$$\begin{aligned}
A_{11}f_{r+1} + A_{12}\theta_{r+1} + A_{13}\phi_{r+1} &= R_f,\\
A_{21}f_{r+1} + A_{22}\theta_{r+1} + A_{23}\phi_{r+1} &= R_\theta,\\
A_{31}f_{r+1} + A_{32}\theta_{r+1} + A_{33}\phi_{r+1} &= R_\phi.
\end{aligned} \tag{43}$$

In matrix for this can be written as

$$\begin{bmatrix} A_{11} & A_{12} & A_{13} \\ A_{21} & A_{22} & A_{23} \\ A_{31} & A_{32} & A_{33} \end{bmatrix} \begin{bmatrix} f_{r+1} \\ \theta_{r+1} \\ \phi_{r+1} \end{bmatrix} = \begin{bmatrix} R_f \\ R_\theta \\ R_\phi \end{bmatrix},$$

where,

$A11 = diag(a_{0,r})D3 + diag(a_{1,r})D2 + diag(a_{2,r})D1 + diag(a_{3,r})I$, $A12 = diag(a_{4,r})I$,

$A13 = diag(a_{5,r})I$, $A21 = diag(b_{3,r})D2+diag(b_{4,r})I$, $A22 = diag(b_{0,r})D2+diag(b_{1,r})D1+diag(b_{2,r})I$, $A23 = diag(b_{5,r})D1$, $A31 = diag(a_{3,r})I$, $A32 = diag(c_{4,r})D2 + diag(c_{5,r})I$,

$A33 = diag(c_{0,r})D2 + diag(c_{1,r})D1 + diag(c_{2,r})I$.

Residual error analysis

In order to get a clear understanding of the behaviour of momentum, heat and mass transfers under different circumstances we solved the governing equation numerically using simulations. To validate the accuracy of our simulations we performed the residual error analysis and the summary of the analysis is given in Table 1 and Figure 2.

Table 1: Residual error for different iterations

i	$f(\eta)$	$\theta(\eta)$	$\phi(\eta)$
1	$1.32746354 \times 10^{-02}$	$5.25566389 \times 10^{00}$	$2.74935787 \times 10^{00}$
2	$7.21041461 \times 10^{-03}$	$1.45963375 \times 10^{00}$	$6.01742660 \times 10^{-01}$
3	$5.52545804 \times 10^{-04}$	$1.00195264 \times 10^{00}$	$9.56003621 \times 10^{-02}$
4	$1.41375059 \times 10^{-04}$	$3.11568082 \times 10^{-02}$	$3.91511992 \times 10^{-02}$
5	$5.27746204 \times 10^{-08}$	$5.34392677 \times 10^{-04}$	$3.30780666 \times 10^{-04}$
6	$2.25804927 \times 10^{-08}$	$4.84693898 \times 10^{-08}$	$1.74715666 \times 10^{-08}$
7	$3.91856085 \times 10^{-08}$	$2.24601493 \times 10^{-09}$	$4.90053051 \times 10^{-11}$
8	$9.85789108 \times 10^{-08}$	$2.35930431 \times 10^{-09}$	$5.04747355 \times 10^{-11}$
9	$2.41516856 \times 10^{-08}$	$2.15273310 \times 10^{-09}$	$4.90303276 \times 10^{-11}$
10	$2.17438490 \times 10^{-08}$	$2.23999219 \times 10^{-09}$	$4.86822695 \times 10^{-11}$

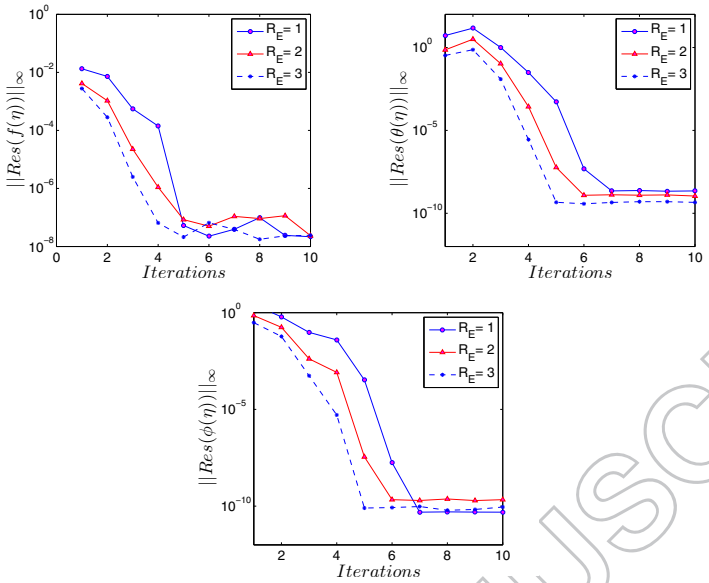

Figure 2: Residual errors for velocity, temperature and concentration profiles

From the results in Table 1 and Figure 2, one can see that the SQLM is a highly accurate numerical technique with a high convergence rate with errors of orders less than 10^{-8}.

6. Discussion and Conclusion

The accuracy of the comparison table is verified with the results previously reported by Tsou et al. [63], Soundalgekar and Murty [61], Ali [6], Moutsoglou and Chen [44] and Patil et al. [50]. They are using finite difference and shooting method for evaluated the Nusselt number. The results of this comparison using the spectral quasilinearization methods are presented in Table 2 and are found to be in excellent agreement. We investigate the impact that certain parameters have on the momentum, heat and mass transfer coefficients. Thus we investigate the impact of these parameters on the local skin friction coefficient, Nusselt number, and the Sherwood number. These are given by values that are proportional to the quantities $-f''(0)$, $-\theta'(0)$ and $-\phi'(0)$ respectively. The values are evaluated numerically and presented in Table 3.

Table 2: Comparison of local Nusselt number (Nu) for different values of *Pr*

Pr	0.7	1.0	2.0	7.0	10.0	100.0
Tsou et al. [63]	0.3492	0.4438	—-	—-	1.6804	5.545
Soundalgekar and Murty [61]	0.3500	—-	0.6831	—-	1.6808	—
Ali [6]	0.3476	0.4416	—-	—-	1.6713	—-
Moutsoglou and Chen [44]	0.34924	—-	—-	1.38703	—-	—-
Patil et al. [50]	0.349235	0.443748	0.683258	1.387033	1.680293	5.544633
Present Results	0.349235	0.443748	0.683258	1.387033	1.680293	5.544633

Table 3: Effect of varying parameters on skin friction coefficient (C_f), local Nusselt number (Nu) and local Sherwood number (Sh) for $Ec = 0.3$, $M = 2$, $Bi = 3$, $Nb = 0.5$, $Nt = 0.5$, $\gamma = 2$, $m = 1$, $\epsilon = 2$

Sc	λ_1	λ_2	n	Pr	E	δ	$-f''(0)$	$-\theta'(0)$	$-\phi'(0)$
0.24	0.4	0.5	2.0	7.0	1.0	0.1	1.18351957	-0.47401062	0.72646868
0.6							1.18765542	-0.65247895	0.97806071
0.8							1.18960295	-0.68810262	1.04550932
0.6	1.0						0.87592336	-0.24563881	0.53240437
	2.0						0.47844063	0.06055691	0.20806346
	0.4	0.0					1.17144241	-0.72590676	1.06026085
		0.95					1.18367187	-0.55914556	0.87956737
		0.5	3.0				1.18088289	-0.52881398	0.76457312
			4.0				1.17859866	-0.44554206	0.64333629
			2.0	6.0			1.19383864	-0.53510821	0.83126379
				8.0			1.18180395	-0.76849254	1.12682774
				7.0	2.0		1.18292761	-0.54338155	0.80241278
					3.0		1.17994759	-0.44336201	0.65370400
					1.0	0.0	1.22241757	-0.17284207	0.47010191
						0.05	1.20729203	-0.37278093	0.67403384

Table 4 gives a summary of the parameters that we used with their sources. The values chosen for this model are consistent with values of a typical nanofluid. For values that have a wide range we chose values for which the numerical scheme was stable.

Table 4: Parameters in the model and their values

Parameter	Symbol	Value	Source
Chemical reaction parameter	γ	(1, 5)	[39] [46], [41]
Heat generation parameter	δ	0.1	[39]
Eckert number	Ec	(0.1, 3)	[39]
Prandtl number	Pr	(4, 7.2)	[46], [43]
Thermal buoyancy	λ_1	(0, 1)	[39]
solute buoyancy	λ_2	(0, 1)	[39]
Magnetic field parameter	M	(0, 6)	[36]
Brownian motion parameter	Nb	(0.1, 5)	[43]
Thermophoresis parameter	Nt	(0.1, 0.5)	[43]
schmidt number	Sc	(0.2, 2.62)	[39]
Constant exponent	m	(-1, 1)	[41]
Temperature relative parameter	ϵ	(0, 3)	[10]
Order of chemical reaction	n	(1, 5)	[48]
Activation energy	E	(1, 3)	[39], [41]
Biot number	Bi	(0.1, 50)	[46], [7]

Brownian motion

Figure 3 shows the impact of Brownian motion on the velocity, temperature and concentration profiles. Brownian motion is the random 'indecisive' movement of particles suspended in a fluid resulting from the collision with the fast-moving molecules of the fluid. An increase in the Brownian motion causes the momentum boundary layer to thin as shown in Figure 3 (a), a result consistent with a result obtained by [58, 8]. The fluid around a particle is

dragged in the direction of the particle. At the same time the motion of the particle is resisted by viscous forces in the fluid [64]. The overall effect is a reduction in the velocity of the fluid. Temperature is shown to increase with increasing values of the Brownian motion as reported by [36]. Increasing the Brownian motion parameter was shown to lead to a decrease in the solute boundary layer. An increase in the Brownian motion parameter boost the movement of particles. This cause the warming of boundary layer which effectively cause nanoparicle to move away of the surfaces inside the inactive fluid. This increases the deposition of the solute particles away from the surface, leading to the reduction of the concentration [22]. The results are shown in Figure 3 (c). Similar results were obtained by [16, 17, 36].

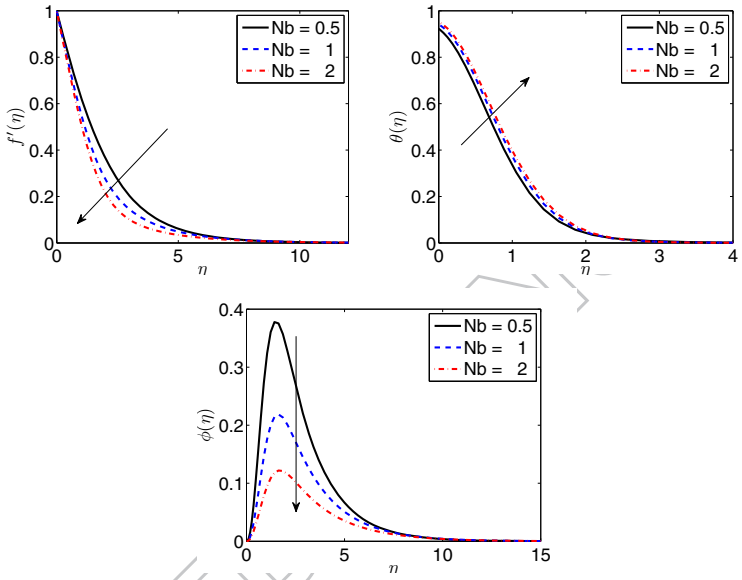

Figure 3: Effect of Brownian motion on the velocity, temperature and concentration profiles

Thermophoresis

Thermophoresis, sometimes called thermo migration is the movement of particles due to a force resulting from a temperature gradient, acting in the direction of high to low-temperature regions. An increase in the thermopheretic parameter is accompanied by by an increase in temperature and fluid velocity. The thermophoretic force for small particles is given as $F_t = -p\lambda d_p^2 \nabla T/T$, where p is the gas pressure, λ gas mean free path, d_p is the particle diameter, ∇T and T is the absolute temperature of the particle. The influence of thermophoretic parameter on velocity and temperature is shown in Figure 4 (a) and (b) respectively. Increasing the thermophoretic parameter leads to an increase in both velocity and thermal boundary layers. This result is associated with an increase in the buoyancy effects [57]. For a small region close to the surface, increasing the thermophoretic parameter decreases the concentration. A phenomenon consistent with the particles being 'pushed' out of the hot boundary layer to the colder free stream region. This, however, changes as we move further away from the surface into the free stream, where increasing the thermophoretic parameter increases the concentration. The concentration dynamics under thermophoretic parameter are depicted in Figure 4 (c). Similar results were obtained by [9, 16, 17, 36]. Close

to the metal plate the concentration of solute decreases with increasing thermophoretic parameter. Increasing the thermophoretic parameter increases the wall slope of the concentration profile and decreasing the concentration of the solute [15, 21]. This is because at the heated wall the thermophoretic force is greatest and will therefore push the solute away leading to the observed decrease in concentration near the hot surface.

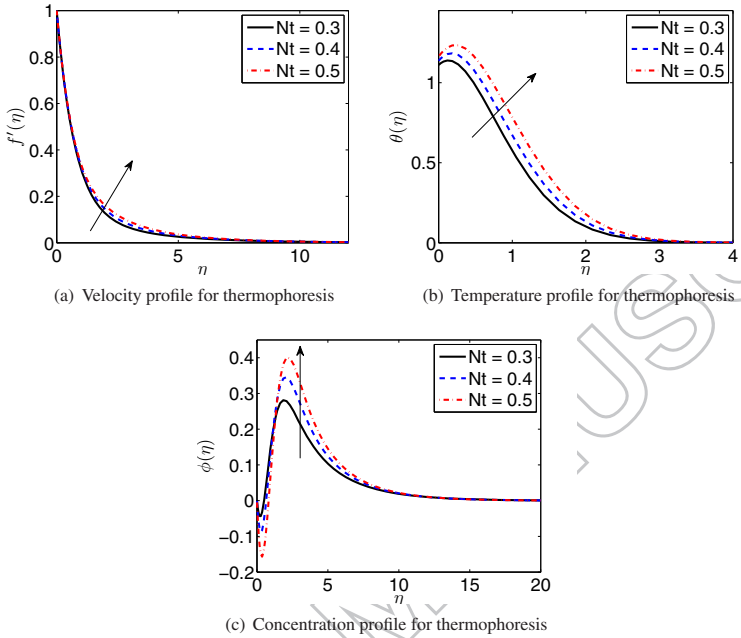

(a) Velocity profile for thermophoresis

(b) Temperature profile for thermophoresis

(c) Concentration profile for thermophoresis

Figure 4: Thermophoresis on the velocity, temperature and concentration profiles

Order of chemical reaction and Activation energy

We asses the impact of activation energy and order of chemical reaction in Figure 5. We observe that the two parameters have similar effects on the velocity, temperature and concentration. Increasing the activation energy slows the rate of reaction leading to an increase in the concentration profile [40, 41]. Although activation energy does not directly appear on the temperature and velocity equation, it's impact is via the mass equation. It is noted that increasing the activation energy increases velocity possible due to solute buoyancy and decreases the temperature. Our results on order are consistent with results in literature e.g see [38, 48]. Increasing the order of chemical reaction increased concentration and velocity while temperature decreases. Ferdows and Al-Mdallal, [18] drew similar conclusion for the velocity and temperature profiles. The concentration profile is consistent with results by Palani *et al.* [49]. The mechanism behind the phenomenon has not yet been fully understood.

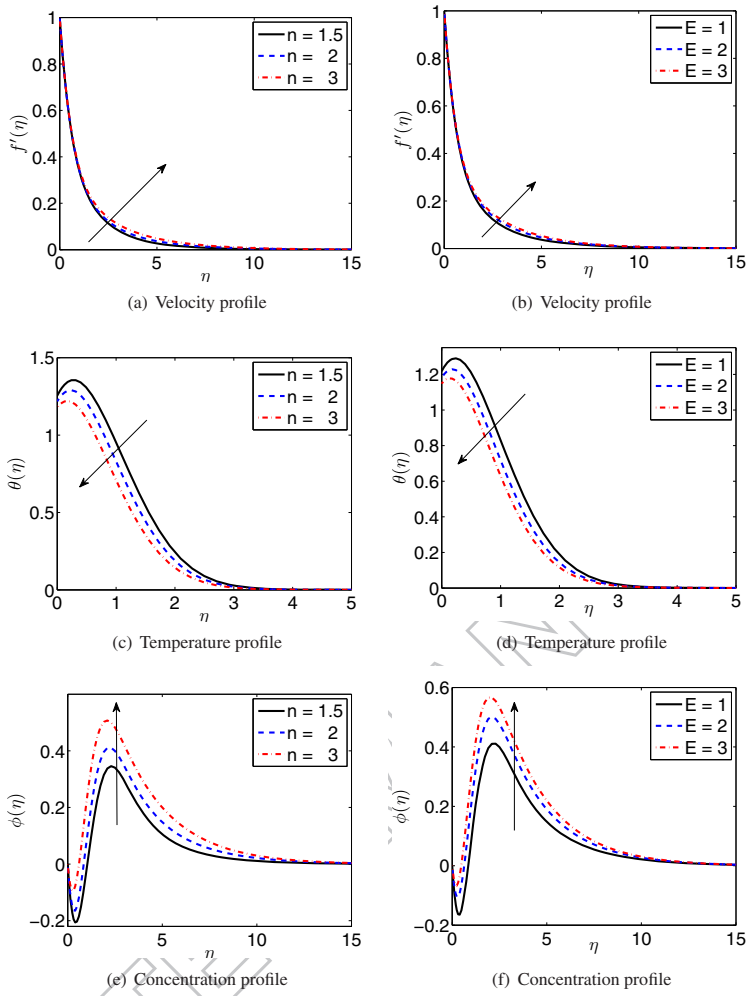

(a) Velocity profile (b) Velocity profile

(c) Temperature profile (d) Temperature profile

(e) Concentration profile (f) Concentration profile

Figure 5: Order of chemical reaction and Activation energy on the velocity, temperature and concentration profiles

Entropy generation: Brinkman and Reynolds number

In Figure 6 we analyze the impact of Brinkman number and Reynolds number on entropy generation and the Bejan number. An increase in the Brinkman number and Reynolds number have the same effect of increasing entropy generation and decreasing the Bejan number. Similar results are reported by [45, 1]. The Bejan number for both the Brinkman and Reynolds number is less than 0.5 and this implies that entropy generation due to heat transfer irreversibility is dominated by the viscous and mass transfer irreversibility. Increasing the Brinkman number and Reynolds increases the entropy generation by viscous dissipation and mass transfer and thus resulting in a decrease in the Bejan number.

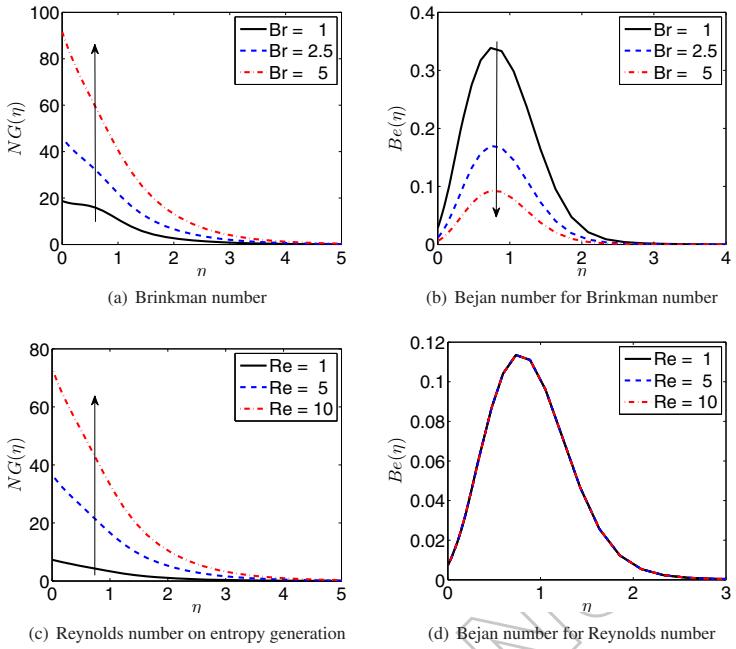

(a) Brinkman number (b) Bejan number for Brinkman number

(c) Reynolds number on entropy generation (d) Bejan number for Reynolds number

Figure 6: Entropy generation and Bejan number for Brinkman and Reynolds numbers

Entropy generation: Activation energy and order of chemical reaction

Figure (7) seeks to give an insight into the influence of activation energy and order of chemical reaction have on the entropy generation and the Bejan number. The two parameters have the same impact on entropy generation and Bejan number. An increase in any one of the parameters leads to an increase in the entropy generation and a decrease in the Bejan number. Our results do not agree with results by Khan *et al* [33]. The graphical result on Bejan number is similar to our result, however the authors contradicted themselves in the discussion section. An increase in activation energy leads to increase in the concentration as shown in Figure 5. This leads to an increase in mass transfer irreversibility which result in the increase in entropy generation and a decrease in the Bejan number.

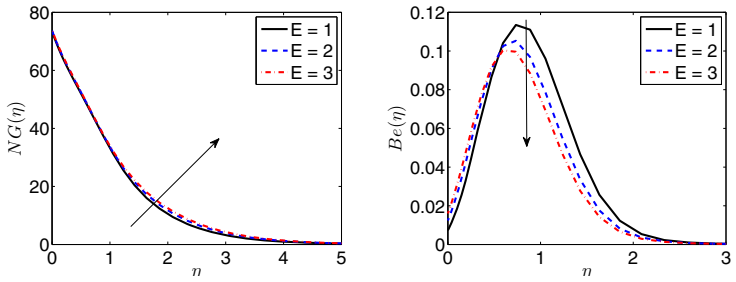

(a) Activation energy on entropy generation (b) Bejan number for Activation energy

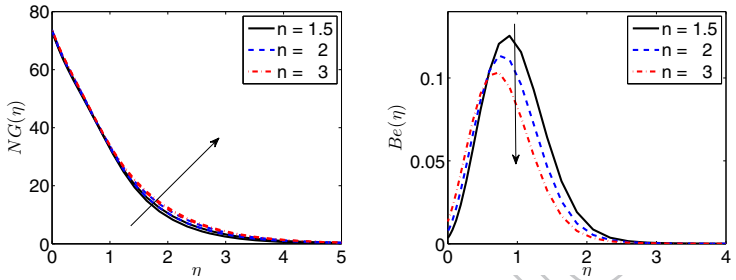

(c) Order of chemical reaction on entropy generation (d) Bejan number for Order of chemical reaction

Figure 7: Entropy generation and Bejan number for Activation energy and order of chemical reaction

Entropy generation: Heat generation

In Figure 8 we plot the graphs for entropy generation and Bejan number for the heat generation parameter, δ. Entropy generation and the Bejan number increase with increasing heat generation. An increase in the Bejan number shoes that the heat transfer irreversibility dominates. We found no study in literature through our intensive study that clearly described or gave an account of effect of heat generation on entropy generation.

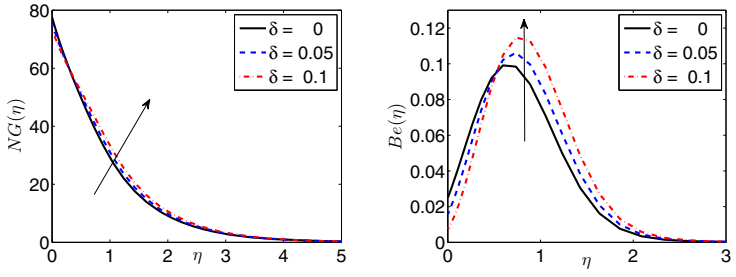

(a) Heat generation on entropy generation (b) Bejan number for heat generation

Figure 8: Entropy generation and Bejan number for heat generation

Conclusion

In this paper a mathematical model that accounts for entropy generation, activation energy and high order of a chemical reactions was formulated and analyzed. The flow was assumed to be initiated by a moving surface in

the fluid. We gain an insight into the flow characteristics, order of chemical reaction and entropy generation by studying the impact of associated parameters. We deduce the following:

- Brownian motion and thermophoresis have opposing effects on velocity and concentration profiles, however both increase the temperature of the fluid,
- activation energy and order of chemical reaction have the same effects on the velocity, temperature and concentration even though the underlying processes may be different,
- viscous dissipation and mass transfer irreversibility dominated the heat transfer irreversibility,
- for increasing heat generation, the heat transfer irreversibility dominates as evidenced by increasing Bejan number.

[1] Abolbashari, M. H., Freidoonimehr, N., Nazari, F. and Rashidi, M. M. [2015], 'Analytical modeling of entropy generation for casson nano-fluid flow induced by a stretching surface', *Advanced Powder Technology* **26**(2), 542–552.

[2] Abu-Hijleh, B. A. [2002], 'Entropy generation due to cross-flow heat transfer from a cylinder covered with an orthotropic porous layer', *Heat and Mass Transfer* **39**(1), 27–40.

[3] Abu-Nada, E. [2008], 'Application of nanofluids for heat transfer enhancement of separated flows encountered in a backward facing step', *International Journal of Heat and Fluid Flow* **29**(1), 242–249.

[4] Al-Rashed, A. A., Kalidasan, K., Kolsi, L., Velkennedy, R., Aydi, A., Hussein, A. K. and Malekshah, E. H. [2018], 'Mixed convection and entropy generation in a nanofluid filled cubical open cavity with a central isothermal block', *International Journal of Mechanical Sciences* **135**, 362–375.

[5] Alharbey, R., Mondal, H. and Behl, R. [2019], 'Spectral quasi-linearization method for non-darcy porous medium with convective boundary condition', *Entropy* **21**(9), 838.

[6] Ali, M. E. [1994], 'Heat transfer characteristics of a continuous stretching surface', *Wärme-und Stoffübertragung* **29**(4), 227–234.

[7] Almakki, M., Dey, S., Mondal, S. and Sibanda, P. [2017], 'On unsteady three-dimensional axisymmetric mhd nanofluid flow with entropy generation and thermo-diffusion effects on a non-linear stretching sheet', *Entropy* **19**(7), 168.

[8] Ardahaie, S. S., Amiri, A. J., Amouei, A., Hosseinzadeh, K. and Ganji, D. [2018], 'Investigating the effect of adding nanoparticles to the blood flow in presence of magnetic field in a porous blood arterial', *Informatics in Medicine Unlocked* **10**, 71–81.

[9] Awad, F. G., Ahamed, S. M. S., Sibanda, P. and Khumalo, M. [2015], 'The effect of thermophoresis on unsteady oldroyd-b nanofluid flow over stretching surface', *PLOS ONE* **10**(8), e0135914.

[10] Awad, F. G., Motsa, S. and Khumalo, M. [2014], 'Heat and mass transfer in unsteady rotating fluid flow with binary chemical reaction and activation energy', *PloS one* **9**(9), e107622.

[11] Bejan, A. [2013], *Convection heat transfer*, John wiley & sons.

[12] Bhattacharyya, K. [2011], 'Effects of radiation and heat source/sink on unsteady mhd boundary layer flow and heat transfer over a shrinking sheet with suction/injection', *Frontiers of Chemical Science and Engineering* **5**(3), 376–384.

[13] Butt, A. S. and Ali, A. [2013], 'Thermodynamical analysis of the flow and heat transfer over a static and a moving wedge', *ISRN Thermodynamics* **2013**, 1–6.

[14] Canuto, C., Hussaini, M. Y., Quarteroni, A., Thomas Jr, A. et al. [2012], *Spectral methods in fluid dynamics*, Springer Science & Business Media.

[15] Chamkha, A. J. and Issa, C. [2000], 'Effects of heat generation/absorption and thermophoresis on hydromagnetic flow with heat and mass transfer over a flat surface', *International Journal of Numerical Methods for Heat & Fluid Flow* **10**(4), 432–449.

[16] Dhlamini, M., Kameswaran, P. K., Sibanda, P., Motsa, S. and Mondal, H. [2018], 'Activation energy and binary chemical reaction effects in mixed convective nanofluid flow with convective boundary conditions', *Journal of Computational Design and Engineering* .

[17] Dhlamini, M., Mondal, H., Sibanda, P. and Motsa, S. [2018], 'Spectral quasi-linearization methods for powell-eyring MHD flow over a nonlinear stretching surface', *Journal of Nanofluids* **7**(5), 917–927.

[18] Ferdows, M. and Al-Mdallal, Q. M. [2013], 'Effectsof order of chemical reaction on a boundary layer flow with heat and mass transfer over a linearly stretching sheet', *American Journal of Fluid Dynamics* **2**(6), 89–94.

[19] Freidoonimehr, N. and Rahimi, A. B. [2016], 'Comment on "effects of thermophoresis and brownian motion on nanofluid heat transfer and entropy generation" by m. mahmoodi, sh. kandelousi, journal of molecular liquids, 211 (2015) 15–24', *Journal of Molecular Liquids* **216**, 99–102.

[20] Goqo, S. P., Oloniiju, S. D., Mondal, H., Sibanda, P. and Motsa, S. S. [2018], 'Entropy generation in mhd radiative viscous nanofluid flow over a porous wedge using the bivariate spectral quasi-linearization method', *Case studies in thermal engineering* **12**, 774–788.

[21] Goren, S. L. [1977], 'Thermophoresis of aerosol particles in the laminar boundary layer on a flat plate', *Journal of Colloid and Interface Science* **61**(1), 77–85.

[22] Goyal, R. and Bhargava, R. [2017], 'Gfem study of magnetohydrodynamics thermo-diffusive effect on nanofluid flow over power-law stretching sheet along with regression analysis', *arXiv preprint arXiv:1708.05609* .

[23] Hayat, T., Khan, M. I., Farooq, M., Alsaedi, A., Waqas, M. and Yasmeen, T. [2016], 'Impact of cattaneo–christov heat flux model in flow of variable thermal conductivity fluid over a variable thicked surface', *International Journal of Heat and Mass Transfer* **99**, 702–710.

[24] Hayat, T., Khan, M. I., Farooq, M., Yasmeen, T. and Alsaedi, A. [2016], 'Stagnation point flow with cattaneo-christov heat flux and homogeneous-heterogeneous reactions', *Journal of Molecular Liquids* **220**, 49–55.

[25] Hayat, T., Khan, M. I., Qayyum, S. and Alsaedi, A. [2018], 'Entropy generation in flow with silver and copper nanoparticles', *Colloids and Surfaces A: Physicochemical and Engineering Aspects* **539**, 335–346.

[26] Hayat, T., Muhammad, T., Shehzad, S. A. and Alsaedi, A. [2015], 'Temperature and concentration stratification effects in mixed convection flow of an oldroyd-b fluid with thermal radiation and chemical reaction', *PloS one* **10**(6), e0127646.

[27] Hayat, T., Qayyum, S., Khan, M. I. and Alsaedi, A. [2018], 'Entropy generation in magnetohydrodynamic radiative flow due to rotating disk in presence of viscous dissipation and joule heating', *Physics of Fluids* **30**(1), 017101.

[28] Hayat, T., Ullah, I., Alsaedi, A. and Farooq, M. [2017], 'Mhd flow of powell-eyring nanofluid over a non-linear stretching sheet with variable thickness', *Results in Physics* **7**, 189–196.

[29] Hussein, A. K. and Hussain, S. H. [2016], 'Heatline visualization of natural convection heat transfer in an inclined wavy cavities filled with nanofluids and subjected to a discrete isoflux heating from its left sidewall', *Alexandria Engineering Journal* **55**(1), 169–186.

[30] Kameswaran, P. K., Sibanda, P. and Motsa, S. S. [2013], 'A spectral relaxation method for thermal dispersion and radiation effects in a nanofluid flow', *Boundary Value Problems* **2013**(1), 242.

[31] Kasmani, R. M., Sivanandam, S., Bhuvaneswari, M., Siri, Z., , and and [2016], 'Effect of chemical reaction on convective heat transfer of boundary layer flow in nanofluid over a wedge with heat generation/absorption and suction', *Journal of Applied Fluid Mechanics* **9**(1), 379–388.

[32] Khan, M. I., Hayat, T., Khan, M. I. and Alsaedi, A. [2018], 'Activation energy impact in nonlinear radiative stagnation point flow of cross nanofluid', *International Communications in Heat and Mass Transfer* **91**, 216–224.

[33] Khan, M. I., Khan, T. A., Qayyum, S., Hayat, T., Khan, M. I. and Alsaedi, A. [2018], 'Entropy generation optimization and activation energy in nonlinear mixed convection flow of a tangent hyperbolic nanofluid', *The European Physical Journal Plus* **133**(8).

[34] Khan, M. I., Waqas, M., Hayat, T. and Alsaedi, A. [2017], 'A comparative study of casson fluid with homogeneous-heterogeneous reactions', *Journal of colloid and interface science* **498**, 85–90.

[35] Khan, M. W. A., Khan, M. I., Hayat, T. and Alsaedi, A. [2018], 'Entropy generation minimization (EGM) of nanofluid flow by a thin moving needle with nonlinear thermal radiation', *Physica B: Condensed Matter* **534**, 113–119.

[36] Mabood, F., Ibrahim, S. and Khan, W. [2016], 'Framing the features of brownian motion and thermophoresis on radiative nanofluid flow past a rotating stretching sheet with magnetohydrodynamics', *Results in Physics* **6**, 1015–1023.

[37] Mahanthesh, B., Gireesha, B. and Gorla, R. S. R. [2017], 'Unsteady three-dimensional mhd flow of a nano eyring-powell fluid past a convectively heated stretching sheet in the presence of thermal radiation, viscous dissipation and joule heating', *Journal of the Association of Arab Universities for Basic and Applied Sciences* **23**, 75–84.

[38] Makinde, O. D., Olanrewaju, P. O. and Charles, W. M. [2011], 'Unsteady convection with chemical reaction and radiative heat transfer past a flat porous plate moving through a binary mixture', *Afrika Matematika* **22**(1), 65–78.

[39] Makinde, O. D. and Sibanda, P. [2011], 'Effects of chemical reaction on boundary layer flow past a vertical stretching surface in the presence of internal heat generation', *International Journal of Numerical Methods for Heat & Fluid Flow* **21**(6), 779–792.

[40] Maleque, K. A. [2013], 'Effects of exothermic/endothermic chemical reactions with arrhenius activation energy on MHD free convection and mass transfer flow in presence of thermal radiation', *Journal of Thermodynamics* **2013**, 1–11.

[41] Maleque, K. et al. [2013], 'Effects of exothermic/endothermic chemical reactions with arrhenius activation energy on mhd free convection and mass transfer flow in presence of thermal radiation', *Journal of Thermodynamics* **2013**, 1–11.

[42] Mohammed, H., Al-Aswadi, A., Abu-Mulaweh, H., Hussein, A. K. and Kanna, P. R. [2014], 'Mixed convection over a backward-facing step in a vertical duct using nanofluid—buoyancy opposing case', *Journal of Computational and Theoretical Nanoscience* **11**(3), 860–872.

[43] Mondal, H., Almakki, M. and Sibanda, P. [2019], 'Dual solutions for three-dimensional magnetohydrodynamic nanofluid flow with entropy generation', *Journal of Computational Design and Engineering* .

[44] Moutsoglou, A. and Chen, T. [1979], 'Buoyancy effects in boundary layers on inclined, continuous, moving sheets'.

[45] Noghrehabadi, A., Saffarian, M. R., Pourrajab, R. and Ghalambaz, M. [2013], 'Entropy analysis for nanofluid flow over a stretching sheet in the presence of heat generation/absorption and partial slip', *Journal of Mechanical Science and Technology* **27**(3), 927–937.

[46] Olanrewaju, P., Arulogun, O. and Adebimpe, K. [2012], 'Internal heat generation effect on thermal boundary layer with a convective surface boundary condition', *American journal of Fluid dynamics* **2**(1), 1–4.

[47] Pal, D., Mondal, S. and Mondal, H. [2019], 'Entropy generation on mhd jeffrey nanofluid over a stretching sheet with nonlinear thermal radiation using spectral quasilinearisation method', *International Journal of Ambient Energy* pp. 1–15.

[48] Palani, S., Kumar, B. R. and Kameswaran, P. K. [2016*a*], 'Unsteady mhd flow of an ucm fluid over a stretching surface with higher order chemical reaction', *Ain Shams Engineering Journal* **7**(1), 399–408.

[49] Palani, S., Kumar, B. R. and Kameswaran, P. K. [2016*b*], 'Unsteady MHD flow of an UCM fluid over a stretching surface with higher order chemical reaction', *Ain Shams Engineering Journal* **7**(1), 399–408.

[50] Patil, P., Roy, S. and Pop, I. [2012], 'Flow and heat transfer over a moving vertical plate in a parallel free stream: Role of internal heat generation or absorption', *Chemical Engineering Communications* **199**(5), 658–672.

[51] Qing, J., Bhatti, M., Abbas, M., Rashidi, M. and Ali, M. [2016], 'Entropy generation on MHD casson nanofluid flow over a porous stretching/shrinking surface', *Entropy* **18**(4), 123.

[52] Rashid, M., Khan, M. I., Hayat, T., Khan, M. I. and Alsaedi, A. [2019*a*], 'Entropy generation in flow of ferromagnetic liquid with nonlinear radiation and slip condition', *Journal of Molecular Liquids* **276**, 441–452.

[53] Rashid, M., Khan, M. I., Hayat, T., Khan, M. I. and Alsaedi, A. [2019*b*], 'Entropy generation in flow of ferromagnetic liquid with nonlinear radiation and slip condition', *Journal of Molecular Liquids* **276**, 441–452.

[54] Reddy, V. P., Kumar, R. K., Reddy, G. V., Prasad, P. D. and Varma, S. [2015*a*], 'Free convection heat and mass transfer flow of chemically reactive and radiation absorption fluid in an aligned magnetic filed', *Procedia Engineering* **127**, 575–582.

[55] Reddy, V. P., Kumar, R. K., Reddy, G. V., Prasad, P. D. and Varma, S. [2015*b*], 'Free convection heat and mass transfer flow of chemically reactive and radiation absorption fluid in an aligned magnetic filed', *Procedia Engineering* **127**, 575–582.

[56] Shafique, Z., Mustafa, M. and Mushtaq, A. [2016], 'Boundary layer flow of maxwell fluid in rotating frame with binary chemical reaction and activation energy', *Results in Physics* **6**, 627–633.

[57] Shateyi, S. [2008], 'Thermal radiation and buoyancy effects on heat and mass transfer over a semi-infinite stretching surface with suction and blowing', *Journal of Applied Mathematics* **2008**, 1–12.

[58] Shehzad, S. A., Abbasi, F. M., Hayat, T. and Alsaadi, F. [2014], 'MHD mixed convective peristaltic motion of nanofluid with joule heating and thermophoresis effects', *PLoS ONE* **9**(11), e111417.

[59] Sithole, H., Mondal, H., Magagula, V. M., Sibanda, P. and Motsa, S. [2019], 'Bivariate spectral local linearisation method (bsllm) for unsteady mhd micropolar-nanofluids with homogeneous–heterogeneous chemical reactions over a stretching surface', *International Journal of Applied and Computational Mathematics* **5**(1), 12.

[60] Sohut, N. F. H. M., Aziz, A. S. A. and Ali, Z. M. [2017], Double stratification effects on boundary layer over a stretching cylinder with chemical reaction and heat generation, *in* 'Journal of Physics: Conference Series', Vol. 890, IOP Publishing, p. 012019.

[61] Soundalgekar, V. and Murty, T. R. [1980], 'Heat transfer in flow past a continuous moving plate with variable temperature', *WaÈrme-und*

stoffuÈbertragung **14**(2), 91–93.
[62] Trefethen, L. N. [2000], *Spectral methods in MATLAB*, SIAM.
[63] Tsou, F., Sparrow, E. M. and Goldstein, R. J. [1967], 'Flow and heat transfer in the boundary layer on a continuous moving surface', *International Journal of Heat and Mass Transfer* **10**(2), 219–235.
[64] Uma, B., Swaminathan, T. N., Radhakrishnan, R., Eckmann, D. M. and Ayyaswamy, P. S. [2011], 'Nanoparticle brownian motion and hydrodynamic interactions in the presence of flow fields', *Physics of Fluids* **23**(7), 073602.
[65] van Boekel, M. A. [2008], 'Kinetic modeling of food quality: A critical review', *Comprehensive Reviews in Food Science and Food Safety* **7**(1), 144–158.
[66] Yu, Y. [2011], 'Importance of cooling rate dependence of thermoremanence in paleointensity determination', *Journal of Geophysical Research* **116**(B9).

Summary

In this chapter, the order of chemical reaction and entropy generation was studied. The system is solved numerically using the spectral quasilinearisation method. Residual errors of orders 10^{-08}, 10^{-09} and 10^{-11} for velocity, temperature and concentration respectively in less than 10 iterations were obtained. The order of chemical reaction increases temperature and solute boundary layer while decreasing the thermal boundary layer. Entropy generation for the order of chemical reaction increased while the associated Bejan number decreased with the increasing the order of the chemical reaction.

Chapter 5

Rotational nanofluids for oxytactic microorganisms with convective boundary conditions using bivariate quasi-linearization method

In this Chapter, we formulated and analysed a model for the rotational flow of a nanofluid with oxytactic microorganisms and convective boundary conditions. Oxytactic microorganisms swim up a concentration gradient. These organisms are used in beer brewery industries [102]. Yeast uses oxygen in processes such as mitochondrial development [102]. Although yeast requires oxygen for this purpose, too much of it causes the yeast to degenerate due to the toxic effect of reactive oxygen species [102]. According to Lee and Kim [103] when the swimming microorganisms accumulate at the top layer of the fluid the density of this layer becomes greater than that of the fluid then the plumes containing microorganisms will fall to the bottom of the chamber. Such a transport mechanism delivers optimal amounts of oxygen to the bottom of the chamber without causing the degradation of microorganisms. For this problem, BSQLM was used to solve the boundary value system.

J. Cent. South Univ. (2020) 27: 824−841
DOI: https://doi.org/10.1007/s11771-020-4334-x

Springer

Rotational nanofluids for oxytactic microorganisms with convective boundary conditions using bivariate spectral quasi-linearization method

Mlamuli DHLAMINI[1], Hiranmoy MONDAL[2], Precious SIBANDA[1], Sandile MOTSA[1, 3]

1. School of Mathematics, Statistics and Computer Science, University of Kwa Zulu-Natal, Private Bag X01, Scottsvile, Pietermaritzburg-3209, South Africa;
2. Department of Mathematics, Brainware University, 398 Ramkrishnapur Road, Barasat, North 24 Parganas, Kolkata-700125, India;
3. Department of Mathematics, University of Swaziland, Private Bag 4, Kwaluseni, Swaziland

Abstract: In this study, we considered the three-dimensional flow of a rotating viscous, incompressible electrically conducting nanofluid with oxytactic microorganisms and an insulated plate floating in the fluid. Three scenarios were considered in this study. The first case is when the fluid drags the plate, the second is when the plate drags the fluid and the third is when the plate floats on the fluid at the same velocity. The denser microorganisms create the bioconvection as they swim to the top following an oxygen gradient within the fluid. The velocity ratio parameter plays a key role in the dynamics for this flow. Varying the parameter below and above a critical value alters the dynamics of the flow. The Hartmann number, buoyancy ratio and radiation parameter have a reverse effect on the secondary velocity for values of the velocity ratio above and below the critical value. The Hall parameter on the other hand has a reverse effect on the primary velocity for values of velocity ratio above and below the critical value. The bioconvection Rayleigh number decreases the primary velocity. The secondary velocity increases with increasing values of the bioconvection Rayleigh number and is positive for velocity ratio values below 0.5. For values of the velocity ratio parameter above 0.5, the secondary velocity is negative for small values of bioconvection Rayleigh number and as the values increase, the flow is reversed and becomes positive.

Key words: bioconvection; oxytactic microorganisms; velocity ratio; rotational nanofluid; bivariate spectral quasilinearization method (BSQLM)

Cite this article as: Mlamuli DHLAMINI, Hiranmoy MONDAL, Precious SIBANDA, Sandile MOTSA. Rotational nanofluids for oxytactic microorganisms with convective boundary conditions using bivariate spectral quasi-linearization method [J]. Journal of Central South University, 2020, 27(3): 824−841. DOI: https://doi.org/10.1007/s11771-020-4334-x.

1 Introduction

The study of boundary layer flow has received a lot of attention since the ground-breaking study by Lewig Prandtl in 1904. Many flows of interest occur within a boundary layer, and often in conjunction with heat and/or mass transport.

In many industrial processes such as the cooling of electronic devices, solar energy collectors, thermal insulation, underground nuclear disposal and chemical processes, heat transfer enhancement is of paramount importance [1]. Of late nanofluids have been identified as the best choice of fluids for heat transfer processes. The term nanofluid refers to a colloidal suspension of submicronic solid particles. A typical nanoparticle is a stable metal (Al, Cu, Ag, Au, Fe), oxide (Al_2O_3,

Received date: 2018-11-05; **Accepted date:** 2019-04-26
Corresponding author: Hiranmoy MONDAL, PhD, Associate Professor; Tel: +91-9434633158; E-mail: hiranmoymondal@yahoo.co.in; ORCID: 0000- 0002-9153-300X

CuO, TiO_2, SiO_2), carbide (SiC), nitrate (AlN, SiN), or non-metal (graphite) with sizes ranging from 1 to 100 nm. The base fluid normally is a conductive fluid, such as water, ethylene glycol, oil, polymer or bio-fluids [1]. The flow of a rotating fluid is encountered in geothermal flows [2]. It is also the reason for the secular variations in geomagnetic fields [3]. In rotating fluids, the Coriolis force is more prominent than the viscous and inertial forces[2]. The viscous forces are balanced by the Coriolis forces instead of the inertial forces. According to HIDE [4, 5], in the study of geophysical flows a key parameter is the Rossby number. The influence of the rotation is said to be weak if the Rossby number is significantly less than unity, and dominant if the Rossby number is significantly larger than unity. The study of rotational viscous fluids sheds some light on the body forces that act on particles immersed in the fluid. This area of study continues to receive considerable attention because of a variety of industrial applications [6]. The motion of rigid particles or drops in rotating fluids is encountered in a number of industrial processes such as in the manufacturing of hallow shells, separation of minerals, extraction of proteins and in waste water treatment [7−11].

Nanofluid bioconvection gives rise to spontaneous pattern formation and density stratification. This is a phenomenon that occurs when instability is induced by the interaction of the swimming of denser self-propelled microorganisms, nanoparticles and buoyancy forces [1, 12]. Bioconvection arises in biological systems, biotechnology such as the mass transport enhancement in microscale mixing and the synthesis of biosensors [13]. Some of microorganisms that normally give rise to bioconvection include gravitaxis, gyrotaxis and oxytaxis. This study considers the movement of oxytactic microorganisms. These are bacteria that consume oxygen such as *Bacillussubtilis*. They swim up the oxygen concentration gradient. KUZNETSOV [12] considered a novel nanofluid with oxytactic microorganisms. The bacteria are oxygen consumers and swim towards the top region when this is exposed to the elements. LEE et al [14] investigated falling bacteria plumes caused by bioconvection. Their study was an extension of work in Ref. [15]. In both studies the falling plumes are attributed to the instability of bacteria-rich boundary layer close to the surface that is denser than the rest of the fluid. The falling plumes transport bacteria and oxygen from the upper boundary layer to the lower region of the chamber, which is depleted of both bacteria and oxygen. The use of microorganisms in delivering oxygen is encountered in industrial processes such as aerobic fermentation [16]. Other uses of microorganisms in industrial processes are encountered in bio-reactors [17].

Bioconvection has been studied by several researchers [18−25]. The current study incorporates a rotational electrically conducting nanofluid with an applied magnetic field to the study of bioconvection induced by oxytactic microorganisms. We also consider the impact of varying the velocity of the plate relative to the fluid velocity and the influence of fluid and flow parameters.

2 Mathematical analysis

The physical model and coordinate system is given in Figure 1, where x, y and z are Cartesian coordinates and u, v and w are the velocity components in the corresponding directions. We consider an insulated flat plate which coincides with the plane z=0. The plate moves with a velocity U_1 in the x direction in a viscous, incompressible, electrically conducting nanofluid that is rotating with constant angular velocity Ω about the x-axis containing oxytaxis microorganisms. There is also a uniform free stream velocity U_2 parallel to the x-axis. A magnetic field B_0 is applied along the z-axis. The temperature and concentration of nanoparticles and free stream microorganisms are kept at constant T_w, C_w and n_w while in the free stream these are assumed to be T_∞, C_∞ and n_∞ respectively. The effects of the Coriolis force and Hall currents give rise to a force in the y-direction, which induces cross flow [2]. The set of equations modeling the flow in a rotating frame of reference with Maxwells electromagnetic equations are given by

$$\frac{\partial u}{\partial x}+\frac{\partial v}{\partial y}=0 \tag{1}$$

$$u\frac{\partial u}{\partial x}+w\frac{\partial u}{\partial z}-2\Omega v=-\frac{1}{\rho}\frac{\partial p}{\partial x}+\upsilon\frac{\partial^2 u}{\partial z^2}+\frac{\sigma B_0^2}{\rho(1+N^2)}\cdot$$

$$(N\upsilon - u)+(1 - C_\infty)\rho f_\infty g\beta(T - T_\infty) - \frac{(\rho_p - \rho_f)}{\rho_f} g(C - C_\infty) - \frac{\gamma g(\rho_p - \rho_f)}{\rho_f} \cdot (n - n_\infty) \quad (2)$$

$$u\frac{\partial v}{\partial x} + w\frac{\partial v}{\partial z} + 2\Omega u = -\frac{1}{\rho}\frac{\partial p}{\partial y} + \upsilon\frac{\partial^2 v}{\partial z^2} + \frac{\sigma B_0^2}{\rho(1+N^2)}(Nu+v) \quad (3)$$

$$u\frac{\partial T}{\partial x} + w\frac{\partial T}{\partial z} = \alpha_m\frac{\partial^2 T}{\partial z^2} + \frac{16\sigma^*}{3\rho C_p}\frac{\partial^2 T}{\partial z^2} + \tau\left[D_B\frac{\partial T}{\partial z}\frac{\partial C}{\partial z} + \frac{D_T}{T_\infty}\left(\frac{\partial T}{\partial z}\right)^2\right] \quad (4)$$

$$u\frac{\partial C}{\partial x} + w\frac{\partial C}{\partial z} = D_B\frac{\partial^2 C}{\partial z^2} + \frac{D_T}{T_\infty}\frac{\partial^2 T}{\partial z^2} \quad (5)$$

$$u\frac{\partial n}{\partial x} + w\frac{\partial n}{\partial z} + \frac{bW_c}{\Delta C}\frac{\partial}{\partial z}\left(n\frac{\partial n}{\partial z}\right) = D_n\frac{\partial^2 n}{\partial z^2} \quad (6)$$

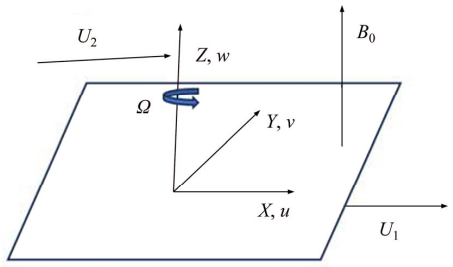

Figure 1 Flow configuration and coordinate system

The boundary conditions for Eqs. (1)−(6) are given in form:

$$u(x, 0)=U_1, v(x, 0)=0, w(x, 0)=0,$$
$$-k_f\frac{\partial T}{\partial z} = h_f(T_w - T), D_z\frac{\partial C}{\partial z} + \frac{D_T}{T_\infty}\frac{\partial T}{\partial z} = 0,$$
$$n=n_w \quad \text{at} \quad z=0,$$
$$u \to U_2, v \to 0, T \to T_\infty, C \to C_\infty, n \to n_\infty, \quad \text{as} \quad z \to \infty \quad (7)$$

where ρ is the density of the base fluid; υ is the kinematic viscosity; σ is the electrical conductivity of the fluid; N is the Hall parameter; g is the gravitational acceleration; β is the volumetric coefficient of expansion for the fluid; ρ_p is the density of the nanoparticles; ρ_f is the density of the nanofluid; γ is the average volume of the microorganisms; ρ_m is the density of microorganisms; α_m is the thermal diffusivity coefficient for microorganisms; τ is the ratio of heat capacitance of nanoparticles to the base fluid; D_B is the Brownian diffusion coefficient; D_T is the thermophoretic diffusion coefficient; σ^* is Stephan Boltzman constant; C_p is the specific heat capacity of the fluid at constant pressure; b is the chemotaxis constant; W_c is the maximum cell swimming speed (bW_c is assumed to be constant); D_n is the microorganism diffusivity; k_f is the thermal conductivity of the solid and h_f is the convective heat transfer coefficient.

Far from the surface, the pressure gradients in the x and y directions, $-\rho^{-1}\rho_x$ and $-\rho^{-1}\rho_y$, must balance the Lorentz and Coriolis forces [2] and are given by the relations:

$$-\frac{1}{\rho}\frac{\partial p}{\partial x} = \frac{\sigma B_0^2}{\rho(1+N^2)}U_2,$$
$$-\frac{1}{\rho}\frac{\partial p}{\partial y} = 2\Omega U_2 + \frac{\sigma B_0^2}{\rho(1+N^2)}U_2 \quad (8)$$

In this study we excluded the effect of viscous dissipation and Joule heating. Viscous dissipation is the heat generated in a fluid due to the frictional forces between fluid layers as they slide over each other. Joule/Ohmic heating is the heat generated due to resistance of a current as it passes through a medium. The effect of both viscous and Joule heating has been studied extensively and is well documented in Refs. [26, 27]. Since we assumed that we have a heated plate, we therefore assume that it is the major contributor of heat and all other heat sources are negligible.

3 Transformation of equations

The following variables are used to transform the system given by Eqs. (1)−(6),

$$\eta = z\sqrt{\frac{U_0}{\upsilon x}}, \psi = \sqrt{U_0\upsilon x}f(\xi, \eta), \xi = \frac{\Omega x}{U_0},$$
$$v = U_0 g(\xi, \eta), U_0 = U_1+U_2, S = \frac{U_1}{U_0},$$
$$\theta(\xi, \eta) = \frac{T - T_\infty}{T_w - T_\infty}, \varphi(\xi, \eta) = \frac{C - C_\infty}{C_w - C_\infty},$$
$$\chi(\xi, \eta) = \frac{n - n_\infty}{n_w - n_\infty} \quad (9)$$

The velocity components $u = \frac{\partial\psi}{\partial z}$ and $w = -\frac{\partial\psi}{\partial x}$ are given as

$$u = U_0 f'(\xi, \eta),$$

$$w = -\sqrt{\upsilon\Omega\xi}\left[\frac{\partial f}{\partial \xi} + \frac{1}{2\xi}\left(f - \eta f'\right)\right] \tag{10}$$

On using Eqs. (8)−(9), Eqs. (2) − (6) and the boundary conditions (7) are transformed into the following boundary value problem:

$$f''' + \frac{1}{2} ff'' + 2\xi g - \frac{M}{1+N^2}\xi(f' - 1 + S - Ng) + Gr\xi(\theta - Nr\varphi - Rb\chi) = \xi\left(f'\frac{\partial f'}{\partial \xi} - f''\frac{\partial f}{\partial \xi}\right) \tag{11}$$

$$g'' + \frac{1}{2} fg' + 2\xi(1 - S - f') - \frac{M}{1+N^2}\xi \cdot \left[g + N(f' + S - 1)\right] = \xi\left(f'\frac{\partial g}{\partial \xi} - g'\frac{\partial f}{\partial \xi}\right) \tag{12}$$

$$\left(1 + \frac{4}{3}Ra\right)\theta'' + \frac{1}{2}Prf\theta' + Nb\theta'\varphi' + Nt\theta'^2 = Pr\xi\left(f'\frac{\partial \theta}{\partial \xi} - \theta'\frac{\partial f}{\partial \xi}\right) \tag{13}$$

$$\varphi'' + \frac{1}{2}Scf\varphi' + \frac{Nt}{Nb}\theta'' = ScPr\xi\left(f'\frac{\partial \varphi}{\partial \xi} - \varphi'\frac{\partial f}{\partial \xi}\right) \tag{14}$$

$$\chi'' + \frac{1}{2}Sbf\chi' - Pb\left[\chi'\varphi' + (\tau_0 + \chi)\varphi''\right] = SbPr\xi\left(f'\frac{\partial \chi}{\partial \xi} - \chi'\frac{\partial f}{\partial \xi}\right) \tag{15}$$

where the prime denotes differentiation with respect to η. The corresponding boundary conditions (7) are transformed as

$$f'(\xi, 0) = S,\ 2\xi\frac{\partial f(\xi, 0)}{\partial \xi} + f(\xi, 0) = 0,\ f'(\xi, 0) \to 1 - S \tag{16}$$

$$g(\xi, 0) = 0,\ g(\xi, \infty) \to 0 \tag{17}$$

$$\theta'(\xi, 0) = -Bi\xi^{\frac{1}{2}}(1 - \theta(\xi, 0)),\ \theta(\xi, \infty) \to 0 \tag{18}$$

$$Nb\varphi'(\xi, 0) + Nt\theta'(\xi, 0) = 0,\ \varphi(\xi, \infty) \to 0 \tag{19}$$

$$\chi(\xi, 0) = 1,\ \chi(\xi, \infty) \to 0 \tag{20}$$

The parameters in the above differential equations and associated boundary conditions are defined as

$$M = \frac{\sigma B_0^2}{\rho U_0 \Omega},\ Gr = \frac{(1 - C_\infty)\rho f_\infty g\beta\Delta T}{U_0\Omega},$$

$$Nr = \frac{(\rho_p - \rho_f)\Delta C}{(1 - C_\infty)\rho f_\infty g\beta\Delta T},\ Nb = \frac{\tau D_B \Delta C}{\alpha_m},$$

$$Rb = \frac{\gamma(\rho_m - \rho_f)(n_w - n_\infty)}{\beta\rho_f \rho f_\infty (1 - C_\infty)\Delta T},\ Pr = \frac{\upsilon}{\alpha},$$

$$Ra = \frac{4\sigma^*}{\rho C_p \alpha},\ Nt = \frac{\tau D_T \Delta T}{\alpha_m T_\infty},\ Sc = \frac{\upsilon}{D_B},$$

$$Sb = \frac{\upsilon}{D_n},\ Pb = \frac{bw_c}{D_n},\ \tau_0 = \frac{n_\infty}{n_w - n_\infty},$$

$$Bi = \frac{h_f}{\kappa_f}\sqrt{\frac{\upsilon}{\Omega}},\ Re_x = \frac{U_0 x}{\upsilon} \tag{21}$$

where M is the modified Hartmann number; Gr is the Grashof number; Nr is the buoyancy ratio; Rb is the bioconvection Rayleigh number; Pr is the Prandtl number; S is the velocity ratio; Ra is the radiation parameter; Nb is the Brownian motion parameter; Nt is thermophoresis parameter; Pb is the bioconvection Peclet number; τ_0 is the constant microorganisms concentration difference parameter; Sc is the Schmidt number; Sb is the bioconvection Schmidt number; Re_x is the Reynolds number; Bi is the Biot number.

4 Momentum, heat and mass transfer coefficients

The parameters that are of interest are the skin friction coefficient, C_f, which measures the shear stress on the surface, the Nusselt number, Nu, which is the ratio of convective to conductive heat transfer across (normal to) the boundary, the Sherwood number, Sh, which is the ratio of the convective mass transfer to the rate of diffusive mass transport and the local density number of the motile microorganisms, Nn, which is the ratio of the convective microorganism transfer to the rate of diffusive microorganism transport.

The local skin friction coefficients in the x and y directions are given as

$$C_{fx} = \frac{\tau_{wx}}{\frac{1}{2}\rho U_0^2} = 2(Re_x)^{-\frac{1}{2}} f''(\xi, 0),$$

$$C_{fy} = \frac{\tau_{wy}}{\frac{1}{2}\rho U_0^2} = 2(Re_y)^{-\frac{1}{2}} g'(\xi, 0) \tag{22}$$

The local Nusselt number, local Sherwood number and local density number of the motile microorganisms are given by

$$Nu_x = \frac{xq_w}{\kappa(T_w - T_\infty)} = -Re_x^{\frac{1}{2}}\theta'(\xi, 0),$$

$$Sh_x = \frac{xq_w}{D_B(C_w - C_\infty)} = -\left(1+\frac{4}{3}Ra\right)Re_x^{\frac{1}{2}}\varphi'(\xi, 0),$$

$$Nn_x = \frac{xq_n}{D_n(n - n_\infty)} = -Re_x^{\frac{1}{2}}\chi'(\xi, 0) \quad (23)$$

where

$$\tau_{wx} = \mu\left(\frac{\partial u}{\partial z}\right)_{|z=0}, \ \tau_{wy} = \mu\left(\frac{\partial v}{\partial z}\right)_{|z=0},$$

$$q_w = -\left(\kappa + \frac{16\sigma^* T_\infty^3}{3K^*\kappa}\right)\left(\frac{\partial T}{\partial z}\right)_{|z=0},$$

$$q_m = -D_B\left(\frac{\partial C}{\partial z}\right)_{|z=0}, \ q_n = -D_n\left(\frac{\partial n}{\partial z}\right)_{|z=0}.$$

5 Numerical solution using bivariate spectral quasi-linearization method

The two-variable nonlinear boundary value problem given by Eqs. (11)−(15) together with the boundary conditions Eqs. (16)−(20) was solved numerically using the bivariate spectral quasilinearization method (BSQLM). The choice of using a spectral-based method is that they require less grid points yet giving accurate results and take less computational time compared to other methods [28, 29]. The flow domain and time interval given by $\eta \in [0, L_x]$ and $\xi \in [0, L_t]$ are transformed to $x \in [-1, 1]$ and $t \in [-1, 1]$ using the linear transformations $\eta \in L_x(x+1)/2$ and $\xi \in L_t(x+1)/2$ respectively. The solution is approximated using Lagrange interpolation polynomial of the form:

$$u(x, t) = \sum_{i=0}^{N_x}\sum_{j=0}^{N_t}\hat{u}(x_i, t_j)L_i(x)L_j(t) \quad (24)$$

where $u(x, t)$ is interpolated at selected grid points both in the x and t directions. The grid points are defined as

$$\{x_i\} = \left\{\cos\left(\frac{\pi i}{N_x}\right)\right\}_0^{N_x}, \ \{t_j\} = \left\{\cos\left(\frac{\pi j}{N_t}\right)\right\}_0^{N_t} \quad (25)$$

The functions $L_i(x)$ are the Lagrange cardinal polynomials given by

$$L_i(x) = \prod_{i=0, i\neq j}^{N_x}\frac{x - x_k}{x_i - x_k} \quad (26)$$

where

$$L_i(x) = \delta_{ik} = \begin{cases} 0, & \text{if } x \neq k \\ 1, & \text{if } x = k \end{cases} \quad (27)$$

$L_j(t)$ is also defined in a similar manner. We begin by defining the functions F, G, Θ, Φ and X for Eqs. (10)−(14) as

$$F = f''' + \frac{1}{2}ff'' + 2\xi g - \frac{M}{1+N^2}\xi(f' - 1 + S - Ng) + Gr\xi(\theta - Nr\varphi - Rb\chi) - \xi\left(f'\frac{\partial f'}{\partial \xi} - f''\frac{\partial f}{\partial \xi}\right) \quad (28)$$

$$G = g'' + \frac{1}{2}fg' + 2\xi(1 - S - f') - \frac{M}{1+N^2}\xi \cdot \left[g + N(f' + S - 1)\right] - \xi\left(f'\frac{\partial g}{\partial \xi} - g'\frac{\partial f}{\partial \xi}\right) \quad (29)$$

$$\Theta = \left(1+\frac{4}{3}Ra\right)\theta'' + \frac{1}{2}Prf\theta' + Nb\theta'\varphi' + Nt\theta'^2 - Pr\xi\left(f'\frac{\partial \theta}{\partial \xi} - \theta'\frac{\partial f}{\partial \xi}\right) \quad (30)$$

$$\Phi = \varphi'' + \frac{1}{2}Scf\varphi' + \frac{Nt}{Nb}\theta'' - ScPr\xi\left(f'\frac{\partial \varphi}{\partial \xi} - \varphi'\frac{\partial f}{\partial \xi}\right) \quad (31)$$

$$X = \chi'' + \frac{1}{2}Sbf\chi' - Pb\left[\chi'\varphi' + (\tau_0 + \chi)\varphi''\right] - SbPr\xi\left(f'\frac{\partial \chi}{\partial \xi} - \chi'\frac{\partial f}{\partial \xi}\right) \quad (32)$$

We construct the solution using the iterative process given by Eqs. (28)−(32):

$$a_{0,r}f'''_{r+1} + a_{1,r}f''_{r+1} + a_{2,r}f'_{r+1} + a_{3,r}f_{r+1} + a_{4,r}\frac{\partial f'_{r+1}}{\partial \xi} + a_{5,r}\frac{\partial f_{r+1}}{\partial \xi} + a_{6,r}\theta_{r+1} + a_{7,r}\varphi_{r+1} + a_{8,r}g_{r+1} + a_{9,r}\chi_{r+1} - F = R_f \quad (33)$$

$$b_{0,r}\theta''_{r+1} + b_{1,r}\theta'_{r+1} + b_{2,r}\frac{\partial \theta_{r+1}}{\partial \xi} + b_{3,r}f'_{r+1} + b_{4,r}f_{r+1} + b_{5,r}\frac{\partial f_{r+1}}{\partial \xi} + b_{6,r}\varphi'_{r+1} - \Theta = R_\theta \quad (34)$$

$$c_{0,r}\varphi''_{r+1} + c_{1,r}\varphi'_{r+1} + c_{2,r}\frac{\partial \varphi_{r+1}}{\partial \xi} + c_{3,r}f'_{r+1} + c_{4,r}f_{r+1} + c_{5,r}\frac{\partial f_{r+1}}{\partial \xi} + c_{6,r}\theta''_{r+1} - \Phi = R_\varphi \quad (35)$$

$$d_{0,r}g''_{r+1} + d_{1,r}g'_{r+1} + d_{2,r}g_{r+1} + d_{3,r}\frac{\partial g_{r+1}}{\partial \xi} + d_{4,r}f'_{r+1} + d_{5,r}f_{r+1} + d_{6,r}\frac{\partial f_{r+1}}{\partial \xi} - G = R_g \quad (36)$$

$$e_{0,r}\chi''_{r+1} + e_{1,r}\chi'_{r+1} + e_{2,r}\chi_{r+1} + e_{3,r}\frac{\partial \chi_{r+1}}{\partial \xi} + e_{4,r}f'_{r+1} +$$

$$e_{5,r}f_{r+1}+e_{6,r}\frac{\partial f_{r+1}}{\partial\xi}+e_{7,r}\varphi''_{r+1}+e_{8,r}\varphi'_{r+1}-X=R_{\chi} \tag{37}$$

subjected to the boundary conditions

$$f'_{r+1}(\xi,0)=S,\ 2\xi\frac{\partial f_{r+1}(\xi,0)}{\partial\xi}+f_{r+1}(\xi,0)=0,$$
$$f'_{r+1}(\xi,\infty)\ \to\ 1-S \tag{38}$$

$$g_{r+1}(\xi,0)=0,\ g_{r+1}(\xi,\infty)\ \to\ 0 \tag{39}$$

$$\theta'_{r+1}(\xi,0)=-Bi\xi^{\frac{1}{2}}(1-\theta_{r+1}(\xi,0)),$$
$$\theta_{r+1}(\xi,\infty)\ \to\ 0 \tag{40}$$

$$Nb\varphi'_{r+1}(\xi,0)+Nt\theta'_{r+1}(\xi,0)=0,$$
$$\varphi_{r+1}(\xi,\infty)\ \to\ \infty \tag{41}$$

$$\chi_{r+1}(\xi,0)=1,\ \chi_{r+1}(\xi,\infty)\ \to\ 0 \tag{42}$$

The coefficients in Eqs. (33)− (37) are given as

$$a_{0,r}=1,\ a_{1,r}=\frac{1}{2}f_r+\xi\frac{\partial f_r}{\partial\xi},$$
$$a_{2,r}=-\frac{M}{1+N^2}\xi-\xi\frac{\partial f'_r}{\partial\xi},\ \cdots$$
$$a_{10,r}=-Gr\xi Rb;$$

$$b_{0,r}=1+\frac{4}{3}Ra,\ b_{1,r}=\frac{1}{2}Prf_r+Nb\varphi'_r+2Nt\theta'_r+$$
$$Pr\xi\frac{\partial f_r}{\partial\xi},\ \cdots,\ b_{6,r}=Nb\theta'_r$$

$$c_{0,r}=1,\ c_{1,r}=\frac{1}{2}Scf_r+Sc\xi\frac{\partial f_r}{\partial\xi},$$
$$c_{2,r}=-Sc\xi f'_r,\ \cdots,\ c_{6,r}=\frac{Nt}{Nb} \tag{43}$$

$$d_{0,r}=1,\ d_{1,r}=\frac{1}{2}f_r+\xi\frac{\partial f_r}{\partial\xi},\ d_{2,r}=-\frac{M}{1+N^2}\xi,$$
$$d_{3,r}=-\xi f'_r,\ d_{4,r}=-2\xi-\frac{MN}{1+N^2}\xi-\xi\frac{\partial g_r}{\partial\xi},$$
$$d_{5,r}=\frac{1}{2}g'_r,\ d_{6,r}=Nb\theta'_r;$$
$$e_{0,r}=1,\ e_{1,r}=\frac{1}{2}Sbf_r-Pb\varphi'_r+Sb\xi\frac{\partial f_r}{\partial\xi},\ \cdots,$$
$$e_{6,r}=Sb\xi\chi'_r,\ e_{7,r}=-Pb(\tau_0+\chi_r),\ e_{8,r}=-Pb\chi'_r.$$

The initial guess functions are selected in such a way that they satisfy the boundary conditions at ξ=0. These are chosen as

$$f_0(\eta)=\eta(1-S)+(1-2S)(e^{-\eta}-1),$$
$$\theta_0(\eta)=\frac{Bi}{1+Bi}e^{-\eta},\ \varphi_0(\eta)=-\frac{Nt}{Nb}\frac{Bi}{1+Bi}e^{-\eta},$$
$$g_0(\eta)=\eta e^{-\eta},\ \chi_0(\eta)=e^{-\eta} \tag{44}$$

For a detailed explanation on how the resulting matrices and corresponding boundary conditions are implemented on a MATLAB code, one can refer to work by MOTSA et al [28, 29].

Table 1 gives parameter values that were used in similar studies.

We validate the accuracy and convergence of

Table 1 Parameter values and their source

Parameter	Mutuku	Khan	Iqbal	Takhar	Others	Current study
Hartmann number, *M*	1,1.5,3	5−0, 1				2
Hall parameter, *N*				0, 0.5, 1		1
Grashof number, *Gr*	0, 5, 10					5
Bioconvective Rayleigh number, *Rb*	0.1−0.5, 0.9	0.5−0.10.3	0.1		0.1, 0.5	0.1
Buoyancy ratio, *Nr*	0.1−0.3, 1.4, 1.8	0.1−0.3	0.1			0.1
Prandtl number, *Pr*		6.2	1, 2, 3, 4			7
Velocity ratio, *S*				0.25		0.25, 0.75
Radiation parameter, *Rd*					2	2
Brownian motion, *Nb*	0.1−2, 6, 10	0.1−0.3, 0.5	0.5−1, 1.5, 2			0.3
Thermophoresis, *Nt*	0.1−2, 6, 10	0.1−0.2, 0.9, 1.1	0.5−0.7			0.5
Schmidt number, *Sc*	5−5.5, 6, 6.5	10	1.6−1.82, 3			5
Bioconvective Schmidt number, *Sb*	1	10				5
Bioconvective Peclet number, *Pb*	1	1−3, 5	0.1			1
Constant, τ_0	0.1−5, 10	0.2				0.2
Biot number, *Bi*			13		0.1−10	0.1

our numerical scheme by performing an error analysis. We plot the norm of residual errors in the variables against the number of iterations. The norm of residual errors for all the variables was less than 10^{-10} after 8 iterations. This shows that the BSQLM is an appropriate scheme for solving the resulting boundary value problem. Figure 2 shows the norm of residual errors for different variables at different number of iterations.

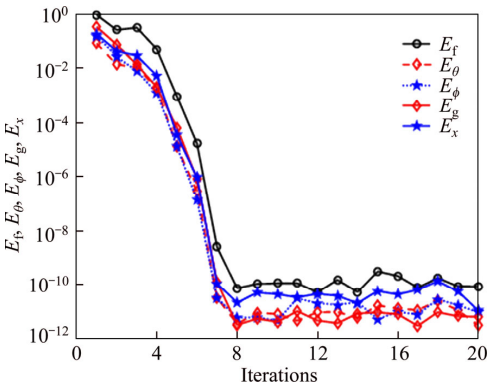

Figure 2 Norm of residual at different iterations

6 Discussion and results

In this section we discuss the results of our findings. We investigate the impact that certain key parameters have on the physical, thermal and concentration properties of the flow. We analyze the variation of the local skin friction coefficient, Nusselt number, Sherwood number and density of motile microorganisms in Table 2.

We investigate the influence of the velocity ratio parameter S in Figure 3. It gives the relative

Table 2 Variation of local skin friction coefficient

S	M	Nr	Rb	Pb	$-f''(\xi, 0)$	$-g'(\xi, 0)$	$-\theta'(\xi, 0)$	$-\phi'(\xi, 0)$	$-\chi'(\xi, 0)$
0.1	2	0.1	0.1	1	−1.181869	0.089125	−0.041784	−0.825765	0.902139
0.25					−0.744698	0.089247	−0.046417	−0.511072	0.883251
0.5					−0.014300	0.089415	−0.056110	0.008863	0.840413
0.75					0.711900	0.089466	−0.069948	0.527703	0.774908
0.9					1.145210	0.089275	−0.084543	0.839662	0.701142
0.25	1				−0.648145	0.089088	−0.045981	−0.500966	0.870135
	3				−0.832141	0.089367	−0.046780	−0.528194	0.893884
0.75	1				0.609104	0.089644	−0.069717	0.512588	0.798809
	2				0.711900	0.089466	−0.069948	0.527703	0.774908
	3				0.804037	0.089308	−0.070131	0.544382	0.754179
0.25		0.3			−0.738647	0.089231	−0.046431	−0.515598	0.881298
		0.5			−0.732591	0.089216	−0.046446	−0.520148	0.879335
0.75		0.1			0.711900	0.089466	−0.069948	0.527703	0.774908
		0.3			0.718898	0.089443	−0.070138	0.521513	0.771126
		0.5			0.725915	0.089420	−0.070333	0.515263	0.767295
0.25			0.3		−0.407902	0.088790	−0.045432	−0.621986	0.829564
			0.5		−0.054057	0.088204	−0.044022	−0.750653	0.767582
0.75			0.1		0.711900	0.089466	−0.069948	0.527703	0.774908
			0.3		1.072758	0.088793	−0.072899	0.380943	0.667118
			0.5		1.480640	0.087539	−0.079719	0.155358	0.479963
0.25				0.1	−0.746320	0.089249	−0.046420	−0.510320	0.925332
				2	−0.742886	0.089243	−0.046414	−0.511915	0.836762
0.75				0.1	0.709670	0.089470	−0.069917	0.528825	0.844309
				1	0.711900	0.089466	−0.069948	0.527703	0.774908
				2	0.714401	0.089461	−0.069982	0.526441	0.698102

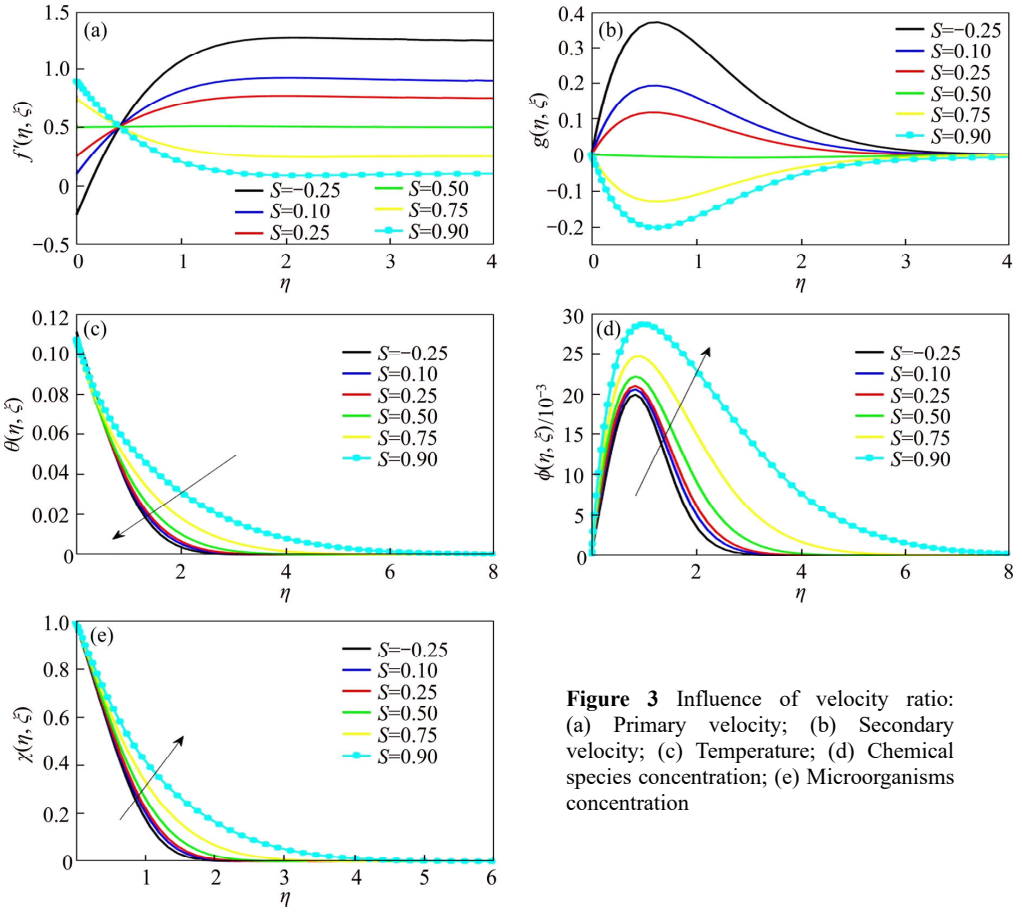

Figure 3 Influence of velocity ratio: (a) Primary velocity; (b) Secondary velocity; (c) Temperature; (d) Chemical species concentration; (e) Microorganisms concentration

velocity of the plate to the velocity of the fluid. A value of zero corresponds to the case of a fluid flowing past a stationary plate. A value of 1 corresponds to the case of a plate moving in a stationary fluid. 0<S<0.5 corresponds the case of a fluid dragging the plate and 0.5<S<1 corresponds to the case of the plate dragging the fluid. Although the phenomenon is not yet fully understood, we observed that increasing the velocity of the plate increases temperature, chemical species concentration and the microorganisms in the boundary layer. This could be due to the fact that as the plate is moving in the fluid so does the boundary layer with respect to space. Our results for both the primary and secondary velocities are consistent with results in Ref. [2]. For values of S below 0.5, the primary velocity increases and the secondary velocity is positive. The primary velocity remains constant while the secondary velocity vanishes at values equal to 0.5. At values greater than 0.5, the primary velocity decreases while the secondary velocity reverses direction and becomes negative.

We analyze the effect of the Hartmann number on the fluid's velocity in Figure 4. The Hartmann number is a dimensionless parameter defined as the ratio of electromagnetic force to the viscous force. An increase in the Hartmann number for the case when the plate is moving relatively faster than the fluid (S>0.5) results in a decrease in the fluid's primary velocity in the boundary layer. This is due to an increase in the Lorentz force that tends to oppose the flow resulting in a frictional drag [30]. An opposite phenomenon is observed for the case when S<0.5, that is, an increase in the Hartmann number results in a velocity increase for the primary flow close to the surface. The Hartmann number causes decrease in the secondary velocity; however, the flow is reversed for values above and below the critical value of 0.5.

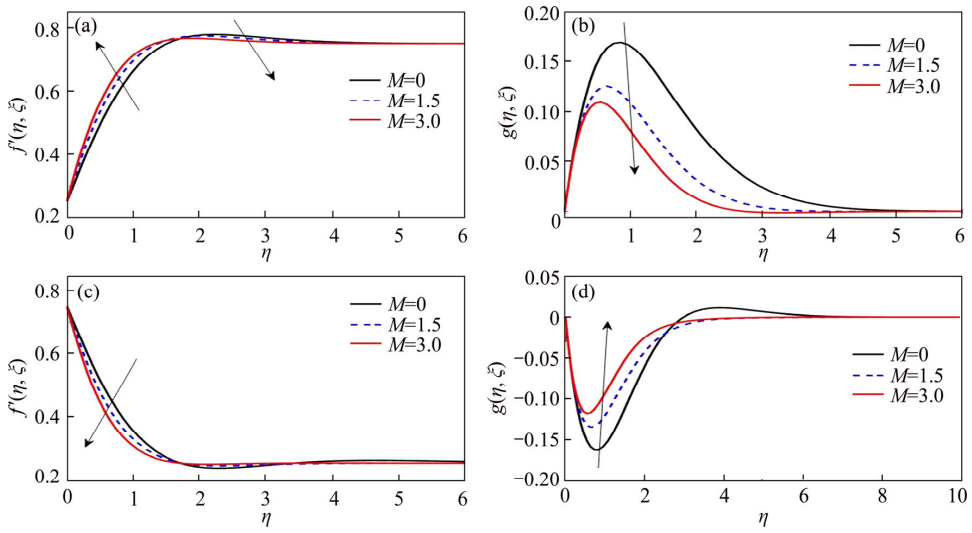

Figure 4 Effect of Hartmann number on fluid's velocity: (a) Primary velocity for S=0.25; (b) Secondary velocity for S=0.25; (c) Primary velocity for S=0.75; (d) Secondary velocity for S=0.75

The influence of the Hartmann number on other parameters is depicted in Figure 5. Our results for the case when S>0.5 are consistent with results found in Ref. [1] that it causes an increase in the temperature chemical species concentration and motile microorganisms. A reverse effect is observed for values of S<0.5.

The buoyancy ratio parameter Nr is analyzed in Figure 6. The buoyancy ratio parameter measures the influence of free and forced convection [31]. In free convection the flow is due to a temperature gradient whereas in forced convection an external device like a pump is used to generate or maintain the flow. It is noticed that for S>0.5 an increase in the buoyancy ratio parameter results in a decrease in both the primary and secondary velocities. An increase in the temperature, chemical species and microorganism concentration is also associated with increasing the buoyancy ratio parameter, results consistent with results in Ref. [32]. In fact, the increase in the chemical species volume fraction is attributed to decrease in the velocity of the fluid [20]. All other parameters behave in a similar manner for values of S<0.5 except the secondary velocity that is in the reverse direction.

The impact of Hall parameter N is assessed in Figure 7. The Hall effect is the production of a voltage difference across an electrical conductor to an applied magnetic field. The Hall parameter is defined to be the ratio of induced electrical field to the applied magnetic field. An increase in the Hall parameter results in an increase in the velocity profile [33, 34]. This is attributed to the fact that the magnetic field on the velocity damping reduces as the Hall parameter is increased. However, there are some studies that reported results are contrary to this [2, 35]. Our results show an increase in the velocity profile for the secondary flow and the primary velocity for the case when S<0.5. When S>0.5, the primary velocity decreases with increasing values of the Hall parameter. The phenomenon responsible for the observed trend is not fully understood.

The impact of thermal radiation is analyzed in Figure 8. The primary velocity increases with increasing values of the thermal radiation parameter for all values of S. This is because an increase in the thermal radiation parameter leads to conduction dominating absorption radiation, resulting in an increase in buoyancy force [33]. Also, an increase in thermal radiation parameter leads to an increase in the fluid's temperature, causing a decrease of the fluid's viscosity making it easier to flow. The secondary velocity increases with increasing values of thermal radiation for values of S>0.5. The result is consistent with result in Ref. [33]. However, for S<0.5, our results show a decrease in the secondary velocity for increasing values of radiation parameter in the reverse direction. Temperature, concentration of chemical species and microorganisms are plotted

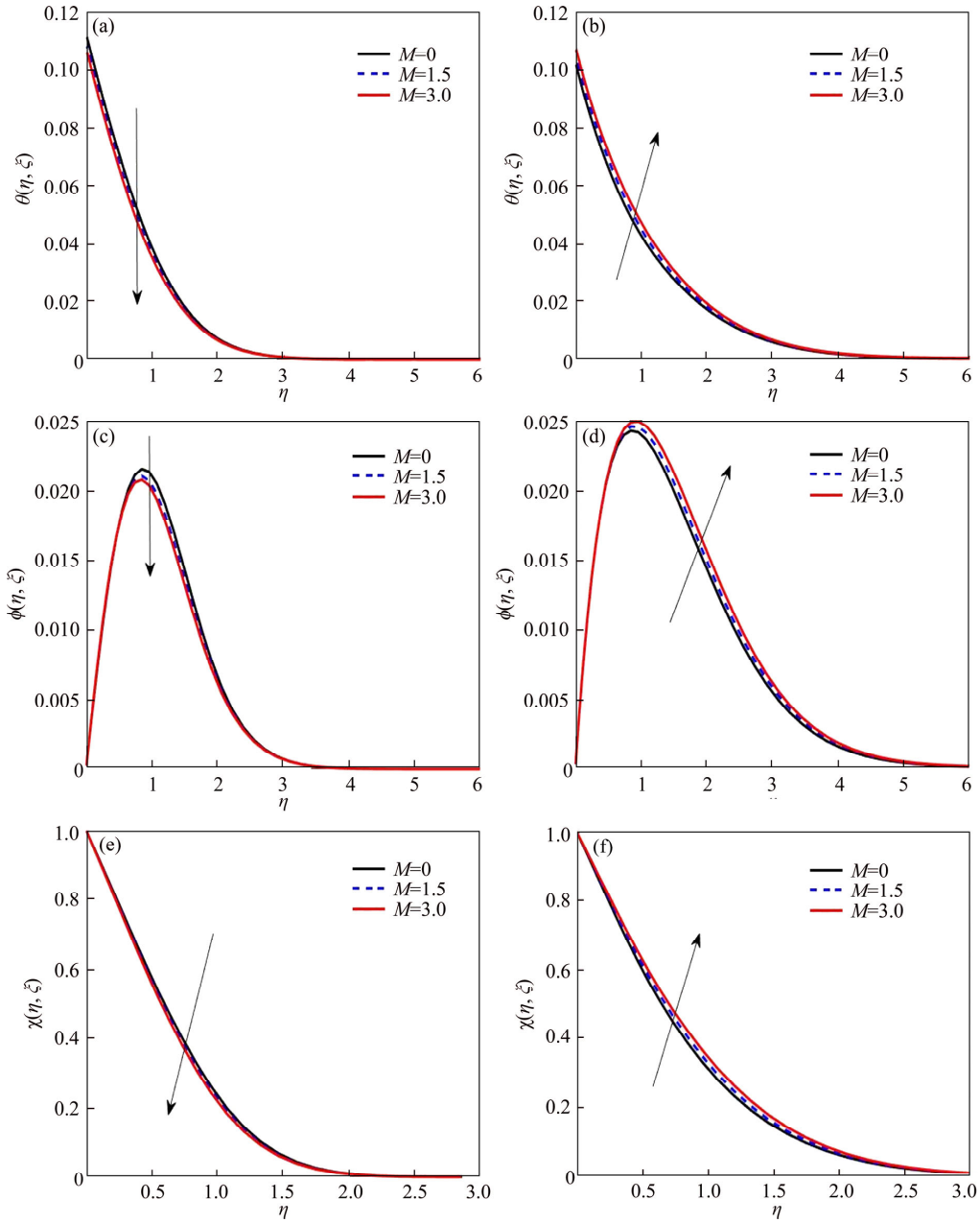

Figure 5 Effect of Hartmann number: (a) Temperature for S=0.25; (b) Temperature for S=0.75; (c) Concentration for S=0.25; (d) Concentration for S=0.75; (e) Microorganisms for S=0.25; (f) Microorganisms for S=0.75

for the case when S=0.75. There are no differences in the graph of these variables for different values of S. From Figure 8 we notice that increasing the radiation parameter results in an increase in the temperature of the fluid. This is because increasing the radiation parameter increases the Rossland diffusion [36], resulting in an increase in the fluid's temperature. Similar results are reported in Refs. [33, 37]. An increase in the radiation parameter results in an initial decrease of the chemical species. Far from the surface, the concentration of the chemical species increases with

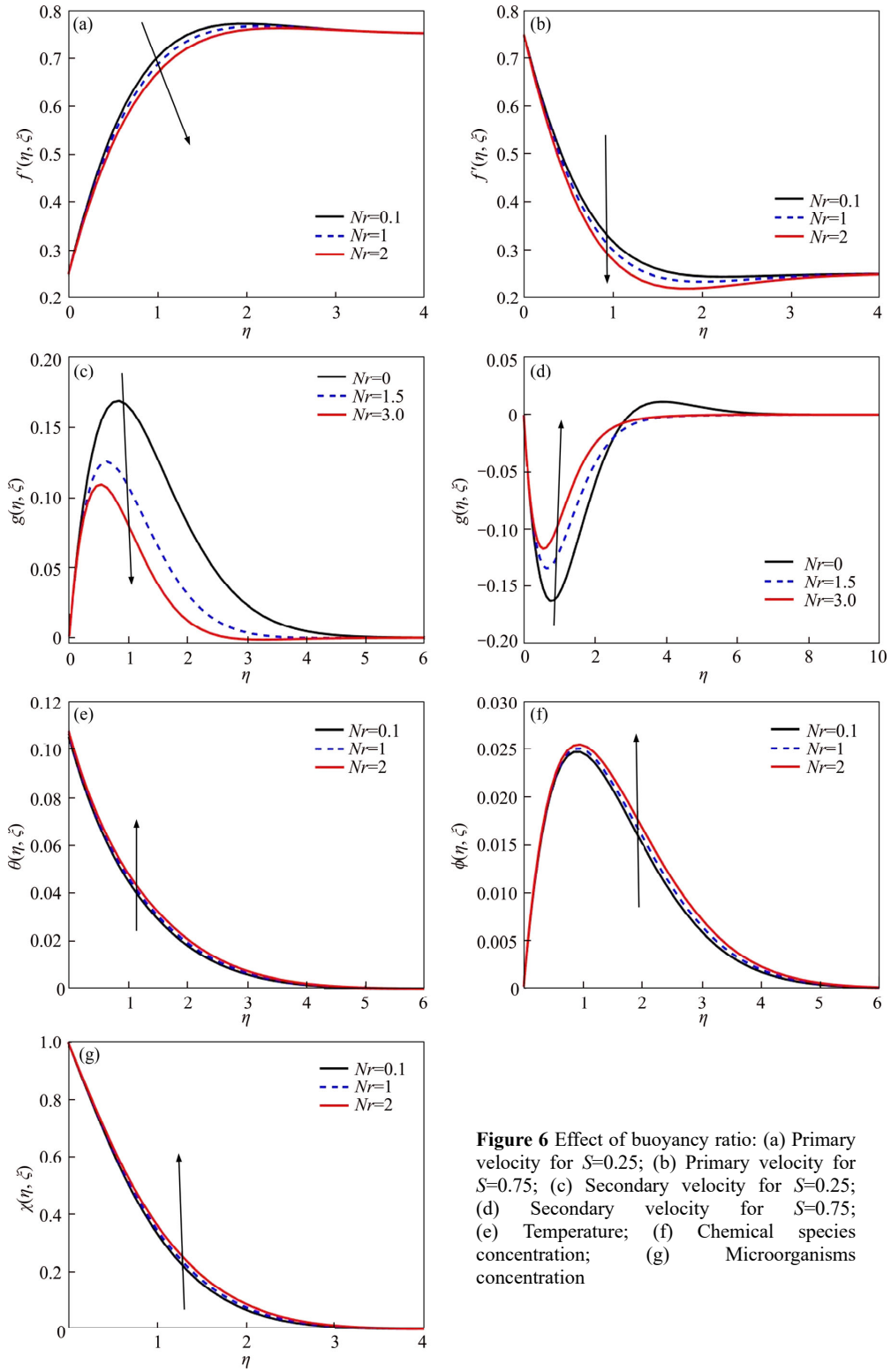

Figure 6 Effect of buoyancy ratio: (a) Primary velocity for S=0.25; (b) Primary velocity for S=0.75; (c) Secondary velocity for S=0.25; (d) Secondary velocity for S=0.75; (e) Temperature; (f) Chemical species concentration; (g) Microorganisms concentration

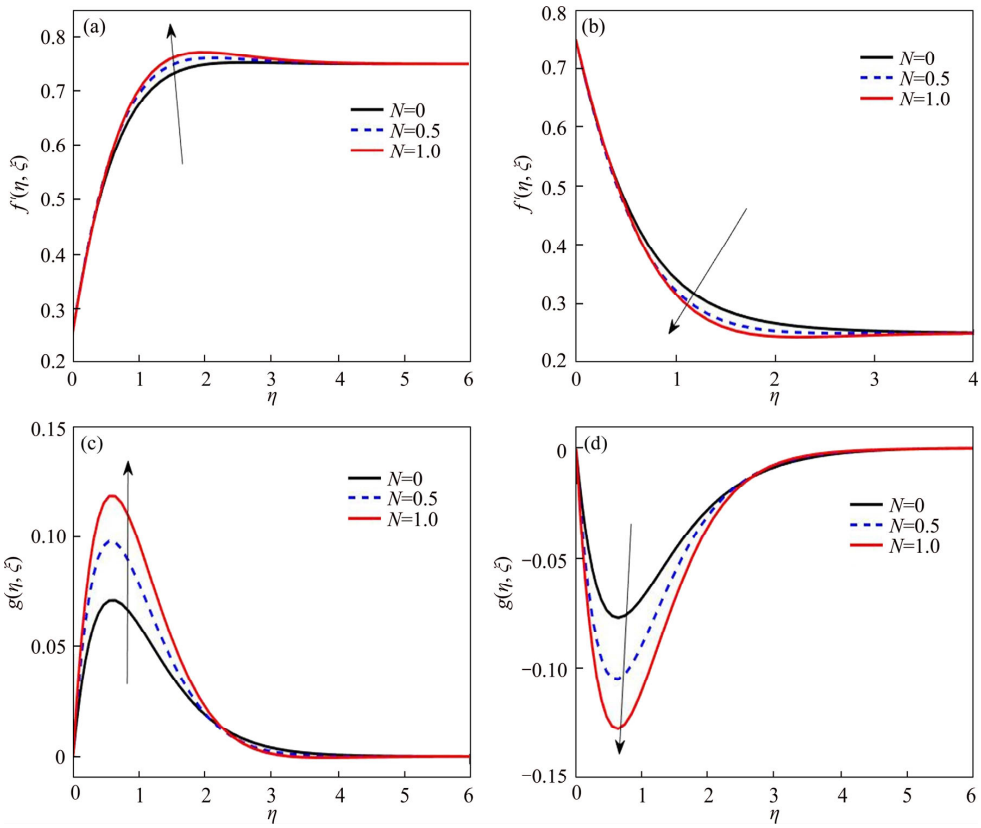

Figure 7 Effect of Hall parameter: (a) Primary velocity for S=0.25; (b) Primary velocity for S=0.75; (c) Secondary velocity for S=0.25; (d) Secondary velocity for S=0.75

increasing values of thermal radiation. REDDY et al [37] also reported similar results; however, no physical explanation was given about the phenomenon of primary velocity for S=0.25. We postulate that this phenomenon is associated with primary velocity, secondary velocity for S=0.25 in the primary velocity profile for the thermal radiation parameter. An increase in the primary velocity in the boundary layer results in the chemical species being carried outside the boundary layer and deposited outside the boundary layer leading to the observed phenomenon. The concentration of the microorganisms decreases with increasing values of thermal radiation parameter.

We analyze the influence of the bioconvective Rayleigh number Rb in Figure 9. The Rayleigh number is defined as a dimensionless number that is associated with buoyancy-driven flow. Below a certain critical value, heat transfer is primarily due to conduction and above that critical value it is due to convection. The primary velocity decreases with increasing values of Rayleigh number for all values of S. Temperature, concentration of chemical species and microorganisms increase with increasing value of Rayleigh number. Similar results were obtained in Ref. [19]. Secondary velocity on the other hand increases with increasing values of Rayleigh number and is positive for S<0.5. For values of S>0.5, the secondary velocity decreases for small values of Rayleigh number and the flow is negative. For large values of Rayleigh number, the flow becomes positive and increases with increasing values of Rayleigh number.

In Figure 10, we analyze the impact of Brownian motion parameter Nb and the thermophoretic parameter Nt on the concentration of chemical species. Brownian motion is the random ‘indeterminate’ movement of microscopic particles in a fluid due to bombardment by molecules of surrounding medium or fluid. Our

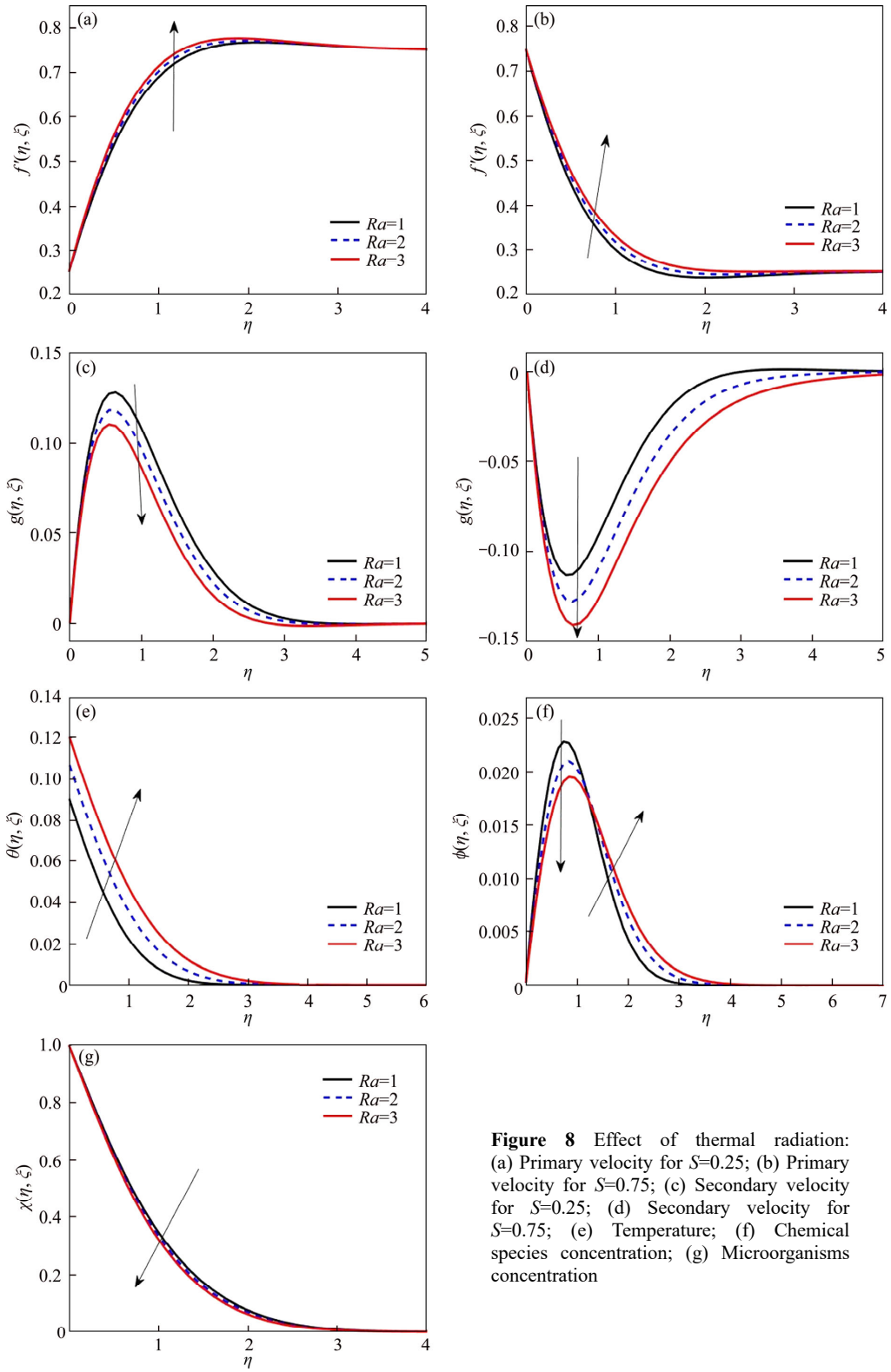

Figure 8 Effect of thermal radiation: (a) Primary velocity for S=0.25; (b) Primary velocity for S=0.75; (c) Secondary velocity for S=0.25; (d) Secondary velocity for S=0.75; (e) Temperature; (f) Chemical species concentration; (g) Microorganisms concentration

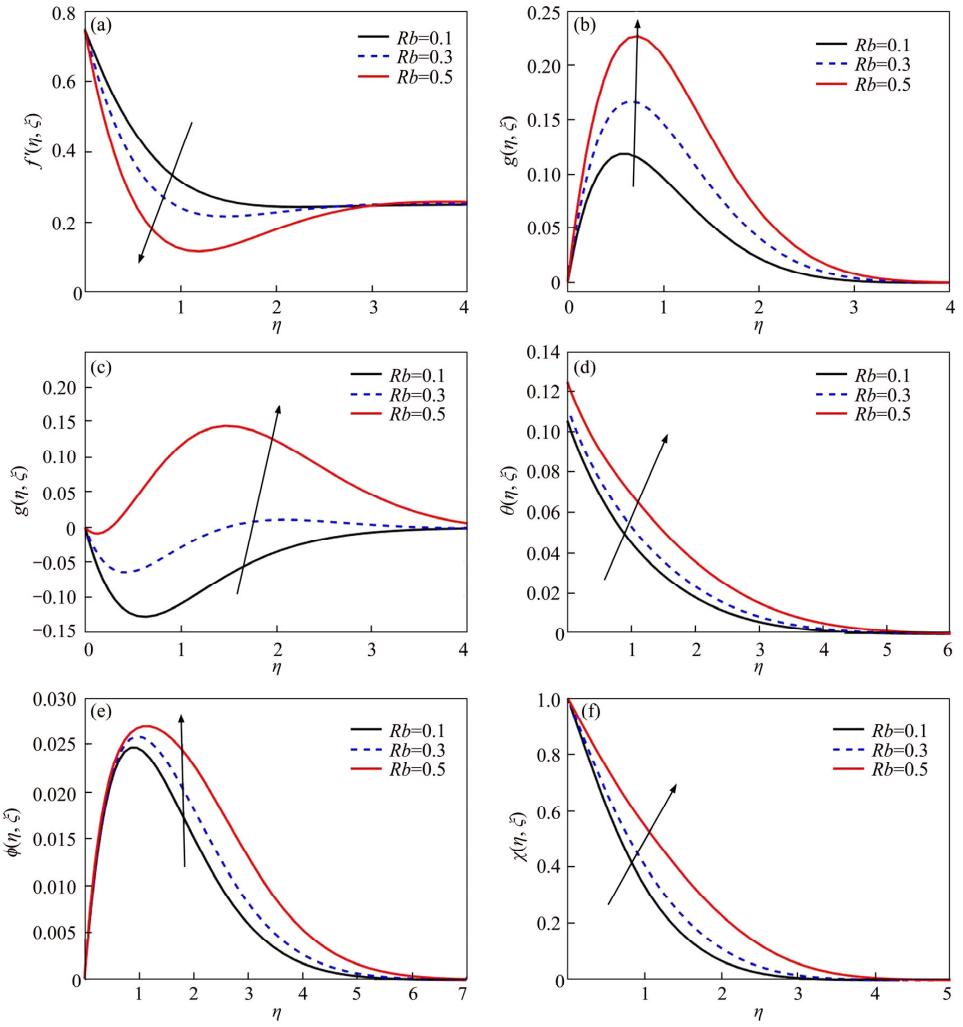

Figure 9 Effect of bioconvective Rayleigh number: (a) Primary velocity; (b) Secondary velocity for S=0.25; (c) Secondary velocity for S=0.75; (d) Temperature; (e) Chemical species concentration; (f) Microorganisms concentration

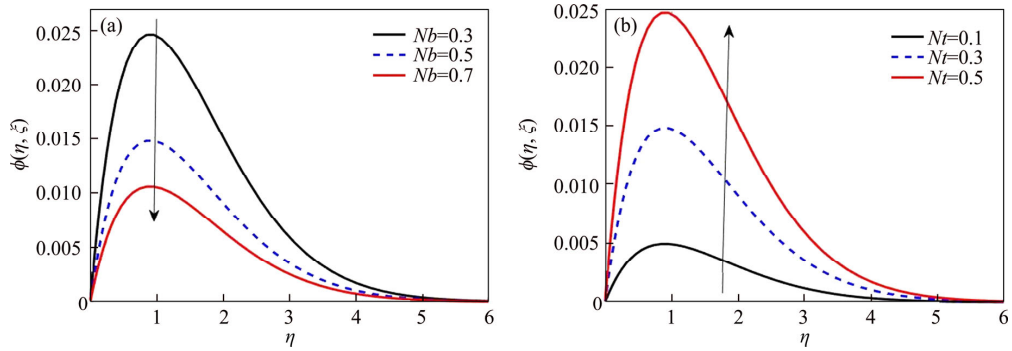

Figure 10 Effect of Brownian motion parameter Nb (a) and thermophoretic parameter Nt (b) on chemical species concentration

results show that an increase in the Brownian motion parameter leads to a decrease in the chemical species concentration in the boundary layer. Similar results for the parameter are reported in Refs. [1, 38, 39]. This is attributed to the fact that increasing the Brownian motion parameter leads to more solute being 'pushed' out of the boundary layer which is relatively 'thin' compared to the rest of the fluid. Thermophoresis, sometimes known as thermo-migration or thermo-diffusion is a phenomenon where microscopic molecules in a fluid exhibit a response to a force that is due to a temperature gradient. The force acts in the direction of a hot region to a cold region. An increase in the thermophoresis parameter leads to an increase in the concentration of chemical species. The result is in agreement with result in Ref. [38] that the fast flow from the stretching sheet carries the nanoparticles leading to an increase in the mass volume fraction boundary layer thickness. Similar conclusions about the parameter were also made in Refs. [1, 40].

In Figure 11, we review the effect of the Schmdit number *Sc* on chemical species concentration, bioconvection Schmdit number and bioconvection Peclet number on microorganisms. An increase in the Schmdit number leads to a decrease in the chemical species concentration in the boundary layer. Similar results were obtained in Ref. [41]. Similarly, an increase in the bioconvection Peclet number causes a decrease in the microorganism's concentration in the boundary layer. An increase in the bioconvection Peclet number increases the microorganism's concentration in the boundary layer. The bioconvection Peclet number is defined as the ratio of swimming microorganisms to the speed of the bulk fluid motion. The bioconvection Peclet number is less than unity if the fluid speed is faster than the microorganisms and greater than unity otherwise. It is equal to unity if the fluid speed equals the speed of microorganisms. Increase in the bioconvection Peclet number increases the motile microorganisms in the boundary layer [42, 43]. This is so because increasing the Peclet number increases the advective transport rate compared to the rate of diffusion. This attracts microorganisms near the boundary and as a result, the microorganisms flux increases. An increase in the bioconvection Schmdit number leads to a decrease in the concentration of microorganisms in the boundary layer. A result similar to ones is reported in Ref. [43].

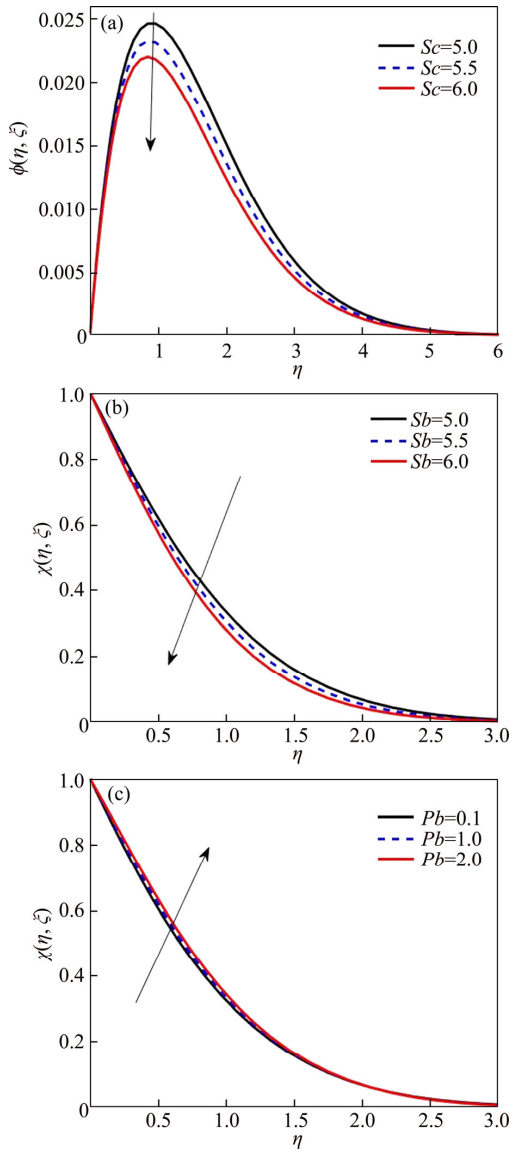

Figure 11 Effect of Schmdit number on chemical species concentration (a), bioconvective Schmidt number (b) and bioconvective Peclet number (c) on microorganism's concentration

7 Conclusions

In this article we formulated and analyzed a

model for a three-dimensional viscous incompressible rotational flow of an electrically conducting fluid with oxytactic microorganisms. The velocity ratio parameter is identified as a key parameter in this study. It has the potential of changing the dynamics of the flow. For values of this parameter above or below a critical value of 0.5 the flow reverses. In some cases, it alters the effect of other parameters, such as the Hartmann number on primary velocity. It is not clear at this point why/how these changes occur. Some of the key findings are:

The thermal radiation parameter increases the primary velocity while decreasing the secondary velocity for $S<0.5$. For $S>0.5$, there is a reverse effect for both the primary and secondary velocities.

Increasing the velocity ratio increases the temperature, concentration of chemical species and microorganisms.

Increasing the bioconvection Peclet number increases the microorganism's concentration in the boundary layer.

Increasing the Schmidt number and bioconvection Schmidt number leads to a decrease in the chemical species concentration and microorganisms, respectively.

References

[1] MUTUKU W N, MAKINDE O D. Hydromagnetic bioconvection of nanofluid over a permeable vertical plate due to gyrotactic microorganisms [J]. Computers & Fluids, 2014, 95: 88−97.

[2] TAKHAR H S, CHAMKHA A J, NATH G. MHD flow over a moving plate in a rotating fluid with magnetic field, hall currents and free stream velocity [J]. International Journal of Engineering Science, 2002, 40(13): 1511−1527.

[3] HIDE R, ROBERTS P. The origin of the main geomagnetic field [J]. Physics and Chemistry of the Earth, 1961, 4: 27−98.

[4] HIDE R. Free hydromagnetic oscillations of the earth's core and the theory of the geomagnetic secular variation [J]. Phil Trans R Soc Lond Series A, 1966, 259 (1107): 615−647.

[5] HIDE R. Magnetohydrodynamics of rotating fluids: A summary of some recent work [J]. Quarterly Journal of the Royal Astronomical Society, 1971, 12: 380−383.

[6] BUSH J, STONE H. Particle motion in rotating viscous fluids: Historical survey and recent developments [J]. J Fluid Mech, 1994, 282(1): 337−355.

[7] ROBERTS G O, KORNFELD D M, FOWLIS W W. Particle orbits in a rotating liquid [J]. J Fluid Mech, 1991, 229(1): 555−567.

[8] ANNAMALAL P, SUBRAMANIAN B, COLE R. Bubble migration inside a liquid drop in a space laboratory [J]. Phys Fluids, 1982, 25(1): 1121−1126.

[9] BOWEN T J, ROWE A J. An introduction to ultracentrifugation[M]. Vol. 4. John Wiley & Sons, 1970.

[10] SHERWOOD J. The hydrodynamic forces on a cylinder touching a permeable wellbore [J]. Physics of Fluids A: Fluid Dynamics, 1990, 2 (10): 1757–1759.

[11] ANNAMALAI P, SHANKAR N, COLE R, SUBRMANIAN R S. Bubble migration inside a liquid drop in a space laboratory [J]. Appl Sci Res, 1982, 38(1): 179−186.

[12] KUZNETSOV A. Nanofluid bioconvection: Interaction of microorganisms oxytactic up-swimming, nanoparticle distribution, and heating/cooling from below [J]. Theoretical and Computational Fluid Dynamics, 2012, 26(1−4): 291−310.

[13] KUZNETSOV A V. Nanofluid bioconvection in water-based suspensions containing nanoparticles and oxytactic microorganisms: Oscillatory instability [J]. Nanoscale Research Letters, 2011, 6: 100. DOI: 10.1186/1556-276X-6-100.

[14] LEE H G, KIM J. Numerical investigation of falling bacterial plumes caused by bioconvection in a three-dimensional chamber [J]. European Journal of Mechanics-B/Fluids, 2015, 52: 120−130.

[15] HILLESDON A, PEDLEY T. Bioconvection in suspensions of oxytactic bacteria: Linear theory [J]. J Fluid Mech, 1996, 324: 223−259.

[16] SAUID S M, KRISHNAN J, LING T H, VELURI M V P S. Enhancement of oxygen mass transfer and gas holdup using palm oil in stirred tank bioreactors with xanthan solutions as simulated viscous fermentation broths [J]. Bio Med Research International, 2013: 409675. DOI: 10.1155/2013/409675.

[17] KRAAKMAN N J R, ROCHA-RIOS J, van LOOSDRECHT M C M. Review of mass transfer aspects for biological gas treatment [J]. Applied Microbiology and Biotechnology, 2011, 91(4): 873−886.

[18] XU H, POP I. Fully developed mixed convection flow in a horizontal channel filled by a nanofluid containing both nanoparticles and gyrotactic microorganisms [J]. European Journal of Mechanics-B/Fluids, 2014, 46: 37−45.

[19] ALSAEDI A, KHAN M I, FAROOQ M, GULL N, HAYAT T. Magnetohydrodynamic (MHD) stratified bioconvective flow of nanofluid due to gyrotactic microorganisms [J]. Advanced Powder Technology, 2017, 28(1): 288−298.

[20] KHAN W, MAKINDE O. MHD nanofluid bioconvection due to gyrotactic microorganisms over a convectively heat stretching sheet [J]. International Journal of Thermal Sciences, 2014, 81: 118−124.

[21] SIDDIQA S, BEGUM N, SALEEM S, HOSSAIN M, GORLA R S R. Numerical solutions of nanofluid bioconvection due to gyrotactic microorganisms along a vertical wavy cone [J]. International Journal of Heat and Mass Transfer, 2016, 101: 608−613.

[22] KHAN W, UDDIN M J, ISMAIL A M. Free convection of non-Newtonian nanofluids in porous media with gyrotactic microorganisms [J]. Transport in Porous Media, 2013, 97(2): 241−252.

[23] IQBAL Z, MEHMOOD Z, MARAJ E. Oblique transport of gyrotactic microorganisms and bioconvection nanoparticles with convective mass ux [J]. Physica E: Low-dimensional Systems and Nanostructures, 2017, 88: 265−271.

[24] ABE T, NAKAMURA S, KUDO S. Bioconvection induced by bacterial chemotaxis in a capillary assay [J]. Biochemical and Biophysical Research Communications, 2017, 483(1): 277−282.

[25] AVINASH K, SANDEEP N, MAKINDE O D, ANIMASAUN I L. Aligned magnetic field effect on radiative bioconvection flow past a vertical plate with thermophoresis and Brownian motion [J]. Defect and Diffusion Forum, 2017, 377: 127−140.

[26] KUMAR K G, RAMESH G, GIREESHA B, GORLA R. Characteristics of Joule heating and viscous dissipation on three-dimensional flow of Oldroyd B nanofluid with thermal radiation [J]. Alexandria Engineering Journal, 2018, 57(3): 2139−2149.

[27] DANIEL Y S, AZIZ Z A, ISMAIL Z, SALAH F. Effects of thermal radiation, viscous and joule heating on electrical MHD nanofluid with double stratification [J]. Chinese Journal of Physics, 2017, 55 (3): 630−651.

[28] MOTSA S, MAGAGULA V, SIBANDA P. A bivariate chebyshev spectral collocation quasi-linearization method for nonlinear evolution parabolic equations [J]. The Scientific World Journal, 2014. DOI: 10.1155/2014/581987.

[29] MOTSA S S, MUTUA S F, SHATEYI S. Solving nonlinear parabolic partial differential equations using multidomain bivariate spectral collocation method [C]// Nonlinear Systems-Design, Analysis, Estimation and Control. 2016.

[30] SURESH M, MANGLIK A. Mathematical analysis of Hall effect on transient Hartman flow about a rotating horizontal permeable surface in a porous medium under inclined magnetic field [R]. International Scholarly Research Notices, 2014: 1−8.

[31] MOHAMED M, SALLEH M, NOAR N, ISHAK A. Buoyancy effect on stagnation point flow past a stretching vertical surface with Newtonian heating [C]// AIP Conference Proceedings. AIP Publishing, 2017: 020005-1-020005-8.

[32] KHAN W, MAKINDE O, KHAN Z. MHD boundary layer flow of a nanofluid containing gyrotactic microorganism past a vertical plate with Navier slip [J]. International Journal of Heat and Mass Transfer, 2014, 74: 285−291.

[33] SHATEYI S, MOTSA S S, SIBANDA P. The effects of thermal radiation, Hall currents, Soret, and Dufour on MHD flow by mixed convection over a vertical surface in porous media [J]. Mathematical Problems in Engineering, 2010: 627475. DOI: 10.1155/2010/627475.

[34] SALEM A M, EL-AZIZ M A. Effect of hall currents and chemical reaction on hydromagnetic flow of a stretching vertical surface with internal heat generation/absorption [J]. Applied Mathematical Modelling, 2008, 32(7): 1236−1254.

[35] NOREEN S, QASIM M. Influence of Hall current and viscous dissipation on pressure driven flow of pseudoplastic fluid with heat generation: A mathematical study [J]. PloS One, 2015, 10(6): e0129588.

[36] REDDY P S, SREEDEVI P, CHAMKHA A J. Heat and mass transfer flow of a nanofluid over an inclined plate under enhanced boundary conditions with magnetic field and thermal radiation [J]. Heat Transfer Asian Research, 2017, 46(7): 815−839.

[37] REDDY M G., KUMARI P V, PADMA P. Effect of thermal radiation on MHD Casson nanofluid over a cylinder [J]. Journal of Nanofluids, 2018, 7(3): 428−438.

[38] AWAD F G, AHAMED S M, SIBANDA P, KHUMALO M. The effect of thermophoresis on unsteady Bldroyd-B nanofluid flow over stretching surface [J]. PloS One, 2015, 10(8): e0135914.

[39] MAKINDE O, ANIMASAUN I. Thermophoresis and Brownian motion effects on MHD bioconvection of nanofluid with nonlinear thermal radiation and quartic chemical reaction past an upper horizontal surface of a paraboloid of revolution [J]. Journal of Molecular Liquids, 2016, 221: 733−743.

[40] ZAIMI K, ISHAK A, POP I. Boundary layer flow and heat transfer over a nonlinearly permeable stretching/shrinking sheet in a nanofluid [J]. Scientific Reports, 2014, 4: 4404

[41] MAKINDE O, ANIMASAUN I. Bioconvection in MHD nanofluid flow with nonlinear thermal radiation and quartic autocatalysis chemical reaction past an upper surface of a paraboloid of revolution [J]. International Journal of Thermal Sciences, 2016, 109: 159−171

[42] CHAKRABORTY T, DAS K, KUNDU P K. Framing the impact of external magnetic field on bioconvection of a nanofluid flow containing gyrotactic microorganisms with convective boundary conditions [J]. Alexandria Engineering Journal, 2016, 57: 61−71.

[43] SHAW S, KAMESWARAN P K, NARAYANA M, SIBANDA P. Biocinvevtion in a non-Darcyporus medium saturated with a nanofluid and oxytactic micro-organisms [J]. International Journal of Biomathematics, 2014, 7(1): 1450005.

(Edited by YANG Hua)

J. Cent. South Univ. (2020) 27: 824−841

中文导读

二元谱拟线性化含嗜氧微生物旋转纳米流体的对流边界条件

摘要：在本研究中，考虑了旋转的含有嗜氧微生物的黏性、不可压缩的导电纳米流体和漂浮在流体中的绝缘板的三维流动动力学。研究考虑了三种情况：一种是流体拖动板，第二种是板拖动流体，第三种是板以与流体相同的速度漂浮在流体上。浓度较高的嗜氧微生物因流体中氧梯度的作用而上浮到顶部时会产生生物对流。速度比在这种流动的动力学中起关键作用。低于临界值或高于临界值时，改变参数会改变流动的动力学。改变速度比使其低于或高于临界值会改变流体流动的动力学，Hartmann 数、浮力比和辐射参数对二次速度有反作用。另一方面，Hall 参数对低于或高于临界值的速度比的初始速度有反作用。生物截面的 Rayleigh 数减慢了初始速度。当速度比低于 0.5 时，二次速度随着生物截面 Rayleigh 数的增大而加快。当速度比高于 0.5 时，对于较小的生物截面 Rayleigh 数，二次速度起反作用，但随着数值的增加，对流动的作用发生被逆转，起正作用。

关键词：生物对流；嗜氧微生物；速度比；旋转纳米流体；二元光谱拟线性化

Summary

In this Chapter, the rotational nanofluid with oxytactic microorganisms and an insulated plate was studied. The bivariate spectral quasilinearisation method was used to solve the resulting system. Varying the velocity of the plate resulted in changes in the flow properties. The secondary velocity changes direction for values above and below a critical value. The Hartmann number and Hall parameter were shown to increase the primary velocity for values of S less than 0.5 and decrease it for S greater than 0.5. Increasing the Rayleigh bioconvective number resulted in some marked changes in all fluid properties. The result suggests the enhancement of convective transfer rates due to microorganisms.

Chapter 6

Numerical studies on temperature-dependent viscosity and thermal conductivity on couple stress fluid

In Chapters 2 to 5 we formulated and analysed models for different non-Newtonian fluid flows under the assumption of constant viscosity and thermal conductivity. In this Chapter, they considered, the flow of industrial fluids in processes that involve heat generation or operate at very high temperatures. In industrial processes such as glass blowing, geothermal systems, crude and oil extraction the machinery operate at high temperature or produce heat at very high temperature [104]. Extremely high temperatures at a local point in sliding metals have been reported in the literature [105]. The viscosity and thermal conductivity of fluids encountered in such engineering settings are affected by high temperatures. A simpler model for the variation of thermal conductivity in couple stress fluid is proposed and analysed.

Contradicting models for variation of thermal conductivity with temperature in fluids are found in the literature. Studies by Devi and Prakash, El-Aziz and Keimanesh [106–108] model the variation of thermal conductivity as a linearly increasing function of temperature. On the other hand studies by Sundar *et al*, Duangthongsuk and Wongwises, and Hazarika [109–111] model the relationship as a nonlinear decreasing function of temperature. Bird *et al* [3] and Polezhaev [112] reported that thermal conductivity decreases with increasing temperature, a consequence of Bridgman's theory. In this chapter, a simpler model that decreases with increasing temperature was developed.

Numerical studies on temperature dependent viscosity and thermal conductivity on a couple stress fluid

Mlamuli Dhlamini[a], Precious Sibanda[a], Sandile Motsa[a,b], Hiranmoy Mondal[a]

[a]*School of Mathematics, Statistics and Computer Science,University of KwaZulu-Natal, Private Bag X01, Scottsvile, Pietermaritzburg-3209, South Africa*

[b]*Department of Mathematics, University of Swaziland, Private Bag 4, Kwaluseni, Swaziland*

Abstract

In this paper, we studied the two-dimensional flow of a steady couple stress fluid with variable viscosity and thermal conductivity. The effect of the three key parameters, temperature dependent viscosity, thermal conductivity and couple stress parameter are analyzed. We adopted simpler parameters for measuring temperature dependent viscosity and thermal conductivity. Increasing the temperature dependent parameter for viscosity is shown to reduce both the heat and mass transfer rates at the surface. Increasing thermal conductivity and the couple stress parameter increased both the heat and mass transfer rates on the boundary surface.

Keywords: Couple stress fluid; variable viscosity; variable thermal conductivity; temperature dependent parameter.

1. Introduction

The study of non-Newtonian fluid is still a growing area of research in engineering. This is because these fluids are encountered in everyday engineering applications such as coal-oil slurries, metal spinning, metal extrusion, continuous casting, glass blowing, extrusion of polymer sheet from die, solidification of liquid crystals (Hayat *et al.*, 2015; Dhlamini *et al.*,

*Corresponding author
Email address: hiranmoymondal@yahoo.co.in (Hiranmoy Mondal)

2018b; Monica *et al.*, 2016; Panigrahi *et al.*, 2015; Khan and Yousafzai, 2014). Couple stress fluids contain base oils (90%) and additives (10%). Some additives that are commonly used include nanoparticles, viscosity index improvers, anti-wear, corrosion inhibitors and friction modifiers (Singh, 1982; Rao *et al.*, 2013). The concept of a couple stress fluid was introduced by Stokes (1966). Most lubricants used in industrial machinery with moving parts contain additives additives that, inter alia, reduce friction and corrosion, aging, contamination and increase fluid viscosity (Bou-Said *et al.*, 2012). The presence of additives lead to changes in the rheological properties of the fluid and for this reason, most lubricants are modeled as couple stress fluids. The couple stress fluid model has also been used to model biological fluids such as blood (Misra *et al.*, 2018; Sahu *et al.*, 2010; Srinivasacharya and Rao, 2016; Sithole *et al.*, 2018) and synovial fluids (Lai *et al.*, 1978; Horibata *et al.*, 2017; Sithole *et al.*, 2018). A number of studies have reported positive results for industrial use of couple stress fluids/lubricants. The benefits reported include an increase in the load-carrying capacity of bearings, decrease in friction, lowering temperature, increase in fluid film stiffness and an increase in the dynamic performance of journal bearing systems when a couple stress lubricants is used compared to Newtonian lubricants (Lin and Lu, 2004; Sinha *et al.*, 1981; Wang *et al.*, 2002; Lin, 2001; Ram, 2017).

Often times when researchers model fluid flow in industrial set-ups they assume that viscosity and thermal conductivity is constant. This assumption is not always true (Cengel and Cimbala, 2004). The fluid and flow properties are significantly affected by temperature fluctuations and in some cases the effect is so significant that it cannot be ignored. The effect of temperature dependent of thermal conductivity is encountered in thermal transportation (Choudhury and Hazarika, 2008). An increase in fluid temperature is associated with a local increase in the momentum transport due to reduction in the viscosity across the momentum boundary layer which also affects heat transfer rate at the wall (Choudhury and Hazarika, 2013). Lai and Kulacki (1990) were the first to introduce a model for variable viscosity, however they did not assume variable thermal conductivity. In this paper we adopt the model by Khound and Hazaika (2000) that preserves the positivity of thermal conductivity in contrast

to the model by Hayat *et al.* (2016b); Manjunatha and Gireesha (2016); Animasaun (2015); Pal and Mondal (2014). Fluids that have viscosity that is a function of temperature are found in polymer processing industries, food processing, bio-chemical industries and in the enhanced recovery of petroleum resources (Kannan and Moorthy, 2016).

In this paper we model the flow of a couple stress fluid with variable viscosity and thermal conductivity. We introduce a new simpler formulation for the temperature dependent parameters. Also, we are cognisant of the fact that some non-dimensionless parameter are not constant in the boundary layer, an assumption that is ignored by many researchers (Choudhury and Hazarika, 2013; Khan *et al.*, 2011; Hayat *et al.*, 2014, 2016a).

2. Mathematical Model

We consider the two dimensional flow of a couple stress fluid over a surface that moves at constant speed U_w and velocity components u and v in the x and y directions respectively. The temperature and concentration on the solid surface are assumed to be constant and given by $T = T_w$ and $C = C_w$ respectively. The free stream conditions are given by $u = 0$, $T = T_\infty$ and $C = C_\infty$. The physical set-up for the flow is given in Figure 1 below

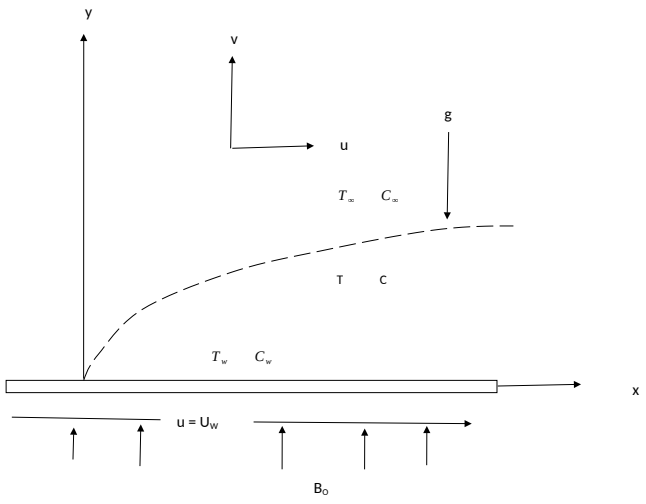

Figure 1: Coordinate system for the flow

The set of equations that describe the flow and the associated boundary conditions are given in Equations (1) - (4) and (5) respectively

$$\frac{\partial u}{\partial x}+\frac{\partial v}{\partial y}=0 \tag{1}$$

$$\rho\left(u\frac{\partial u}{\partial x}+v\frac{\partial u}{\partial y}\right)=\frac{\partial}{\partial y}\left(\mu\frac{\partial u}{\partial y}\right)+\rho g\left[\beta_T\left(T-T_\infty\right)+\beta_C\left(C-C_\infty\right)\right]-$$
$$\xi_1\frac{\partial^4 u}{\partial y^4}-\sigma B_0^2 u, \tag{2}$$

$$\rho C_p\left(u\frac{\partial T}{\partial x}+v\frac{\partial T}{\partial y}\right)=\frac{\partial}{\partial y}\left(\kappa\frac{\partial T}{\partial y}\right)+\tau\rho C_p\left[D_B\frac{\partial C}{\partial y}\frac{\partial T}{\partial y}+\frac{D_T}{T_\infty}\left(\frac{\partial T}{\partial y}\right)^2\right]+$$
$$\mu\left(\frac{\partial u}{\partial y}\right)^2, \tag{3}$$

$$u\frac{\partial C}{\partial x}+v\frac{\partial C}{\partial y}=D_B\frac{\partial^2 C}{\partial y^2}+\frac{D_T}{T_\infty}\frac{\partial^2 T}{\partial y^2}. \tag{4}$$

The boundary conditions for the system given by equations (2) - (4) are given as

$$u=U_w,\ v=0,\ \frac{\partial^2 u}{\partial y^2}=0,\ T=T_w,\ D_B\frac{\partial C}{\partial y}+\frac{D_T}{T_\infty}\frac{\partial T}{\partial y}=0,\ at\ y=0,$$
$$u\to 0,\quad \frac{\partial u}{\partial y}=0,\quad T\to T_\infty,\quad C\to C_\infty,\ as\ y\to\infty. \tag{5}$$

ρ is the density of the fluid, μ is the viscosity, g is the gravitational acceleration, β_T and β_C are the thermal and solute coefficients of expansion, ξ_1 is the couple stress parameter, σ is the conductivity of the fluid, B_0 is the applied magnetic field, Cp is the specific heat capacity of the fluid, κ is the thermal conductivity, τ is the ratio between effective heat capacity of nanoparticles and the base fluid, D_B and D_T are the mass and thermophoretic diffusion coefficients.

The following variables are introduced to transform the system of equations by (2) - (4).

$$\eta=y\sqrt{\frac{U_w}{\nu x}},\quad \psi=\sqrt{U_w\nu x}f(\eta),\quad \theta(\eta)=\frac{T-T_\infty}{T_w-T_\infty},\quad \phi(\eta)=\frac{C-C_\infty}{C_w-C_\infty}. \tag{6}$$

The velocity components are $u = \partial\psi/\partial y$ and $v = -\partial\psi/\partial x$ are given as

$$u = U_w f', \quad v = \frac{1}{2}\sqrt{\frac{U_w \nu}{x}}(\eta f' - f). \tag{7}$$

The viscosity μ and thermal conductivity κ depend on the temperature. In general, both the fluid viscosity and thermal conductivity decrease with increasing temperatures due to a decreases in attraction forces at the molecular level (Bird *et al.*, 2001; Polezhaev, 2011). We model both the viscosity and thermal conductivity as decreasing functions given as

$$\mu(T) = \frac{\mu_\infty}{1 + \epsilon_1(T - T_\infty)}, \quad \kappa(T) = \frac{\kappa_\infty}{1 + \epsilon_2(T - T_\infty)}. \tag{8}$$

Using equations (6) and (7) in equations (2) - (4) and the boundary conditions (5), the system is transformed into a fifth order ordinary boundary value problem,

$$Ca^2 f^v - \frac{1}{1+\Omega_1\theta} f''' + \frac{\Omega_1}{(1+\Omega_1\theta)^2} f''\theta' - \frac{1}{2} f f'' + M f' - \lambda_T \theta - \lambda_C \phi = 0, \tag{9}$$

$$\frac{1}{1+\Omega_2\theta}\theta'' - \frac{\Omega_2}{(1+\Omega_2\theta)^2}\theta'^2 + Pr_\infty \left[\frac{1+\Omega_2\theta}{1+\Omega_1\theta}\right]\left[\frac{1}{2} f\theta' + Ec f''^2\right] + Nb_\infty (1+\Omega_2\theta)\,\theta'\phi' + Nt_\infty (1+\Omega_2\theta)\,\theta'^2 = 0, \tag{10}$$

$$\phi'' + \frac{1}{2}\frac{Sc_\infty}{(1+\Omega_1\theta)} f\phi' + \frac{Nt}{Nb}\theta'' = 0. \tag{11}$$

The associated boundary conditions in (8) are transformed to

$$f(0) = 0, \quad f'(0) = 1, \quad f'''(0) = 0, \quad \theta(0) = 1, \quad Nb\phi'(0) + Nt\theta'(0) = 0,$$
$$f'(\infty) \to 0, \quad f''(\infty) \to 0, \quad \theta(\infty) \to 0, \quad \phi(\infty) \to 0. \tag{12}$$

The parameters in the ordinary differential equation and associated boundary conditions are defined as

$$\Omega_1 = \epsilon_1(T_w - T_\infty), \quad Re = \frac{U_w x}{\nu_\infty}, \quad G_T = \frac{\beta_T(T_w - T_\infty)x^3}{\nu_\infty^2}, \quad G_C = \frac{\beta_C(C_w - C_\infty)x^3}{\nu_\infty^2},$$
$$\lambda_T = \frac{G_T}{Re^2}, \quad \lambda_C = \frac{G_C}{Re^2}, \quad Ca = \frac{1}{x}\sqrt{\frac{\xi_1}{\mu}}, \quad M = \frac{\sigma B_0^2 x}{\rho U_w}, \quad \Omega_2 = \epsilon_2(T_w - T_\infty),$$
$$Pr_\infty = \frac{\nu_\infty}{\alpha_\infty}, \quad Ec = \frac{U_w^2}{C_p(T_w - T_\infty)}, \quad Nb_\infty = \frac{\tau D_B(C_w - C_\infty)}{\alpha_\infty},$$
$$Nt_\infty = \frac{\tau D_T(T_w - T_\infty)}{\alpha_\infty T_\infty}, \quad Sc_\infty = \frac{\nu_\infty}{D_B}. \tag{13}$$

The prime denotes differentiation with respect to η, Ω_1 is the temperature dependent parameter for viscosity, Re is the Reynolds number, G_T and G_C are the thermal and solutal Grashof number, Ca is the couple stress parameter, λ_T is the mixed convective parameter, λ_C is the solute buoyancy parameter, Ω_2 is the temperature dependent parameter for thermal conductivity, Pr_∞ is the ambient Prandtl number, Ec is the Eckert number, Nb_∞ is the ambient Brownian motion parameter, Nt_∞ is the ambient thermophoresis parameter and Sc_∞ is the ambient Schmdit number.

3. Momentum, heat and mass transfer coefficients

We evaluate the parameters of interest in the model, namely the local skin friction coefficient (C_f), Nusselt number (Nu) and the Sherwood number. The local skin friction coefficient measures the shear stress on the surface. The Nusselt number is defined as the ratio of convective heat transfer to conduction across a boundary. The Sherwood number on the other hand is the ratio of convective mass transfer to the diffusive mass transfer. These are given as

$$C_f = \frac{\tau_w}{\frac{1}{2}\rho U_w^2} = 2Re^{-\frac{1}{2}}\left(f''(0) - Ca^2 f''''(0)\right), \tag{14}$$
$$Nu = \frac{x q_w}{\kappa(T_w - T_\infty)} = -Re^{\frac{1}{2}}\theta'(0), \tag{15}$$
$$Sh = \frac{x q_m}{D_B(C_w - C_\infty)} = -Re^{\frac{1}{2}}\phi'(0), \tag{16}$$

where

$$\tau_w = \mu\left(\frac{\partial u}{\partial y}\right) - \frac{\eta_1}{\rho}\left(\frac{\partial^3 u}{\partial y^3}\right)\Big|_{y=0}, q_w = -\kappa\left(\frac{\partial T}{\partial y}\right)\Big|_{y=0}, q_m = -D_B\left(\frac{\partial C}{\partial y}\right)\Big|_{y=0}. \tag{17}$$

4. Numerical solution using the Spectral Quasi-Linearization Method

The nonlinear boundary value problem in equations (9) - (11) with associated boundary conditions (12) are solved numerically using the spectral quasilinearization method (SQLM). The choice to to use a spectral-based method is that they have been shown to produce accurate results using less grid points and hence less computational time (Motsa *et al.*, 2016, 2014). The interval given by $\eta = [0, L_x]$ is transformed to the regions $x = [-1, 1]$ using the linear transformations $\eta = Lx(x+1)/2$. For the implementation of the scheme we start by defining the functions F, Θ and Φ for the equations (9), (10) and (11) respectively as

$$F = Ca^2 f^v - \frac{1}{1+\Omega_1\theta} f''' + \frac{\Omega_1}{(1+\Omega_1\theta)^2} f''\theta' - \frac{1}{2} f f'' + M f' - \lambda_T \theta - \lambda_C \phi, \tag{18}$$

$$\Theta = \frac{1}{1+\Omega_2\theta}\theta'' - \frac{\Omega_2}{(1+\Omega_2\theta)^2}\theta'^2 + Pr_\infty\left[\frac{1+\Omega_2\theta}{1+\Omega_1\theta}\right]\left[\frac{1}{2} f\theta' + Ecf''^2\right] + Nb_\infty\left(1+\Omega_2\theta\right)\theta'\phi' + Nt_\infty\left(1+\Omega_2\theta\right)\theta'^2, \tag{19}$$

$$\Phi = \phi'' + \frac{1}{2}\frac{Sc_\infty}{(1+\Omega_1\theta)} f\phi' + \frac{Nt}{Nb}\theta''. \tag{20}$$

The iterative process is constructed as follows

$$a_{0r} f^v_{r+1} + a_{1r} f'''_{r+1} + a_{2r} f''_{r+1} + a_{3r} f'_{r+1} + a_{4r} f_{r+1} + a_{5r}\theta'_{r+1} + a_{6r}\theta_{r+1} + a_{7r}\phi_{r+1} - F = R_f, \tag{21}$$

$$b_{0r}\theta''_{r+1} + b_{1r}\theta'_{r+1} + b_{2r}\theta_{r+1} + b_{3r} f''_{r+1} + b_{4r} f_{r+1} + b_{5r}\phi'_{r+1} - \Theta = R_\theta, \tag{22}$$

$$c_{0r}\phi''_{r+1} + c_{1r}\phi'_{r+1} + c_{2r} f_{r+1} + c_{3r}\theta''_{r+1} + c_{4r}\theta_{r+1} - \Phi = R_\phi. \tag{23}$$

Subject to the boundary conditions

$$f_{r+1}(0) = f'_{r+1}(0) = 0,\ \theta_{r+1}(0) = 1,\ Nb\phi'_{r+1}(0) + Nt\theta'_{r+1}(0) = 0,$$
$$f'_{r+1}(\infty) \to 1, \quad \theta_{r+1}(\infty) \to 0, \quad \phi_{r+1}(\infty) \to 0. \tag{24}$$

The coefficients in equations (21) - (23) are given as

$$a_{0r} = Ca^2,\ a_{1r} = -\frac{1}{1+\Omega_1\theta_r},\ a_{2r} = \frac{\Omega_1}{(1+\Omega_1\theta_r)^2}\theta'_r - \frac{1}{2}f_r,\ a_{3r} = M,\ a_{4r} = -\frac{1}{2}f''_r,$$
$$a_{5r} = \frac{\Omega_1}{(1+\Omega_1\theta_r)^2}f'',\ a_{6r} = \frac{\Omega_1}{(1+\Omega_1\theta_r)^2}f'''_r - \frac{2\Omega_1^2}{(1+\Omega_1\theta_r)^3}f''_r\theta'_r - \lambda_T,\ a_{7r} = -\lambda_C,$$
$$b_{0r} = \frac{1}{1+\Omega_2\theta_r},\ b_{1r} = \frac{2\Omega_2}{(1+\Omega_2\theta_r)^2}\theta'_r +$$
$$\frac{1}{2}Pr_\infty\left(\frac{1+\Omega_2\theta_r}{1+\Omega_1\theta_r}\right)f_r + Nb_\infty\phi'_r\left(1+\Omega_2\theta_r\right) + 2Nt\theta'_r\left(1+\Omega_2\theta_r\right),$$
$$b_{2r} = -\frac{\Omega_2}{(1+\Omega_2\theta_r)^2}\theta''_r + \frac{2\Omega_2^2}{(1+\Omega_2\theta_r)^3}\theta'^2_r + Nb_\infty\Omega_2\theta'_r\phi'_r +$$
$$Nt_\infty\Omega_2\theta'^2_r + \frac{Pr_\infty\left(\Omega_2-\Omega_1\right)}{\left(1+\Omega_1\theta_r\right)^2}\left[\frac{1}{2}f_r\theta' + Ecf''^2\right],\ b_{3r} = 2Pr_\infty Ecf''_r\left[\frac{1+\Omega_2\theta_r}{1+\Omega_1\theta_r}\right],$$
$$b_{4r} = \frac{1}{2}Pr_\infty\theta'_r\left[\frac{1+\Omega_2\theta_r}{1+\Omega_1\theta_1}\right],\ b_{5r} = Nb_\infty\theta'_r\left(1+\Omega_2\theta_r\right),\ c_{0r} = 1,\ c_{1r} = \frac{1}{2}\frac{Sc_\infty}{\left(1+\Omega_1\theta_r\right)}f_r,$$
$$c_{2r} = \frac{1}{2}\frac{Sc_\infty}{\left(1+\Omega_1\theta_r\right)}\phi'_r,\ c_{3r} = \frac{Nt}{Nb}, c_{4r} = -\frac{1}{2}\frac{\Omega_1 Sc_\infty}{\left(1+\Omega_1\right)^2}f_r\phi'_r. \tag{25}$$

The initial guess functions are given as

$$f_0(\eta) = \frac{1}{2}\left[3 - 3e^{-\eta} - \eta e^{-\eta}\right],\ \theta_0(\eta) = \frac{Bi}{1+Bi}e^{-\eta},\ \phi_0(\eta) = -\frac{Nt}{Nb}\frac{Bi}{1+Bi}e^{-\eta}. \tag{26}$$

5. Results and Discussion

We solved the fifth order boundary value problem numerically using the spectral-quasilinearization method. To check for the accuracy of the numerical scheme the residual errors are computed and analyzed. The residual errors are given in Figure 2.

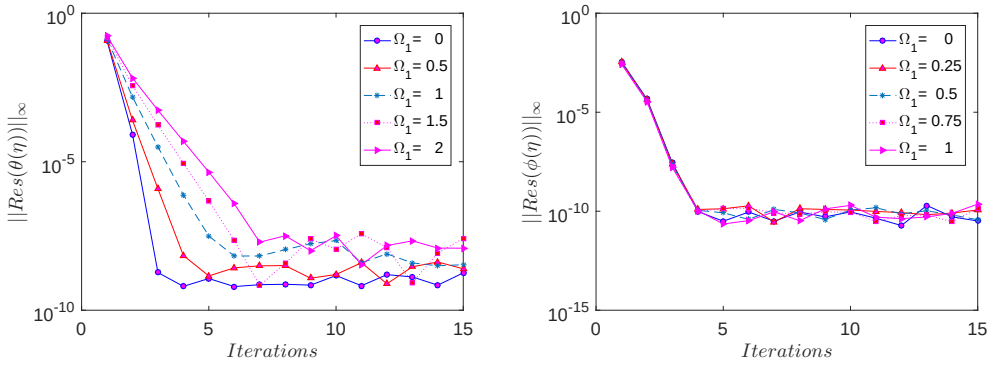

(a) Residual error for temperature

(b) Residual error for concentration

Figure 2: Residual errors

Table 1 shows the variation of the Nusselt and Sherwood number with the temperature dependent parameters Ω_1 and Ω_2 and the couple stress parameter Ca. Ω_2 and Ca increase both the Nusselt and Sherwood numbers while Ω_1 has an opposite effect on both. Increasing Ω_1 decreases velocity leading to the formation of an insulating 'blanket' thereby lowering the heat transfer rate. Increasing Ca increases the velocity leading to destruction of any insulating 'blanket' thereby increasing heat transfer rate. Increasing Ω_2 leads to reduction of thermal conductivity. A reduction in thermal conductivity leads to an increase in the Nusselt number hence increasing heat transfer rate at the surface.

Table 1: Variation of Nusselt number and Sherwwod number for M = 0.3, $\lambda_T = 0.5$, $\lambda_C = 0.5$, Pr = 8, Ec = 0.3, Nb = 0.3, Nt = 0.2, Sc = 10

Ω_1	Ω_2	Ca	-$\theta(0)$	-$\phi(0)$
0	0.2	0.5	1.140843	-0.340881
0.5			1.007528	-0.269538
1.0			0.921115	-0.226829
1.5			0.859877	-0.198561
2.0			0.813770	-0.178560
0.2	0		0.958828	-0.248035
	0.5		1.237629	-0.386604
	1.0		1.449109	-0.494242
	1.5		1.605156	-0.573162
	2.0		1.713117	-0.625464
	0.2	0	0.958829	-0.248035
		0.5	1.237627	-0.386604
		1.0	1.449110	-0.494241
		1.5	1.605156	-0.573162
		2.0	1.713117	-0.625464

The impact of certain critical parameter on the fluid and flow properties are presented graphically and explained. In Figure 3 we present the impact of the temperature dependent parameter for viscosity Ω_1. An increase in the parameter is associated with a decrease in the velocity profile and an increase in the temperature profile. The concentration profile decrease for increasing values of the parameter near the plate and increase far from it. Our results are in agreement with results by Hazarika and Jadav (2014).

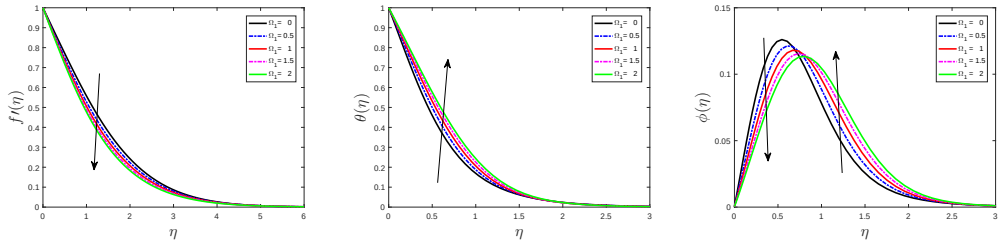

(a) Effect on velocity (b) Effect on temperature (c) Effect on concentration

Figure 3: Effect of temperature dependent parameter for viscosity Ω_1 on velocity, temperature and concentration profiles

Figure 4 depicts the influence of the temperature dependent parameter for thermal conductivity Ω_2 on temperature and concentration. An increase in Ω_2 is associated with a decrease in the thermal boundary layer a result consistent with conclusion by Choudhury and Hazarika (2008) and an increase in the concentration profile. Our results on temperature profile are not in agreement with results by Elbarbary and Elgazery (2004); Hassanien *et al.* (2003) and also not consistent with results by Hassanien *et al.* (2003) for the concentration profile. This may be due to the different choices of models for variation of thermal conductivity with temperature.

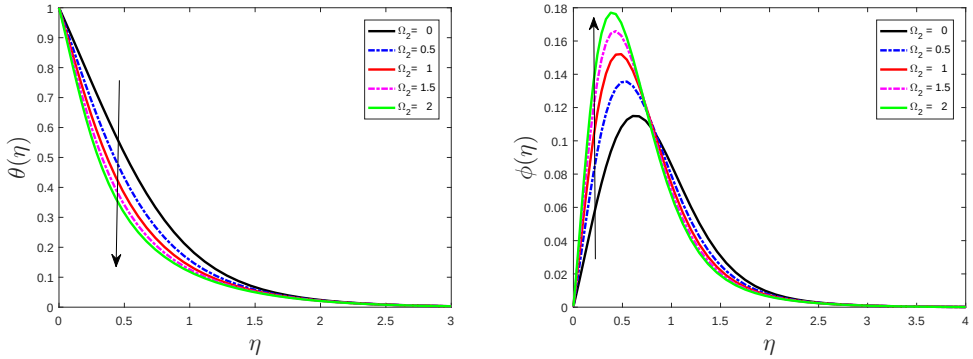

(a) Effect on temperature (b) Effect on concentration

Figure 4: Effect of the temperature dependent parameter for thermal conductivity Ω_2 on temperature and concentration profiles

We show the effect of couple stress parameter in Figure 5. We note that velocity and temperature decrease with an increase in the couple stress parameter a results consistent with results by Kaladhar (2015); Sithole *et al.* (2018); Srinivasacharya and Kaladhar (2012). Concentration on the other hand increases near the boundary surface with increasing values of the couple stress parameter and this result is in agreement with results by Srinivasacharya and Kaladhar (2012).

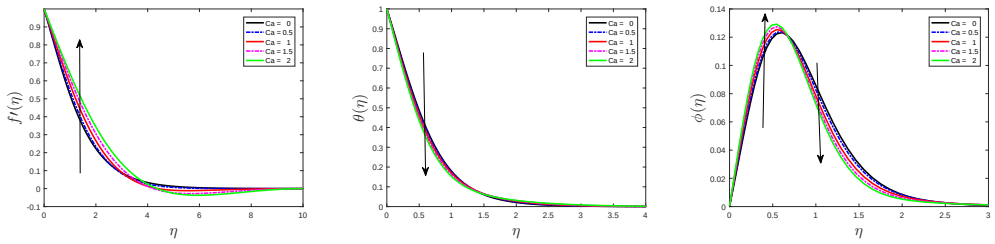

(a) Effect on velocity (b) Effect on temperature (c) Effect on concentration

Figure 5: Effect of the couple stress parameter Ca on velocity, temperature and concentration profiles

The influence of other parameters (magnetic field M, Eckert number Ec, Prandtl number Pr, thermophoresis parameter Nt, Brownian motion Nb, mixed convective parameter λ_T, solutal buoyancy parameter λ_C, and Schmidt number Sc) are consistent with results in literature, e.g see Goqo *et al.* (2018); Dhlamini *et al.* (2018a,b); Hazarika and Jadav (2014)

6. Conclusion

In this research article we formulated and analyzed a model of flow of a couple stress fluid with temperature dependent variable viscosity and thermal conductivity. The temperature dependent parameters and the couple stress parameters were shown to have an effect on the fluid and flow properties of the couple fluid. Some of the notable effects are:

- Velocity and concentration boundary layers decrease while temperature boundary layer increase for increasing Ω_1.

- Temperature decrease for increasing Ω_2 while the concentration was shown to increase for this parameter.
- Increasing the couple stress Ca parameter increases velocity and concentration boundary layers while decreasing the temperature boundary layer.

References

Animasaun, I., 2015. Effects of thermophoresis, variable viscosity and thermal conductivity on free convective heat and mass transfer of non-darcian mhd dissipative casson fluid flow with suction and n^{th} order of chemical reaction. Journal of the Nigerian Mathematical Society 34 (1), 11–31.

Bird, R. B., Stewart, W. E., Lightfoot, E. N., 2001. Transport Phenomena. Vol. 55. Wiley.

Bou-Said, B., Boucherit, H., Lahmar, M., 2012. On the influence of particle concentration in a lubricant and its rheological properties on the bearing behavior. Mechanics & Industry 13 (2), 111–121.

Cengel, Y. A., Cimbala, J. M., 2004. Fluid Mechanics (Mcgraw-Hill Series in Mechanical Engineering). Vol. 9. McGraw-Hill Science/Engineering/Math.

Choudhury, M., Hazarika, G., 2013. The effects of variable viscosity and thermal conductivity on mhd oscillatory free convective flow past a vertical plate in slip flow regime with variable suction and periodic plate temperature. Journal of Applied Fluid Mechanics 6 (2), 277–283.

Choudhury, M., Hazarika, G. C., 2008. The effects of variable viscosity and thermal conductivity on mhd flow due to a point sink. Matemáticas: Enseñanza Universitaria 16 (2).

Dhlamini, M., Kameswaran, P. K., Sibanda, P., Motsa, S., Mondal, H., 2018a. Activation energy and binary chemical reaction effects in mixed convective nanofluid flow with convective boundary conditions. Journal of Computational Design and Engineering.

Dhlamini, M., Mondal, H., Sibanda, P., Motsa, S., 2018b. Spectral quasi-linearization methods for powell-eyring MHD flow over a nonlinear stretching surface. Journal of Nanofluids 7 (5), 917–927.

Elbarbary, E. M. E., Elgazery, N. S., 2004. Chebyshev finite difference method for the effects of variable viscosity and variable thermal conductivity on heat transfer from moving surfaces with radiation. International Journal of Thermal Sciences 43 (9), 889–899.

Goqo, S., Oloniiju, S., Mondal, H., Sibanda, P., Motsa, S., 2018. Entropy generation in MHD radiative viscous nanofluid flow over a porous wedge using the bivariate spectral quasi-linearization method. Case Studies in Thermal Engineering 12, 774–788.

Hassanien, I., Essawy, A., Moursy, N., 2003. Variable viscosity and thermal conductivity effects on combined heat and mass transfer in mixed convection over a UHF/UMF wedge in porous media: the entire regime. Applied Mathematics and Computation 145 (2-3), 667–682.

Hayat, T., Abbasi, F., Ahmad, B., Alsaedi, A., 2014. Mhd mixed convection peristaltic flow with variable viscosity and thermal conductivity. Sains Malays 43 (10), 1583–1590.

Hayat, T., Imtiaz, M., Alsaedi, A., 2015. Effects of homogeneous-heterogeneous reactions in flow of powell-eyring fluid. Journal of Central South University 22 (8), 3211–3216.

Hayat, T., Khan, M. I., Farooq, M., Gull, N., Alsaedi, A., nov 2016a. Unsteady three-dimensional mixed convection flow with variable viscosity and thermal conductivity. Journal of Molecular Liquids 223, 1297–1310.

Hayat, T., Waqas, M., Shehzad, S. A., Alsaedi, A., 2016b. Mixed convection flow of viscoelastic nanofluid by a cylinder with variable thermal conductivity and heat source/sink. International Journal of Numerical Methods for Heat & Fluid Flow 26 (1), 214–234.

Hazarika, G., Jadav, K., 2014. Effects of variable viscosity and thermal conductivity on mhd free convective flow along a vertical porous plate with viscous dissipation. International Journal of Mathematics Trends and Technology 15 (1), 70–85.

Horibata, S., Yarimitsu, S., Fujie, H., 2017. Influence of synovial fluid pressure increase on the biphasic lubrication property of articular cartilage. The Proceedings of Mechanical Engineering Congress, Japan 2017 (0), J0260104.

Kaladhar, K., 2015. Natural convection flow of couple stress fluid in a vertical channel with hall and joule heating effects. Procedia Engineering 127, 1071–1078.

Kannan, T., Moorthy, M., 2016. Effects of variable viscosity on power-law fluids over a permeable moving surface with slip velocity in the presence of heat generation and suction. Journal of Applied Fluid Mechanics 9 (6), 9–22.

Khan, W., Yousafzai, F., 2014. On the exact solutions of couple stress fluids. Advanced Trends in Mathematics 1, 27–32.

Khan, Y., Wu, Q., Faraz, N., Yildirim, A., 2011. The effects of variable viscosity and thermal conductivity on a thin film flow over a shrinking/stretching sheet. Computers & Mathematics with Applications 61 (11), 3391–3399.

Khound, P., Hazaika, G., 2000. The effect of variable viscosity and thermal conductivity on liquid film on an unsteady stretching surface. Proc. of 46th Annual Tech. Session, Ass. Sc. Soc 22, 47–56.

Lai, F., Kulacki, F., 1990. The effect of variable viscosity on convective heat transfer along a vertical surface in a saturated porous medium. International Journal of Heat and Mass Transfer 33 (5), 1028–1031.

Lai, W. M., Kuei, S. C., Mow, V. C., 1978. Rheological equations for synovial fluids. Journal of Biomechanical Engineering 100 (4), 169.

Lin, J.-R., 2001. Linear stability analysis of rotor-bearing system: couple stress fluid model. Computers & Structures 79 (8), 801–809.

Lin, J.-R., Lu, Y.-M., 2004. Steady-state performance of wide parabolic-shaped slider bearings with a couple stress fluid. Journal of Marine Science and Technology 12 (4), 239–246.

Manjunatha, S., Gireesha, B., 2016. Effects of variable viscosity and thermal conductivity on MHD flow and heat transfer of a dusty fluid. Ain Shams Engineering Journal 7 (1), 505–515.

Misra, J. C., Adhikay, S. D., Mallick, B., Sinha, A., 2018. Mathematical modeling of blood flow in arteries subject to vibrating environment. Journal of Mechanics in Medicine and Biology 18 (01), 1850001.

Monica, M., Vittal, C., Reddy, M. C. K., 2016. Stagnation point flow of a mhd powell-eyring fluid over a nonlinearly stretching sheet in the presence of heat source/sink. Journal of Progressive Research in Mathematics 8 (2), 1290–1300.

Motsa, S. S., Magagula, V. M., Sibanda, P., 2014. A bivariate chebyshev spectral collocation quasilinearization method for nonlinear evolution parabolic equations. The Scientific World Journal 2014, 1–13.

Motsa, S. S., Mutua, S. F., Stanford, S., 2016. Solving nonlinear parabolic partial differential equations using multidomain bivariate spectral collocation method. In: Nonlinear Systems - Design, Analysis, Estimation and Control. InTech.

Pal, D., Mondal, H., 2014. Effects of temperature-dependent viscosity and variable thermal conductivity on MHD non-darcy mixed convective diffusion of species over a stretching sheet. Journal of the Egyptian Mathematical Society 22 (1), 123–133.

Panigrahi, S., Reza, M., Mishra, A. K., 2015. Mixed convective flow of a powell-eyring fluid over a non-linear stretching surface with thermal diffusion and diffusion thermo. Procedia Engineering 127, 645–651.

Polezhaev, Y. V., 2011. Thermal conductivity. In: A-to-Z Guide to Thermodynamics, Heat and Mass Transfer, and Fluids Engineering. Begellhouse.

Ram, N., 2017. Influence of couple stress lubricants on hole-entry hybrid journal bearings. Jurnal Tribologi 14, 32–49.

Rao, T. V. V. L. N., Sufian, S., Mohamed, N. M., 2013. Analysis of nanoparticle additive couple stress fluids in three-layered journal bearing. Journal of Physics: Conference Series 431, 012023.

Sahu, M., Sharma, S., Agrawal, A., 2010. Study of arterial blood flow in stenosed vessel using non-newtonian couple stress fluid model. International Journal of Dynamics of Fluids 6 (2), 248–257.

Singh, C., 1982. Lubrication theory for couple stress fluids and its application to short bearings. Wear 80 (3), 281–290.

Sinha, P., Singh, C., Prasad, K., 1981. Couple stresses in journal bearing lubricants and the effect of cavitation. Wear 67 (1), 15–24.

Sithole, H., Mondal, H., Goqo, S., Sibanda, P., Motsa, S., 2018. Numerical simulation of couple stress nanofluid flow in magneto-porous medium with thermal radiation and a chemical reaction. Applied Mathematics and Computation 339, 820–836.

Srinivasacharya, D., Kaladhar, K., 2012. Mixed convection flow of couple stress fluid in a non-darcy porous medium with soret and dufour effects. Journal of Porous Media 15 (4), 415–422.

Srinivasacharya, D., Rao, G. M., 2016. Mathematical model for blood flow through a bifurcated artery using couple stress fluid. Mathematical Biosciences 278, 37–47.

Stokes, V. K., 1966. Couple stresses in fluids. Physics of Fluids 9 (9), 1709–1715.

Wang, X., Zhu, K., Gui, C., 2002. A study of a journal bearing lubricated by couple stress fluids considering thermal and cavitation effects. Proceedings of the Institution of Mechanical Engineers, Part J: Journal of Engineering Tribology 216 (5), 293–305.

Summary

In this chapter, viscosity and thermal conductivity were not taken as constant in the boundary layer as assumed in chapters 2 to 5. The two properties were assumed to be temperature dependent. A new simpler model for temperature-dependent thermal conductivity that correctly models the variation of thermal conductivity as a function of temperature was formulated. Results for the temperature-dependent thermal conductivity model were found to be consistent with results found in the literature that used a decreasing function and were different from those that used a linearly increasing function.

Chapter 7

Conclusion

In this thesis, we set out to study the convective flow of nanofluids with convective boundary conditions. The nonlinear partial differential equations were transformed to boundary value problems via similarity transformations. The spectral quasilinearisation and the bivariate spectral quasilinearisation methods were used to solve the boundary value problems numerically. The spectral methods were shown to be accurate, stable and had fast convergence rates. The successful modeling of the notorious convection-diffusion term was demonstrated. Modeling of the convection-diffusion models has been a challenge in computational fluid dynamics [113]. We were able to numerically solve the convection-reaction models using spectral quasilinearisation methods without having to introduce some additional terms as suggested by Wang and Hutter [113]. There were no numerical instabilities observed when using spectral methods. They also showed that convective transport was enhanced by the use of nanofluids and motile microorganisms as evidenced by the thickening of both the momentum and thermal boundary layers.

Further, the flow of a nanofluid with an applied transverse magnetic field, particle Brownian motion and thermophoresis was considered. It was observed that increasing the magnetic field parameter leads to a decrease in fluid velocity. This is attributed to the Lorentz force generated that acts in the opposite direction of flow [114, 115]. An increase in the magnetic field parameter was shown to increase temperature and concentration in Chapter 2. The results are consistent with findings by Noghrehabadi *et al* [115]. Increasing the Brownian motion parameter was shown to lead to a decrease in the solute boundary layer. An increase in the Brownian motion parameter boosts the movement of particles. This causes the warming of the boundary layer which effectively causes

the nanoparticle to move away from the surfaces inside the inactive fluid. This increases the deposition of the solute particles away from the surface, leading to the reduction of the concentration [116]. These results are in agreement with the findings by Makinde and Animasaun [117] and Malvandia and Ganji [118]. Thermophoresis, on the other hand, which is a force exerted on the solute particle due to a temperature acts to oppose the Brownian motion [118]. Increasing the thermophoretic parameter increases the solute boundary layer and our results are consistent with the results by Makinde and Animasaun [117],Malvandi and Ganji, [118] and Sheikholeslami *et al* [119]. The buoyancy parameters were also shown to increase velocity while causing a decrease in temperature and concentration. The results are in agreement with the results by Hayat *et al* [120].

In Chapter 2, we studied Powell-Eyring MHD Flow over a nonlinear stretching surface and the other parameter of interest was the thinning parameter. It was shown that increasing the thinning parameter increased the velocity of the fluid as well as the thermal boundary layer. Jalil *et al* [92] drew a similar conclusion on this parameter.

In Chapters 3 and 4, the impact of activation energy and binary chemical reaction effects in mixed convective nanofluid flow with convective boundary conditions and activation energy and entropy generation in viscous nanofluid with higher-order chemically reacting species was studied. The unsteady parameter decreased velocity, temperature and concentration profiles. Activation energy increased concentration while the chemical reaction constant decreased it. Similar results were obtained by Maleque [121, 122]. Increasing the Biot number was shown to increase the temperature and concentration profiles. Higher-order chemical reactions increase the solute boundary layer, a result that is consistent with results by Palani *et al* [123]. Heat generation is the only process that was shown to increase the Bejan number. This suggests that heat transfer irreversibility was dominant. All other processes/parameters lead to a decrease in the Bejan number suggesting that heat transfer irreversibility was dominated by other processes.

In Chapter 5, the impact of oxytactic microorganisms in a rotational nanofluid with convective boundary conditions was studied. The velocity ratio parameter plays a pivotal role in the dynamics and direction of the flow. The bioconvection Peclet number is shown to increase the concentration of microorganisms in the boundary layer.

In Chapter 6, a system that describes the flow of couple stress fluids assuming that viscosity and thermal conductivity are not constant but rather they depend on temperature was formulated. The simpler model for the variation of thermal conductivity produced results that were consistent with findings in literature [124, 125]. In this study, we set to assess the impact of certain key parameters on the flow dynamics of nanofluids. The following conclusions were made: (1) Order of chemical reaction increases the fluid velocity and concentration of chemical species while decreasing the temperature. (2) Above or below a critical value the velocity parameter alters the flow dynamics. (3) Having the plate move in the opposite direction as the fluid does not change the dynamics of the flow, changes occur at the critical value. (4) The new model for the variation of thermal conductivity with temperature is consistent with models in the literature.

7.1 Recommendations for future work

Further, some new results were obtained through the theoretical study of nanofluid flow with convective boundary conditions. The validity of these results requires, in some instances, experimental results to confirm. Moving forward we propose to investigate, inter alia, modeling the flow of a nanofluid with variable viscosity and thermal conductivity due to nanoparticle volume fraction and develop models that incorporate conjugate heat transfer analysis for the nanofluid flow with convective boundary conditions.

Several studies have reported a change in the viscosity of fluid due to nanoparticle addition [126–130]. Most mathematical simulation models haven't incorporated this phenomenon. Hence it is prudent to interrogate the impact that this has on the flow properties of nanofluids.

The conjugate heat transfer analysis predicts heat transfer by solving all relevant solid and fluid field heat transfer processes simultaneously instead of solving it as a separate coefficient [131, 132]. Conjugate heat transfer is suitable for a problem where two different materials or where heat is modeled by different equations in different sub-domains [131]. This is the set-up encountered in most convective heat transfer problems where heat transfer within the solid is modeled by elliptical Laplace's equation or parabolic differential equation, while heat transfer in the fluid is modeled by

the elliptical Navier-Stokes equations. Conjugate heat transfer analysis is beneficial for those applications where heat transfer is non-uniform or difficult to calculate empirically. Using conjugate heat transfer analysis will result in more realistic results than those that we used in this study where heat transfer coefficients were used. The main setback in using the heat transfer coefficient is that the value is determined experimentally. The actual wall temperature distribution is often neglected resulting in calculations that are not very accurate [131, 133].

References

[1] Y. A. Cengel and J. M. Cimbala, *Fluid mechanics : fundamentals and applications.*, vol. 31. Wiley, 2005.

[2] F. M. White, *Fluid Mechanics*. McGraw Hill, 2011.

[3] R. B. Bird, W. E. Stewart, and E. N. Lightfoot, *Transport phenomena*, vol. 31. John Wiley & Sons, 2007.

[4] C. T. Simmons, T. R. Fenstemaker, and J. M. Sharp Jr, "Variable-density groundwater flow and solute transport in heterogeneous porous media: approaches, resolutions and future challenges," *Journal of Contaminant Hydrology*, vol. 52, no. 1-4, pp. 245–275, 2001.

[5] R. Sankarasubramanian and W. N. Gill, "Unsteady convective diffusion with interphase mass transfer," *Proceedings of the Royal Society A: Mathematical, Physical and Engineering Sciences*, vol. 333, no. 1592, pp. 115–132, 1973.

[6] K. Vafai and C. Tien, "Boundary and inertia effects on convective mass transfer in porous media," *International Journal of Heat and Mass Transfer*, vol. 25, no. 8, pp. 1183–1190, 1982.

[7] S. Kumar and G. Tiwari, "Estimation of convective mass transfer in solar distillation systems," *Solar Energy*, vol. 57, no. 6, pp. 459–464, 1996.

[8] M. Y. Jaffrin, "Convective mass transfer in hemodialysis," *Artificial Organs*, vol. 19, no. 11, pp. 1162–1171, 1995.

[9] Z. Guo, D. Li, and B. Wang, "A novel concept for convective heat transfer enhancement," *International Journal of Heat and Mass Transfer*, vol. 41, no. 14, pp. 2221–2225, 1998.

[10] H. L. Stone and P. L. T. Brian, "Numerical solution of convective transport problems," *AIChE Journal*, vol. 9, no. 5, pp. 681–688, 1963.

[11] G. Ruocco, *Introduction to Transport Phenomena Modeling: A Multiphysics, General Equation-Based Approach*. Springer, 2018.

[12] I. A. Popov, Y. F. Gortyshov, and V. V. Olimpiev, "Industrial applications of heat transfer enhancement: The modern state of the problem (a review)," *Thermal Engineering*, vol. 59, no. 1, pp. 1–12, 2012.

[13] M. Nebyla, M. Přibyl, and I. Schreiber, "Effects of convective transport on chemical signal propagation in epithelia," *Biophysical Journal*, vol. 102, no. 5, pp. 990–1000, 2012.

[14] M. A. Swartz and M. E. Fleury, "Interstitial flow and its effects in soft tissues," *Annual Review of Biomedical Engineering*, vol. 9, no. 1, pp. 229–256, 2007.

[15] L. T. K.Jain, "Transport of fluid and macromolecules in tumors. i. role of interstitial pressure and convection," *Microvascular Research*, vol. 37, pp. 77–104, 1989.

[16] L. Ray, J. J. Iliff, and J. J. Heys, "Analysis of convective and diffusive transport in the brain interstitium," *Fluids and Barriers of the CNS*, vol. 16, no. 1, 2019.

[17] D. Liu, A. Chalkidou, D. B. Landau, P. K. Marsden, and J. D. Fenwick, "Interstitial diffusion and the relationship between compartment modelling and multi-scale spatial-temporal modelling of18f-FLT tumour uptake dynamics," *Physics in Medicine and Biology*, vol. 59, no. 17, pp. 5175–5202, 2014.

[18] R. K. Zeytounian, *Convection in fluids: a rational analysis and asymptotic modelling*, vol. 90. Springer Science & Business Media, 2009.

[19] Z. Svoboda, "The convective-diffussion equation and its use in building physics," *International Journal on Architectural Science*, vol. 114, no. A2, 2000.

[20] W. Q. Tao and E. M. Sparrow, "The transportive and convective numerical stability of the steady-state convection-diffussion finite-difference equation," *Numerical Heat Transfer*, vol. 11, no. 4, pp. 491–497, 1987.

[21] J. L. Siemieniuch and I. Gladwell, "Analysis of explicit difference methods for a diffusion-convection equation," *International Journal for Numerical Methods in Engineering*, vol. 12, no. 6, pp. 899–916, 1978.

[22] N. Dalir, "Numerical study of entropy generation for forced convection flow and heat transfer of a jeffrey fluid over a stretching sheet," *Alexandria Engineering Journal*, vol. 53, no. 4, pp. 769–778, 2014.

[23] M. Ramzan, M. Bilal, and J. D. Chung, "Radiative flow of powell-eyring magneto-nanofluid over a stretching cylinder with chemical reaction and double stratification near a stagnation point," *PLOS ONE*, vol. 12, no. 1, p. e0170790, 2017.

[24] K. Kaladhar, "Natural convection flow of couple stress fluid in a vertical channel with hall and joule heating effects," *Procedia Engineering*, vol. 127, pp. 1071–1078, 2015.

[25] S. Shateyi, S. S. Motsa, and P. Sibanda, "The effects of thermal radiation, hall currents, soret, and dufour on MHD flow by mixed convection over a vertical surface in porous media," *Mathematical Problems in Engineering*, vol. 2010, pp. 1–20, 2010.

[26] D. Srinivasacharya, B. Mallikarjuna, and R. Bhuvanavijaya, "Soret and dufour effects on mixed convection along a vertical wavy surface in a porous medium with variable properties," *Ain Shams Engineering Journal*, vol. 6, no. 2, pp. 553–564, 2015.

[27] F. Awad and P. Sibanda, "Dufour and soret effects on heat and mass transfer in a micropolar fluid in a horizontal channel," *WSEAS Trans. Heat Mass Transfer*, vol. 5, pp. 165–177, 2010.

[28] F. P. Incropera, A. S. Lavine, T. L. Bergman, and D. P. DeWitt, *Fundamentals of heat and mass transfer*. Wiley, 2007.

[29] J. Gustin, "Runaway reactions, their courses and the methods to establish safe process conditions," *Journal de Physique III*, vol. 1, no. 8, pp. 1401–1419, 1991.

[30] M. Rashidi, S. Bagheri, E. Momoniat, and N. Freidoonimehr, "Entropy analysis of convective MHD flow of third grade non-newtonian fluid over a stretching sheet," *Ain Shams Engineering Journal*, vol. 8, no. 1, pp. 77–85, 2017.

[31] R. Ogulata and F. Doba, "Experiments and entropy generation minimization analysis of a cross-flow heat exchanger," *International Journal of Heat and Mass Transfer*, vol. 41, no. 2, pp. 373–381, 1998.

[32] I. L. Mostinsky, "Mass transfer," in *A-to-Z Guide to Thermodynamics, Heat and Mass Transfer, and Fluids Engineering*, Begellhouse, 2011.

[33] S. U. Choi and J. A. Eastman, "Enhancing thermal conductivity of fluids with nanoparticles," Tech. Rep. 2, Argonne National Lab., IL (United States), 1995.

[34] R. Saidur, K. Leong, and H. Mohammad, "A review on applications and challenges of nanofluids," *Renewable and Sustainable Energy Reviews*, vol. 15, no. 3, pp. 1646–1668, 2011.

[35] S. Kim, I. C. Bang, J. Buongiomo, and L. Hu, "Study of pool boiling and critical heat flux enhancement in nanofluids," *International Journal of Energy Research*, vol. 39, no. 10, pp. 1391–1401, 2007.

[36] K. V. Wong and O. D. Leon, "Applications of nanofluids: Current and future," *Advances in Mechanical Engineering*, vol. 2, p. 519659, 2010.

[37] R. Ramakoteswaa, L. Gahane, and S. Ranganayakulu, "Synthesis applications and challenges of nanofluids–review," *IOSR J. Appl. Phys*, vol. 6, no. 1, pp. 21–28, 2014.

[38] W. N. Mutuku and O. D. Makinde, "Hydromagnetic bioconvection of nanofluid over a permeable vertical plate due to gyrotactic microorganisms," *Computers & Fluids*, vol. 95, pp. 88–97, 2014.

[39] S. Lee, S. U.-S. Choi, S. Li, and J. A. Eastman, "Measuring thermal conductivity of fluids containing oxide nanoparticles," *Journal of Heat Transfer*, vol. 121, no. 2, p. 280, 1999.

[40] J. C. Maxwell, *A treatise on electricity and magnetism*, vol. 1. Clarendon press, 1881.

[41] J. Lee and I. Mudawar, "Assessment of the effectiveness of nanofluids for single-phase and two-phase heat transfer in micro-channels," *International Journal of Heat and Mass Transfer*, vol. 50, no. 3-4, pp. 452–463, 2007.

[42] R. Taylor, S. Coulombe, T. Otanicar, P. Phelan, A. Gunawan, W. Lv, G. Rosengarten, R. Prasher, and H. Tyagi, "Small particles, big impacts: A review of the diverse applications of nanofluids," *Journal of Applied Physics*, vol. 113, no. 1, p. 011301, 2013.

[43] P. Keblinski, R. Prasher, and J. Eapen, "Thermal conductance of nanofluids: is the controversy over?," *Journal of Nanoparticle Research*, vol. 10, no. 7, pp. 1089–1097, 2008.

[44] W. Evans, R. Prasher, J. Fish, P. Meakin, P. Phelan, and P. Keblinski, "Effect of aggregation and interfacial thermal resistance on thermal conductivity of nanocomposites and colloidal nanofluids," *International Journal of Heat and Mass Transfer*, vol. 51, no. 5-6, pp. 1431–1438, 2008.

[45] R. Prasher, W. Evans, P. Meakin, J. Fish, P. Phelan, and P. Keblinski, "Effect of aggregation on thermal conduction in colloidal nanofluids," *Applied Physics Letters*, vol. 89, no. 14, p. 143119, 2006.

[46] S.-Q. Zhou and R. Ni, "Measurement of the specific heat capacity of water-based al2o3 nanofluid," *Applied Physics Letters*, vol. 92, no. 9, p. 093123, 2008.

[47] D. Shin and D. Banerjee, "Enhancement of specific heat capacity of high-temperature silica-nanofluids synthesized in alkali chloride salt eutectics for solar thermal-energy storage applications," *International Journal of Heat and Mass Transfer*, vol. 54, no. 5-6, pp. 1064–1070, 2011.

[48] H. Masuda, A. Ebata, and K. Teramae, "Alteration of thermal conductivity and viscosity of liquid by dispersing ultra-fine particles. dispersion of al2o3, sio2 and tio2 ultra-fine particles," *Netsu Bussei*, vol. 7, no. 4, pp. 227–233, 1993.

[49] P. Senapati, B. Mishra, and A. Parida, "Modeling of viscosity for power plant ash slurry at higher concentrations: Effect of solids volume fraction, particle size and hydrodynamic interactions," *Powder Technology*, vol. 197, no. 1-2, pp. 1–8, 2010.

[50] R. Prasher, D. Song, J. Wang, and P. Phelan, "Measurements of nanofluid viscosity and its implications for thermal applications," *Applied Physics Letters*, vol. 89, no. 13, p. 133108, 2006.

[51] J. Buongiorno, "Convective transport in nanofluids," *Journal of Heat Transfer*, vol. 128, no. 3, p. 240, 2006.

[52] I. M. Jánosi, A. Czirók, D. Silhavy, and A. Holczinger, "Is bioconvection enhancing bacterial growth in quiescent environments?," *Environmental Microbiology*, vol. 4, no. 9, pp. 525–531, 2002.

[53] O. A. Bég, "Nonlinear multiphysical laminar nanofluid bioconvection flows: Models and computation," in *Computational Approaches in Biomedical Nano-Engineering*, pp. 113–145, Wiley-VCH Verlag GmbH & Co. KGaA, 2018.

[54] A. Kage, C. Hosoya, S. A. Baba, and Y. Mogami, "Drastic reorganization of the bioconvection pattern of chlamydomonas: quantitative analysis of the pattern transition response," *Journal of Experimental Biology*, vol. 216, no. 24, pp. 4557–4566, 2013.

[55] B. Mallikarjuna, A. Rashad, A. J. Chamkha, and M. Abdou, "Mixed bioconvection flow of a nanofluid containing gyrotactic microorganisms past a vertical slender cylinder," *Frontiers in Heat and Mass Transfer*, vol. 10, 2018.

[56] S. Shaw, P. K. Kameswaran, M. Narayana, and P.Sibanda, "Bioconvection in a non-darcy porus medium saturated with a nanofluid and oxytactic micro-organisms," *International Journal of Biomathematics*, vol. 07, no. 01, p. 1450005, 2014.

[57] N. Sato, K. Sato, and M. Toyoshima, "Analysis and modeling of the inverted bioconvection in chlamydomonas reinhardtii : emergence of plumes from the layer of accumulated cells," *Heliyon*, vol. 4, no. 3, p. e00586, 2018.

[58] T. Abe, S. Nakamura, and S. Kudo, "Bioconvection induced by bacterial chemotaxis in a capillary assay," *Biochemical and Biophysical Research Communications*, vol. 483, no. 1, pp. 277–282, 2017.

[59] S. Shaw, S. S. Motsa, and P. Sibanda, "Magnetic field and viscous dissipation effect on bioconvection in a permeable sphere embedded in a porous medium with a nanofluid containing gyrotactic micro-organisms," *Heat Transfer-Asian Research*, vol. 47, no. 5, pp. 718–734, 2018.

[60] A. Kuznetsov, "The onset of nanofluid bioconvection in a suspension containing both nanoparticles and gyrotactic microorganisms," *International Communications in Heat and Mass Transfer*, vol. 37, no. 10, pp. 1421–1425, 2010.

[61] T. Pedley and J. Kessler, "Bioconvection," *Science Progress (1933-)*, vol. 37, pp. 105–123, 1992.

[62] M. Bees and N. Hill, "Wavelengths of bioconvection patterns," *Journal of Experimental Biology*, vol. 200, no. 10, pp. 1515–1526, 1997.

[63] J. O. Kessler and N. A. Hill, "Complementarity of physics, biology and geometry in the dynamics of swimming micro-organisms," in *Physics of Biological Systems*, pp. 325–340, Springer, 1997.

[64] S. Mohd Sauid, J. Krishnan, T. Huey Ling, and M. V. Veluri, "Enhancement of oxygen mass transfer and gas holdup using palm oil in stirred tank bioreactors with xanthan solutions as simulated viscous fermentation broths," *BioMed research international*, vol. 2013, pp. 1–9, 2013.

[65] S. Siddiqa, G. e Hina, N. Begum, S. Saleem, M. Hossain, and R. S. R. Gorla, "Numerical solutions of nanofluid bioconvection due to gyrotactic microorganisms along a vertical wavy cone," *International Journal of Heat and Mass Transfer*, vol. 101, pp. 608–613, 2016.

[66] Y. Deleuze, C.-Y. Chiang, M. Thiriet, and T. W. Sheu, "Numerical study of plume patterns in a chemotaxis–diffusion–convection coupling system," *Computers & Fluids*, vol. 126, pp. 58–70, 2016.

[67] W. A. Khan, M. J. Uddin, and A. I. M. Ismail, "Free convection of non-newtonian nanofluids in porous media with gyrotactic microorganisms," *Transport in Porous Media*, vol. 97, no. 2, pp. 241–252, 2013.

[68] A. Kuznetsov, "Nanofluid bioconvection: interaction of microorganisms oxytactic upswimming, nanoparticle distribution, and heating/cooling from below," *Theoretical and Computational Fluid Dynamics*, vol. 26, no. 1-4, pp. 291–310, 2012.

[69] B. Mallikarjuna, A. Rashad, A. Chamkha, and M. Abdou, "Mixed bioconvection flow of a nanofluid containing gyrotactic microorganisms past a vertical slender cylinder," *Frontiers in Heat and Mass Transfer (FHMT)*, vol. 10, 2018.

[70] P. E. Hydon and P. E. Hydon, *Symmetry methods for differential equations: a beginner's guide*, vol. 22. Cambridge University Press, 2000.

[71] A. K. M. Al-Salihi, "Study of similarity techniques in differential equations and applications," *Journal of Applied Mathematics and Physics*, vol. 02, no. 03, pp. 22–32, 2013.

[72] G. I. Barenblatt and G. I. Barenblatt, *Scaling, self-similarity, and intermediate asymptotics: dimensional analysis and intermediate asymptotics*, vol. 14. Cambridge University Press, 1996.

[73] I. Fris and P. Winternitz, "Invariant expansions of relativistic amplitudes and subgroups of the proper lorentz group," tech. rep., Joint Inst. of Nuclear Research, Dubna, USSR Lab. of Theoretical Physics, 1964.

[74] P. A. Clarkson and M. D. Kruskal, "New similarity reductions of the boussinesq equation," *Journal of Mathematical Physics*, vol. 30, no. 10, pp. 2201–2213, 1989.

[75] D. J. Arrigo, *Symmetry analysis of differential equations: an introduction*, vol. 9. John Wiley & Sons, 2015.

[76] S. S. Motsa, V. M. Magagula, and P. Sibanda, "A bivariate chebyshev spectral collocation quasilinearization method for nonlinear evolution parabolic equations," *The Scientific World Journal*, vol. 2014, pp. 1–13, 2014.

[77] S. Liao, *Beyond Perturbation :'Introduction to the Homotopy Analysis Method'*. Chapman and Hall/CRC, 2003.

[78] R. W. Lewis, P. Nithiarasu, and K. N. Seetharamu, *Fundamentals of the finite element method for heat and fluid flow*. John Wiley & Sons, 2004.

[79] H. Kreiss and G. Scherer, "Finite element and finite difference methods for hyperbolic partial differential equations," in *Mathematical Aspects of Finite Elements in Partial Differential Equations*, pp. 195–212, Elsevier, 1974.

[80] B. Hamilton, "Finite volume perspectives on finite difference schemes and boundary formulations for wave simulation.," in *DAFx*, pp. 295–302, 2014.

[81] J. P. Boyd, *Chebyshev and Fourier spectral methods*, vol. 295. Courier Corporation, 2001.

[82] D. Dutykh, "A brief introduction to pseudo-spectral methods: application to diffusion problems," *arXiv preprint arXiv:1606.05432*, vol. 131, pp. 54–71, 2016.

[83] D. A. Kopriva, *Implementing Spectral Methods for Partial Differential Equations*. Springer Netherlands, 2009.

[84] S. S. Motsa, "A new spectral local linearization method for nonlinear boundary layer flow problems," *Journal of Applied Mathematics*, vol. 2013, pp. 1–15, 2013.

[85] L. N. Trefethen, *Spectral methods in MATLAB*, vol. 10. Siam, 2000.

[86] R. E. Bellman and R. E. Kalaba, "Quasilinearization and nonlinear boundary-value problems," *Mathematics of Computation*, vol. 21, no. 97, p. 121, 1965.

[87] A. Krysko, J. Awrejcewicz, S. Pavlov, M. Zhigalov, and V. Krysko, "On the iterative methods of linearization, decrease of order and dimension of the karman-type pdes," *The Scientific World Journal*, vol. 2014, pp. 1–15, 2014.

[88] V. Lakshmikantham and A. S. Vatsala, *Generalized quasilinearization for nonlinear problems*, vol. 440. Springer Science & Business Media, 2013.

[89] F. C. G. Santos, "The linearization method for the numerical analysis of finite element solutions to quasi-linear elliptic partial differential equations," *SIAM Journal on Numerical Analysis*, vol. 38, no. 1, pp. 227–266, 2000.

[90] S. S. Motsa, P. G. Dlamini, and M. Khumalo, "Spectral relaxation method and spectral quasilinearization method for solving unsteady boundary layer flow problems," *Advances in Mathematical Physics*, vol. 2014, pp. 1–12, 2014.

[91] J. S. Hesthaven, S. Gottlieb, and D. Gottlieb, *Spectral methods for time-dependent problems*, vol. 21. Cambridge University Press, 2007.

[92] M. Jalil, S. Asghar, and S. Imran, "Self similar solutions for the flow and heat transfer of powell-eyring fluid over a moving surface in a parallel free stream," *International Journal of Heat and Mass Transfer*, vol. 65, pp. 73–79, 2013.

[93] N. A. Khan, S. Aziz, and N. A. Khan, "MHD flow of powell–eyring fluid over a rotating disk," *Journal of the Taiwan Institute of Chemical Engineers*, vol. 45, no. 6, pp. 2859–2867, 2014.

[94] T. Agbaje, S. Mondal, S. Motsa, and P. Sibanda, "A numerical study of unsteady non-newtonian powell-eyring nanofluid flow over a shrinking sheet with heat generation and thermal radiation," *Alexandria Engineering Journal*, vol. 56, no. 1, pp. 81–91, 2017.

[95] R. E. Powell and H. Eyring, "Mechanisms for the relaxation theory of viscosity," *Nature*, vol. 154, no. 3909, pp. 427–428, 1944.

[96] I. L. Animasaun, B. Mahanthesh, and O. K. Koriko, "On the motion of non-newtonian eyring–powell fluid conveying tiny gold particles due to generalized surface slip velocity and buoyancy," *International Journal of Applied and Computational Mathematics*, vol. 4, no. 6, 2018.

[97] A. Bestman, "Natural convection boundary layer with suction and mass transfer in a porous medium," *International journal of energy research*, vol. 14, no. 4, pp. 389–396, 1990.

[98] S. K. Upadhyay, *Chemical kinetics and reaction dynamics*, vol. 15. Springer Science & Business Media, 2007.

[99] J. Sethna, *Statistical mechanics: entropy, order parameters, and complexity*, vol. 14. Oxford University Press, 2006.

[100] A. Bejan, *Entropy generation through heat and fluid flow*, vol. 50. Wiley, 1982.

[101] A. Bejan, "Entropy generation minimization: The new thermodynamics of finite-size devices and finite-time processes," *Journal of Applied Physics*, vol. 79, no. 3, pp. 1191–1218, 1996.

[102] P. J. Verbelen, S. A. Depraetere, J. Winderickx, F. R. Delvaux, and F. Delvaux, "The influence of yeast oxygenation prior to brewery fermentation on yeast metabolism and the oxidative stress response," *FEMS Yeast Research*, vol. 9, no. 2, pp. 226–239, 2009.

[103] H. G. Lee and J. Kim, "Numerical investigation of falling bacterial plumes caused by bioconvection in a three-dimensional chamber," *European Journal of Mechanics - B/Fluids*, vol. 52, pp. 120–130, 2015.

[104] S. A. Devi and M. Prakash, "Temperature dependent viscosity and thermal conductivity effects on hydromagnetic flow over a slendering stretching sheet," *Journal of the Nigerian Mathematical Society*, vol. 34, no. 3, pp. 318–330, 2015.

[105] F. P. Bowden and F. Thomas, "The surface temperature of sliding solids," *Proceedings of the Royal Society of London. Series A. Mathematical and Physical Sciences*, vol. 223, no. 1152, pp. 29–40, 1954.

[106] S. A. Devi and M. Prakash, "Temperature dependent viscosity and thermal conductivity effects on hydromagnetic flow over a slendering stretching sheet," *Journal of the Nigerian Mathematical Society*, vol. 34, no. 3, pp. 318–330, 2015.

[107] M. A. El-Aziz, "Temperature dependent viscosity and thermal conductivity effects on combined heat and mass transfer in MHD three-dimensional flow over a stretching surface with ohmic heating," *Meccanica*, vol. 42, no. 4, pp. 375–386, 2007.

[108] C. A. Reza Keimanesh, "The effect of temperature-dependent viscosity and thermal conductivity on micropolar fluid over a stretching sheet," *Tehnicki vjesnik - Technical Gazette*, vol. 24, no. 2, 2017.

[109] L. S. Sundar, M. K. Singh, and A. C. Sousa, "Investigation of thermal conductivity and viscosity of fe3o4 nanofluid for heat transfer applications," *International Communications in Heat and Mass Transfer*, vol. 44, pp. 7–14, 2013.

[110] W. Duangthongsuk and S. Wongwises, "Measurement of temperature-dependent thermal conductivity and viscosity of TiO2-water nanofluids," *Experimental Thermal and Fluid Science*, vol. 33, no. 4, pp. 706–714, 2009.

[111] S. H. G. C. Hazarika, "Effects of variable viscosity and thermal conductivity on magneto hydrodynamics mixed convective flow over a stretching surface with radiation," *International Journal of Scientific Research Engineering & Technology*, vol. 9, pp. 1282–1291, 2015.

[112] Y. V. Polezhaev, "Thermal conductivity," in *A-to-Z Guide to Thermodynamics, Heat and Mass Transfer, and Fluids Engineering*, Begellhouse, 2011.

[113] Y. Wang and K. Hutter, "Comparisons of numerical methods with respect toconvectively dominated problems," *International Journal for Numerical Methods in Fluids*, vol. 37, pp. 721–745, 2001.

[114] D. Khan, A. Khan, I. Khan, F. Ali, F. ul Karim, and I. Tlili, "Effects of relative magnetic field, chemical reaction, heat generation and newtonian heating on convection flow of casson fluid over a moving vertical plate embedded in a porous medium," *Scientific Reports*, vol. 9, no. 1, 2019.

[115] A. Noghrehabadi, M. Ghalambaz, E. Izadpanahi, and R. Pourrajab, "Effect of magnetic field on the boundary layer flow, heat, and mass transfer of nanofluids over a stretching cylinder," *Journal of Heat and Mass Transfer Research (JHMTR)*, vol. 1, no. 1, pp. 9–16, 2014.

[116] R. Goyal and R. Bhargava, "Gfem study of magnetohydrodynamics thermo-diffusive effect on nanofluid flow over power-law stretching sheet along with regression analysis," *arXiv preprint arXiv:1708.05609*, 2017.

[117] O. Makinde and I. Animasaun, "Thermophoresis and brownian motion effects on MHD bio-convection of nanofluid with nonlinear thermal radiation and quartic chemical reaction past an upper horizontal surface of a paraboloid of revolution," *Journal of Molecular Liquids*, vol. 221, pp. 733–743, 2016.

[118] A. Malvandi and D. Ganji, "Brownian motion and thermophoresis effects on slip flow of alumina/water nanofluid inside a circular microchannel in the presence of a magnetic field," *International Journal of Thermal Sciences*, vol. 84, pp. 196–206, 2014.

[119] M. Sheikholeslami, D. D. Ganji, M. Y. Javed, and R. Ellahi, "Effect of thermal radiation on magnetohydrodynamics nanofluid flow and heat transfer by means of two phase model," *Journal of Magnetism and Magnetic Materials*, vol. 374, pp. 36–43, 2015.

[120] T. Hayat, Y. Saeed, A. Alsaedi, and S. Asad, "Effects of convective heat and mass transfer in flow of powell-eyring fluid past an exponentially stretching sheet," *Plos One*, vol. 10, no. 9, p. e0133831, 2015.

[121] K. A. Maleque, "Effects of binary chemical reaction and activation energy on MHD boundary layer heat and mass transfer flow with viscous dissipation and heat generation/absorption," *ISRN Thermodynamics*, vol. 2013, pp. 1–9, 2013.

[122] K. A. Maleque, "Effects of exothermic/endothermic chemical reactions with arrhenius activation energy on MHD free convection and mass transfer flow in presence of thermal radiation," *Journal of Thermodynamics*, vol. 2013, pp. 1–11, 2013.

[123] S. Palani, B. R. Kumar, and P. K. Kameswaran, "Unsteady MHD flow of an UCM fluid over a stretching surface with higher order chemical reaction," *Ain Shams Engineering Journal*, vol. 7, no. 1, pp. 399–408, 2016.

[124] G. Hazarika and U. S. Gopal Ch, "Effects of variable viscosity and thermal conductivity on mhd flow past a vertical plate," *Matemáticas: Enseñanza Universitaria*, vol. 20, no. 2, pp. 70–84, 2012.

[125] M. Choudhury and G. C. Hazarika, "The effects of variable viscosity and thermal conductivity on mhd flow due to a point sink," *Matemáticas: Enseñanza Universitaria*, vol. 16, no. 2, 2008.

[126] E. A. Taborda, C. A. Franco, S. H. Lopera, V. Alvarado, and F. B. Cortés, "Effect of nanoparticles/nanofluids on the rheology of heavy crude oil and its mobility on porous media at reservoir conditions," *Fuel*, vol. 184, pp. 222–232, 2016.

[127] M. S. A. Ruqeishi, Y. A. Salmi, and T. Mohiuddin, "Nanoparticles as drilling fluids rheological properties modifiers," *Progress in Petrochemical Science*, vol. 1, 2018.

[128] P. C. Mishra, S. Mukherjee, S. K. Nayak, and A. Panda, "A brief review on viscosity of nanofluids," *International Nano Letters*, vol. 4, no. 4, pp. 109–120, 2014.

[129] A. Agi, R. Junin, and A. Gbadamosi, "Mechanism governing nanoparticle flow behaviour in porous media: insight for enhanced oil recovery applications," *International Nano Letters*, vol. 8, no. 2, pp. 49–77, 2018.

[130] A. V. Minakov, V. Y. Rudyak, and M. I. Pryazhnikov, "About rheology of nanofluids," Author(s), 2018.

[131] A. Dorfman and Z. Renner, "Conjugate problems in convective heat transfer: Review," *Mathematical Problems in Engineering*, vol. 2009, pp. 1–27, 2009.

[132] T. J. Macbeth, "Conjugate heat transfer and average versusvariable heat transfer coefficients," Master's thesis, Department of Mechanical EngineeringBrigham Young University, 2016.

[133] A. S. Dorfman, *Conjugate problems in convective heat transfer*. CRC Press, 2009.